# LEVEL II

# NAVAL POSTGRADUATE SCHOOL
## Monterey, California

DTIC
ELECTE
AUG 1 1 1981
D
C

# THESIS

A SENSITIVITY STUDY OF THE
PARABOLIC EQUATION MODEL TO
BOTTOM TYPE AND GEOMETRY

by

Antonio Ruiz Cañavate

March 1981

| Thesis Co-Advisors: | R. H. Bourke |
| | R. W. Garwood, Jr |

81 8 11 044

| REPORT DOCUMENTATION PAGE | | READ INSTRUCTIONS BEFORE COMPLETING FORM |
|---|---|---|
| 1. REPORT NUMBER | 2. GOVT ACCESSION NO. $AD$-$A102661$ | 3. RECIPIENT'S CATALOG NUMBER |
| 4. TITLE (and Subtitle) A Sensitivity Study of the Parabolic Equation Model to Bottom Type and Geometry | | 5. TYPE OF REPORT & PERIOD COVERED Master's thesis; March 1981 |
| | | 6. PERFORMING ORG. REPORT NUMBER |
| 7. AUTHOR(s) Antonio Ruiz Cañavate | | 8. CONTRACT OR GRANT NUMBER(s) |
| 9. PERFORMING ORGANIZATION NAME AND ADDRESS Naval Postgraduate School Monterey, California 93940 | | 10. PROGRAM ELEMENT, PROJECT, TASK AREA & WORK UNIT NUMBERS |
| 11. CONTROLLING OFFICE NAME AND ADDRESS Naval Postgraduate School Monterey, California 93940 | | 12. REPORT DATE March 1981 |
| | | 13. NUMBER OF PAGES 95 |
| 14. MONITORING AGENCY NAME & ADDRESS(If different from Controlling Office) | | 15. SECURITY CLASS. (of this report) Unclassified |
| | | 15a. DECLASSIFICATION/DOWNGRADING SCHEDULE |

16. DISTRIBUTION STATEMENT (of this Report)

Approved for public release; distribution unlimited.

17. DISTRIBUTION STATEMENT (of the abstract entered in Block 20, if different from Report)

18. SUPPLEMENTARY NOTES

19. KEY WORDS (Continue on reverse side if necessary and identify by block number)

Parabolic Equation Model

20. ABSTRACT (Continue on reverse side if necessary and identify by block number)

The effect of several types of flat and sloping bottom configurations and bottom geophysical properties are studied using the parabolic equation model in a sensitivity analysis to determine the importance of such environmental parameters. Low frequency and fixed source and receiver depths have been used along with a single sound speed profile, in both deep and shallow water cases. For a fully absorbing bottom, only the

1

SECURITY CLASSIFICATION OF THIS PAGE(When Data Entered)

#20 - ABSTRACT - (CONTINUED)

refracted energy paths remain, making the model insensitive to the bottom geometry. For a perfectly reflecting bottom, both the refracted and the reflected paths were present in deep water tests, and only the reflected paths in shallow water cases. For the sloping bottom geometries a periodic interference pattern was found in transmission loss, with a wavelength inversely related to the bottom slope. A more realistic partially-absorbing bottom proved to have properties very similar to those of the perfectly reflecting bottom.

Accession For

NTIS GRA&I

DTIC TAB

Unannounced

Justification

By

Distribution/

Availability Codes

Avail and/or

Dist Special

A

A Sensitivity Study of the
Parabolic Equation Model to
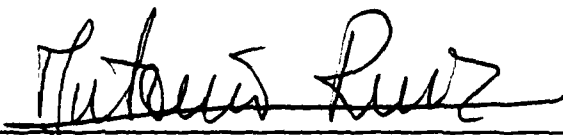Bottom Type and Geometry

by

Antonio Ruiz Cañavate
Lieutenant, Spanish Navy

Submitted in partial fulfillment of the
requirements for the degree of

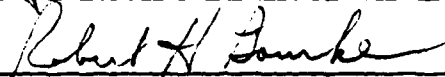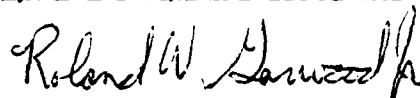MASTER OF SCIENCE IN OCEANOGRAPHY
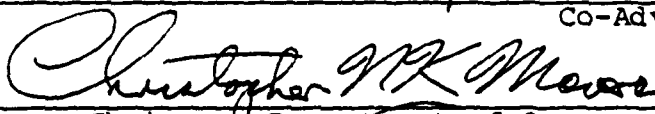
from the
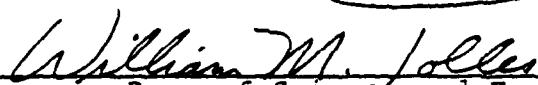
NAVAL POSTGRADUATE SCHOOL

March 1981

Author _____

Approved by: _____

_____ Co-Advisor

_____

_____ Co-Advisor

_____

Chairman, Department of Oceanography

_____

Dean of Science and Engineering

3

## ABSTRACT

The effect of several types of flat and sloping bottom configurations and bottom geophysical properties are studied using the parabolic equation model in a sensitivity analysis to determine the importance of such environmental parameters. Low frequency and fixed source and receiver depths have been used along with a single sound speed profile, in both deep and shallow water cases. For a fully absorbing bottom, only the refracted energy paths remain, making the model insensitive to the bottom geometry. For a perfectly reflecting bottom, both the refracted and the reflected paths were present in deep water tests, and only the reflected paths in shallow water cases. For the sloping bottom geometries a periodic interference pattern was found in transmission loss, with a wavelength inversely related to the bottom slope. A more realistic partially-absorbing bottom proved to have properties very similar to those of the perfectly reflecting bottom.

4

# TABLE OF CONTENTS

# I.  INTRODUCTION

The usually accepted procedure for the evaluation of
acoustic field measurements has been to compare observed
propagation loss with an analytical expression for propaga-
tion loss versus distance from the acoustic source.

Not much is known beyond these kinds of semiempirical
expressions for transmissions losses.  This is especially
true at low frequencies.  The type or kind of bottom from a
geophysical point of view has not been included, except for
some shallow-water, high-frequency cases in a very limited
sense with coefficients that may account for the "strength"
of the bottom.  Not much work has been published on acoustic
transmission with sloping or range-dependent bottom geometry.
Northrop et al. (1968) comment on the effect of variations
in the observed signal level received from shots fired over
the edge of the continental shelf, attributing these varia-
tions to changes in bottom slope, bottom material, and water
depth in the source area.  Another study analyzing the influ-
ence of sound speed fluctuations of a CW signal in an ocean
with a uniformly sloping bottom has been made by Hamilton
et al. (1979).  One of the reasons for considering the uni-
form slope was that bottom variation had been excluded from
most previous published studies.

The effect of a sloping bottom on propagation could be
divided into two categories:  purely geometric effects

(iso-velocity case) and refraction effects caused by a
variable sound speed. In the first category, perhaps the
most apparent effects are the funnel effect and its inverse,
the megaphone effect (Fig. 1). These effects are simply
changes in acoustic energy density due to changes in water
cross sectional area at any fixed range. This effect is
maximized in the case of a perfectly reflecting bottom
(Hawker et al., 1976). Another interesting effect found in
the sloping bottom context has been the slope enhancement
effect (Hawker et al., 1976). Several sets of experimental
data were examined for slope effects showing a strong slope
enhancement feature for all receiver depths. The enhancement
increased with decreasing depth and began approximately 40%
up the slope, peaking at the top of the slope.

With the introduction of the parabolic equation (PE)
model in acoustics, an accurate description of the acoustic
field is now available for many of the actual situations that
can be found in underwater acoustics.

Possibly one of the most complete numerical models for
the PE equations is that of Brock (1978). This model treats
the acoustic propagation phenomenon from a deep water point
of view.

With the incorporation of the bottom into the PE algor-
itehm (Stieglitz et al., 1979), it is possible to simulate
practically all kinds of environments for either shallow or
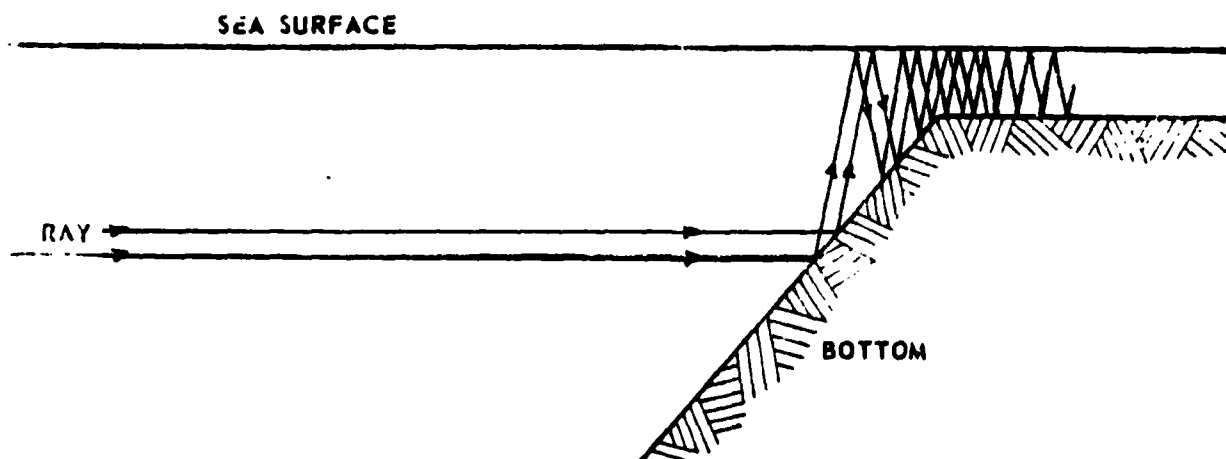deep water cases.

Figure 1. Funnel effect

This study is intended to be a preliminary sensitivity
test for bottom-related model parameters. The scope of the
present work is to explore the importance of the oceanic
bottom in the transmission of sound from two points of
view: type and geometry. Under the first, three kinds
of bottoms that, in theory, span all the possible situations
were studied. Under the second, several different bottom
geometries were modeled.

## II. THE PARABOLIC EQUATION (PE) MODEL

### A. THE ALGORITHM

The parabolic equation (PE) model is one of the latest
major developments in the field of acoustic modeling.  It
was introduced into underwater acoustics by Tappert and
Hardin in 1972, and the first paper showing practical re-
sults of applying the method to underwater sound propagation
was published by Spofford(1973).  Since then, the PE method
has been tested and evaluated at various laboratories,
especially in the United States, and several variants of
the numerical model have been developed.

An outline of the derivation of the PE equation is de-
scribed below, showing the steps and approximations employed.

Basically, the parabolic equation involves replacing the
elliptic reduced wave equation (the Helmholtz equation) with
a parabolic differential equation.

Starting with the Helmholtz equation,

$$\nabla^2 \phi + k^2 \phi = 0 \tag{1}$$

where:

$\nabla^2$ = Laplacian operator,

$\phi$ = velocity potential,

and

$k$ = Wave number $(w/c)$.

Defining a reference sound speed $c_0$ gives

$$k_0 = \text{reference wave number} = w/c_0, \text{ and}$$

$$n = \text{refraction index} = c_0/c.$$

This results in the Helmholtz equation in terms of the reference sound speed:

$$\nabla^2 \phi + k_0^2 n^2 \phi = 0 . \tag{2}$$

Assuming cylindrically symmetric propagation, gives

$$\frac{\partial^2 \phi}{\partial r^2} + \frac{1}{r} \frac{\partial \phi}{\partial r} + \frac{\partial^2 \phi}{\partial z^2} + k_0^2 n^2 \phi = 0 . \tag{3}$$

With the separation of variables,

$$\phi = \psi(r,z) \cdot S(r) \tag{4}$$

equation (3) becomes

$$\psi \left[ \frac{\partial^2 S}{\partial r^2} + \frac{1}{r} \frac{\partial S}{\partial r} \right] + S \cdot \left[ \frac{\partial^2 \psi}{\partial r^2} + \frac{\partial^2 \psi}{\partial z^2} \right.$$

$$\left. + \left( \frac{1}{r} + \frac{2}{S} \frac{\partial S}{\partial r} \right) \cdot \frac{\partial \psi}{\partial r} + k_0^2 n^2 \psi \right] = 0 . \tag{5}$$

If we set the terms in the first bracket equal to $(-Sk_0^2)$, and the terms in the second bracket equal to $(\psi k_0^2)$, the equation can be separated into two differential equations:

$$\frac{\partial^2 S}{\partial r^2} + \frac{1}{r} \frac{\partial S}{\partial r} + k_0^2 S = 0 \tag{6}$$

and

$$\frac{\partial^2 \psi}{\partial r^2} + \frac{\partial^2 \psi}{\partial z^2} + \left(\frac{1}{r} + \frac{2}{S} \cdot \frac{\partial S}{\partial r}\right) \cdot \frac{\partial \psi}{\partial r} + k_0^2 n^2 \psi - k_0^2 \psi = 0 \qquad (7)$$

Equation (6) is the zero-order Bessel equation, and its solution in terms of outgoing waves is given by the zero-order Hankel function of the first kind:

$$S = H_0^{(1)}(k_0 r) \qquad (8)$$

Introducing the far field approximation,

$$k_0 r \gg 1 \qquad (9)$$

and replacing the Hankel function by its asymptotic value, gives

$$S(r) \simeq \sqrt{2/\pi k_0 r} \; e^{i(k_0 r - \frac{\pi}{4})} . \qquad (10)$$

The variable S can be eliminated from equation (7) using (10):

$$\frac{\partial^2 \psi}{\partial r^2} + \frac{\partial^2 \psi}{\partial z^2} + 2ik_0 \frac{\partial \psi}{\partial r} + k_0^2 (n^2 - 1) \psi = 0 \qquad (11)$$

Next, the small angle approximation is introduced:

$$\frac{\partial^2 \psi}{\partial r^2} \ll 2k_0 \frac{\partial \psi}{\partial r} . \qquad (12)$$

11

The physical meaning of this fundamental approximation in the parabolic equation method is that, if the acoustic field were represented by rays, these would be inclined only at small angles with respect to the horizontal.

This yields the parabolic wave equation:

$$\frac{\partial^2 \psi}{\partial z^2} + 2ik_0 \frac{\partial \psi}{\partial r} + k_0^2 (n^2 - 1)\psi = 0 . \tag{13}$$

## B. THE NUMERICAL MODEL

The parabolic equation model is an acoustic wave model designed for the computation of acoustic transmission loss as a function of range and depth in range-dependent ocean environments.

The elliptic-reduced wave equation, Eq. (1), is approximated by a parabolic differential equation, Eq. (13), that can be numerically integrated by marching the solution forward in range, using the Tappert-Hardin split-step Fourier algorithm (Brock, 1978).

The parabolic wave equation includes diffraction and all other full-wave effects as well as the possibility of dealing with range dependent environments. The numerical algorithm has exponential accuracy in depth, second order accuracy in range and is unconditionally stable. As the solution is marched forward in range, the entire range and depth dependent acoustic field is computed.

The model assumes a flat pressure release ocean surface and a vanishing field at the maximum depth of the finite

12

Fourier transform. That is, an artificial horizontal bottom boundary below the physical bottom is introduced, and the field is assumed to satisfy a zero boundary condition there. This was required as a periodic boundary condition in z because of the use of the finite Fourier Transform in the split-step algorithm. A pseudo radiation condition is introduced at the water-bottom interface by smoothly attenuating the field.

Since the computing time increases as frequency increases, the model is primarily useful for predicting low-frequency acoustic propagation of energy along water-borne or shallow angle bottom-bounce paths.

On the other hand, the treatment of paths which intersect the ocean bottom has been a major limitation of the algorithm ever since it was first introduced by Tappert and Hardin. The two reasons for this limitation are inherent in the numerical scheme. First, the narrow-band (angular aperture) approximation employed in deriving the PE equation produces an intolerable phase-error for the steep angles associated with the bottom-interacting paths. Second, the stringent requirements of the discrete Fast Fourier Transform (FFT) permit only "smooth" transitions in both the sound speed profile and the attenuation of the pressure field. This makes the implementation of geophysical models for the ocean bottom difficult unless the characteristics of smooth transition are met.

13

With the incorporation of a rather general ocean bottom model (Stieglitz et al., 1979), it is possible, by applying certain restrictions to the bottom-interacting field of the PE model, to realize a workable ocean bottom model. There are two alternative ways to characterize the ocean bottom: by specification of both the sound-speed variation ard attenuation in the bottom or by specification of loss versus grazing angle. The first alternative is directed towards a geophysical description of the bottom while the second lends itself to a simple bottom-reflected ray analog.

There are three specific restrictions to the above specifications, however. First, all bottom sound-speed and attenuation profiles must be point-continuous at the bottom-water interface. Second, the maximum bottom grazing angle considered is approximately 33 degrees. Beyond this angle, independent of what is specified, the attenuation of the field is assumed to be infinite. Finally, the minimum range interval over which a set of bottom specifications, such as grazing angle vs. loss, are held constant should equate to the range-cycle or periodicity of the maximum range ray.

Nevertheless, even with these limitations, the class of bottom characteristics which can be realized under these restrictions is large enough to cover most of the more generally accepted bottom models.

C. COMPARISONS WITH OTHER MODELS

Although there are many models based on the parabolic equation method, the only significant differences among them

14

are the numerical solution technique used to solve the
equation (13), the handling of the bottom absorption, and
the treatment of range dependence.

The PE numerical model used in the present work is in-
stalled on the main frame of the W.R. Church Computer Center
at the Naval Postgraduate School. The program is documented
by Brock (1978) and by Stieglitz et al., (1979). An advan-
tage over other PE models is the possibility to choose
either of the two alternative bottom characterizations des-
cribed previously. The loss versus grazing angle method is
a particularly important option for problems of naval warfare
interest.

Lee and Papadakis (1980) applied an improved numerical
technique to solve the parabolic equation. They used the
numerical ordinary differential equation methods combined
with a predictor-corrector procedure. Apparently, this new
procedure has some advantages over the split-step Fourier
algorithm developed by Tappert and Hardin and later imple-
mented by Brock (1978) and Jensen and Kroll (1975).

In implementing the split-step algorithm described previ-
ously, the second order differential operator in z, in
Eq. (13), is represented by the inverse transform of its
Fourier transform. The resulting equation is transformed
into a system of ordinary differential equations by approxi-
mating the forward and inverse Fourier transform by the Fast
Fourier Transform (FFT) numerical algorithm in z. When the

15

index of refraction has a large change across the bottom interface, there is the possibility of a large error. This error is proportional to the square of the z-derivative of the index of refraction multiplied by the cube of the range step. This error is avoided by using a very small range step, but this may result in unacceptably long computation times for long range calculations. Brock's model (1978), incorporates a warning if the predicted range step is less than the acoustic wavelength. Five such warnings terminate the calculation.

Lee and Papadakis (1980) approximate the second-order differential operator in z by a central finite difference operator which converts the partial differential equation into a system of first order ordinary differential equations. The system is solved numerically by nonlinear multistep methods. This procedure avoids the introduction of an artificial horizontal bottom boundary below the physical bottom. This was required because of the use of the finite Fourier Transform in the split-step algorithm as a periodic boundary condition in z.

The arbitrary boundary condition at the bottom is incorporated into the system of first order ordinary differential equations, treating the bottom boundary condition realistically.

Among the currently working PE models in different centers and laboratories, special mention is made of the SACLANTCEN parabolic equation model (PAREQ) (Jensen and

Kuperman, 1979; Jensen and Martinelli, 1980). This model is essentially a shallow-water version of the Brock model (Brock, 1978) and has been compared successfully with other non-PE models for different environmental conditions.

Even without having the useful alternative characterizations of the bottom that are possible in the model used here, the PAREQ program adds some subroutines, mainly related to output options, such as a routine for creating smoothed propagation loss curves and contour programs for use either in demand or batch modes. This makes the PAREQ program especially useful for certain applications. An example is the study of the sound propagation in the ocean with a sloping penetrable bottom (Jensen and Kuperman, 1980) where modal cutoff during upslope propagation in a wedge-shaped ocean was studied using the PAREQ model, taking advantage of the special contouring features. The PAREQ model has been selected for a comparison with the results from the PE model used here. Three typical cases were compared: One deep-water case, one shallow-water case and an upslope propagation case. The comparisons were sufficiently good to warrant use of the model to study more complicated propagation phenomena.

In the following section, a general description of the model input parameters is presented along with the results achieved and the conclusions that may be drawn.

## III.  TREATMENT OF DATA AND ANALYSIS OF RESULTS

Before discussing the PE model results, it is convenient
to list the main parameters employed in the tests.

Bottom.  Three different types of bottom were studied.
Two of them were limiting situations.  The first is a per-
fectly reflecting bottom for which there is no attenuation
and the sound is not transmitted but is entirely reflected
at the water-bottom interface.  The other limiting situation
is that of a fully absorbing bottom in which all the inci-
dent energy is absorbed.  Finally there is a third type of
bottom resembling more realistic conditions.  This latter
type simulates results from a compilation of low frec   icy
measurements of bottom loss.  These situations were examined
in order to establish the limits of the behavior of the
energy in normal acoustic propagation for each case.

With respect to the geometry of the bottom, three differ-
ent cases were examined:  Flat, sloping, and combinations
of these two types of bottom configurations, termed a "mixed
bottom".

For simplification, it is useful to introduce some short-
hand notation:

F       means flat.

SL=1    means upslope of 1°.

SL=2    means upslope of 2°.

--------------------------------

18

MIXF1     mixed bottom:  upslope of 1° (0-25 nm) and
          flat (25-50 nm).

MIXF2     mixed bottom:  upslope of 2° (0-25 nm) and
          flat (25-50 nm).

------------------------------------

MF1       mixed bottom:  flat (0-30 nm) and upslope of 1°
          (30-50 nm)

------------------------------------

SL=1 MXF   mixed bottom:  flat (0-10 nm), upslope of 1°
           (10-15 nm) and again flat (15-50 nm).

ISL=1 MXF  mixed bottom:  flat (0-10 nm), downslope of 1°
           (10-15 nm) and again flat (15-50 nm).

------------------------------------



F                                           SL=1

MIXF1                            ISL=1MXF

MF1                              SL=1MXF
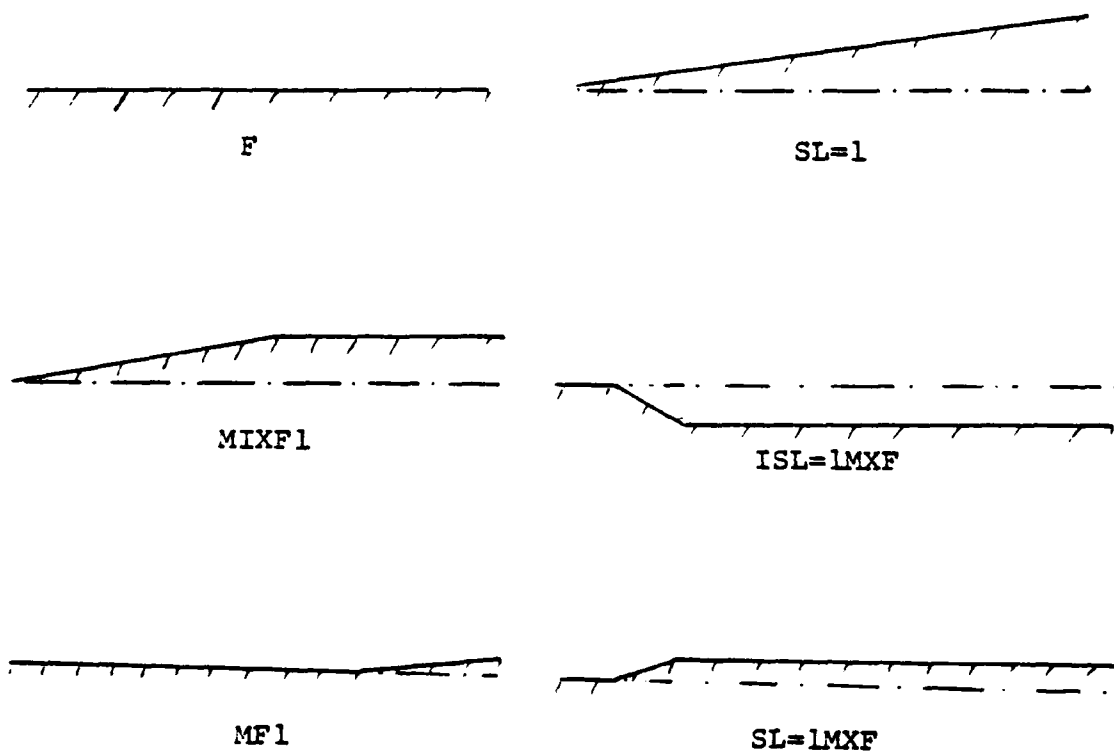
Figure 2.  Bottom Geometries

19

Frequency. Three different frequencies have been employed: 50, 100, and 300 Hz. Due to the constraint of computational time required for the higher frequencies, more cases have been studied at 50 Hz.

Range. For most cases the maximum range used is 50 nm.

Depth. Both deep and shallow water cases were examined with water depths of 12000, 5000, and 1000 feet.

Sound Speed Profiles (SSP). In the tests presented in this work, a single SSP profile documented by Johnson and Norris (1968), Fig. 3, has been employed in order to compare results attributable only to variation of the bottom characteristics, thus avoiding possible "contamination" due to other "weight" parameters related to the SSP.

Source-Receiver Depths. These parameters have been fixed in most of the cases studied, with 300 feet for the receiver, and 50 feet for the source.

Source Beam Size. The half-beam size was 20°.

Spherical Earth Correction. Applied in all the tests.

Volume Attenuation. Omitted.

Horizontal Range Period (for rays in the partially absorbing bottom). This is the distance that the rays travel in the partially absorbing bottom before they again encounter the water. In the model used here this range period is constant for all the rays, and the value used was the default value of 6000 feet. For the fully absorbing bottom cases, the value was 0.

20

Bottom Loss Information. Given by grazing angle (degress) vs. loss (dB).

The information analyzed included transmission loss versus range plots (TL vs. R), tabular listings of TL vs R, and in some selected cases, a contouring of the whole field (TL vs. R and Depth).
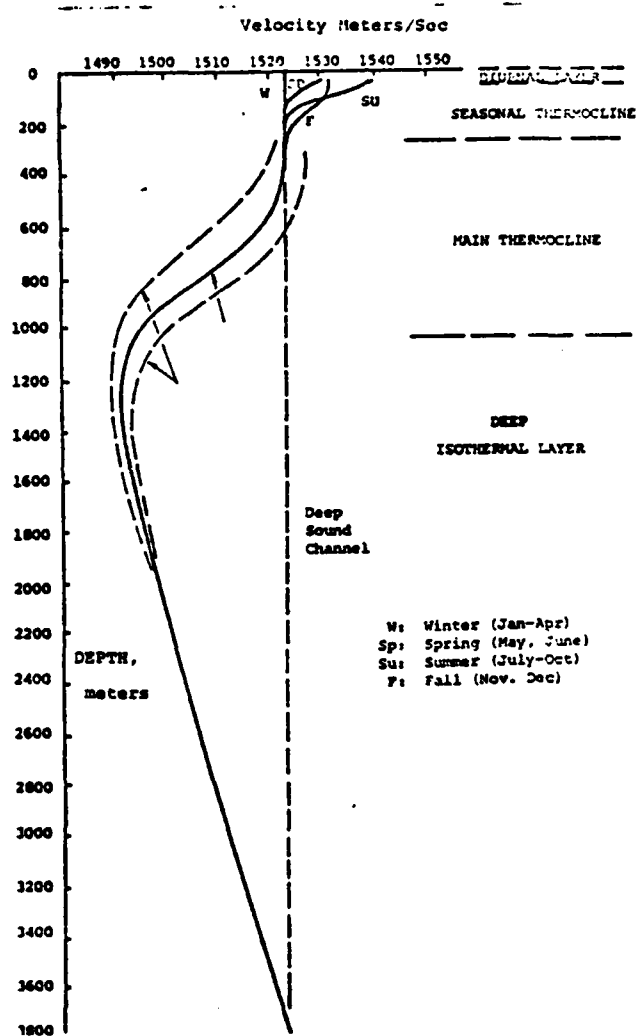


Figure 3. SSP PROF1 (Winter)

## A. FULLY ABSORBING BOTTOM

A series of figures are presented that show the behavior of the acoustic energy in the presence of this type of bottom using several geometries and frequencies.

The remaining parameters are held constant:

Range = 50 nm.

SSP = PROF1.

Source Depth = 50 ft.

Receiver Depth = 300 ft.

Maximum Water Depth = 12000 ft.

The tests are summarized in a tabular format, using the nomenclature above defined for the bottom geometry (Table I).

### Table I

### Fully Absorbing Bottom Tests

| FIGURE | BOTTOM GEOMETRY | FREQUENCY |
|--------|-----------------|-----------|
| 4 | F | 50 |
| 5 | SL=1 | 50 |
| 6 | SL=2 | 50 |
| 7 | F | 100 |
| 8 | SL=1 | 100 |
| 9 | SL=2 | 100 |
| 10 | F | 300 |
| 11 | SL=1 | 300 |
| 12 | SL=2 | 300 |
| 13 | MIXF1 | 50 |
| 14 | MIXF2 | 50 |
| 15 | MIXF3 | 50 |
| 16 | MIXF1 | 100 |
| 17 | MIXF2 | 100 |
| 18 | MIXF1 | 300 |
| 19 | MIXF2 | 300 |
| 20 | MF1 | 50 |

22

An analysis of the figures reveals that for a flat bottom, refractive rays can exist for deep water, and convergence zones are seen at about 40 nm for the three frequencies tested (Figs. 4, 7 and 10). Introducing an upslope of 1° or more causes downward refracted rays to be reflected and therefore absorbed, eliminating the convergence zones (in 50 nm 1° upslope decreases the depth by 5236 ft).

For all three frequencies the slope of the bottom (either flat or upsloping) has no effect on the transmission loss out to ranges where upward refraction begins. There are generally larger signal fluctuations with increased frequency, however.

Summarizing, the convergence zones only appear in the cases where there is absolutely no bottom interaction with refracted rays. All other cases (either an upsloping bottom or a mixed bottom, deep or shallow depth) result in identical TL for each frequency. Thus, no convergence zones can be expected when the change in bottom slope occurs at ranges less than the turning depth of the deeply refracted rays. When the change in slope occurs at ranges beyond the range of the first turning point, as in Fig. 21 where the slope begins at 30 nm from the source and the first turning point occurs at 20 nm, the refracted rays can intersect with the bottom and become absorbed before the second turning point.
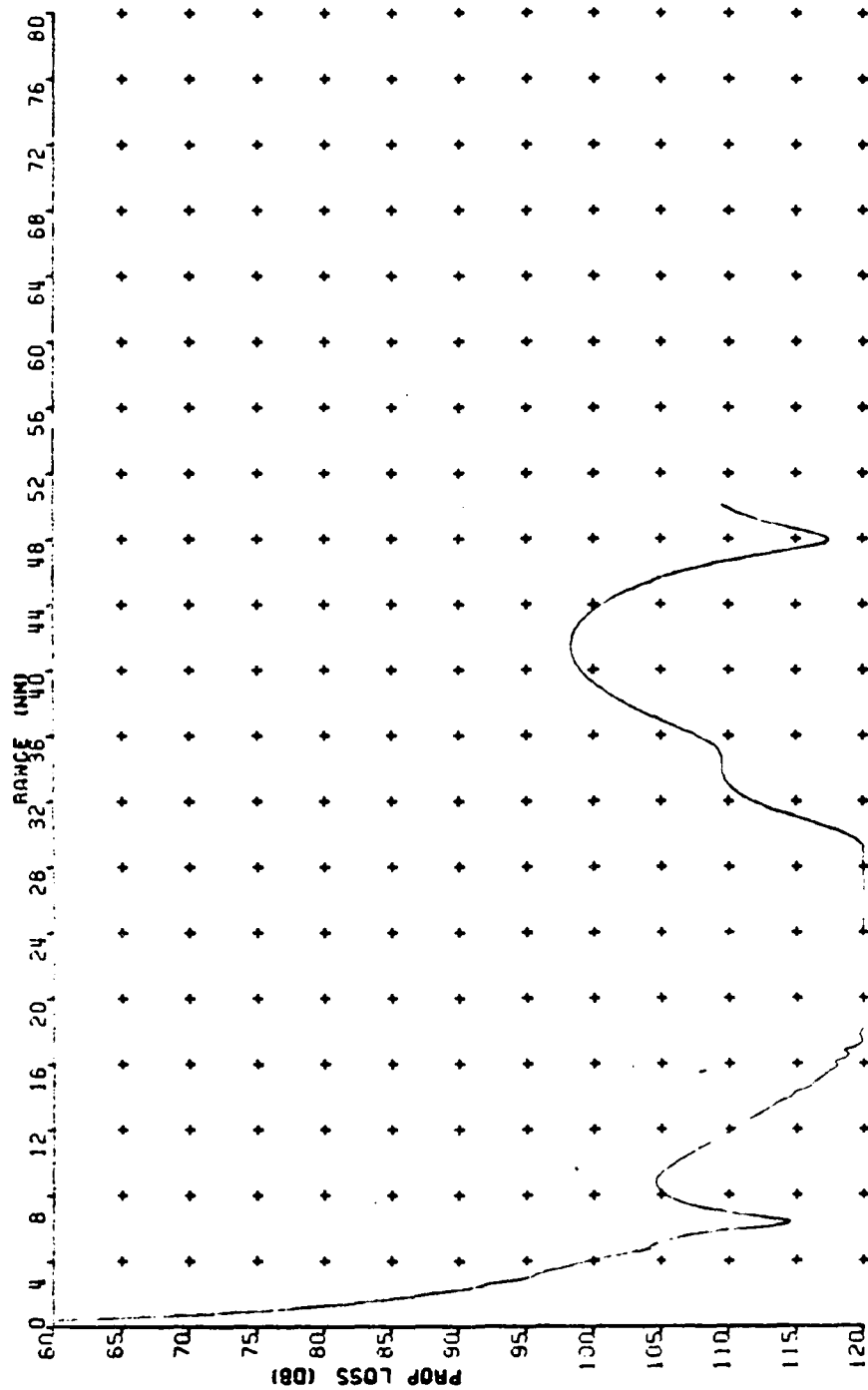
Figure 4.   Fully Absorbing Flat Bottom (50 Hz)
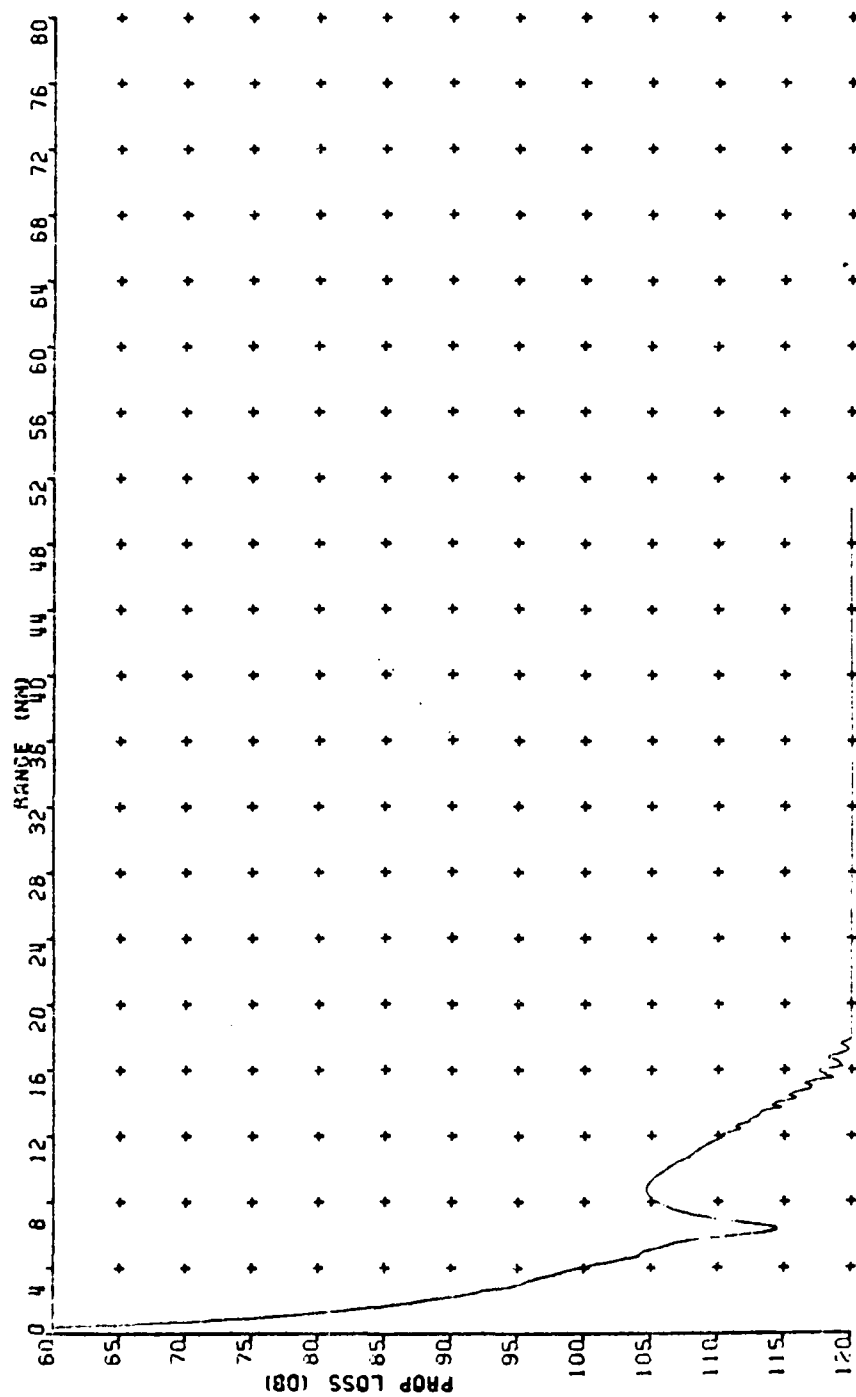
Figure 5. Fully Absorbing SL=1 Bottom (50 Hz)

25
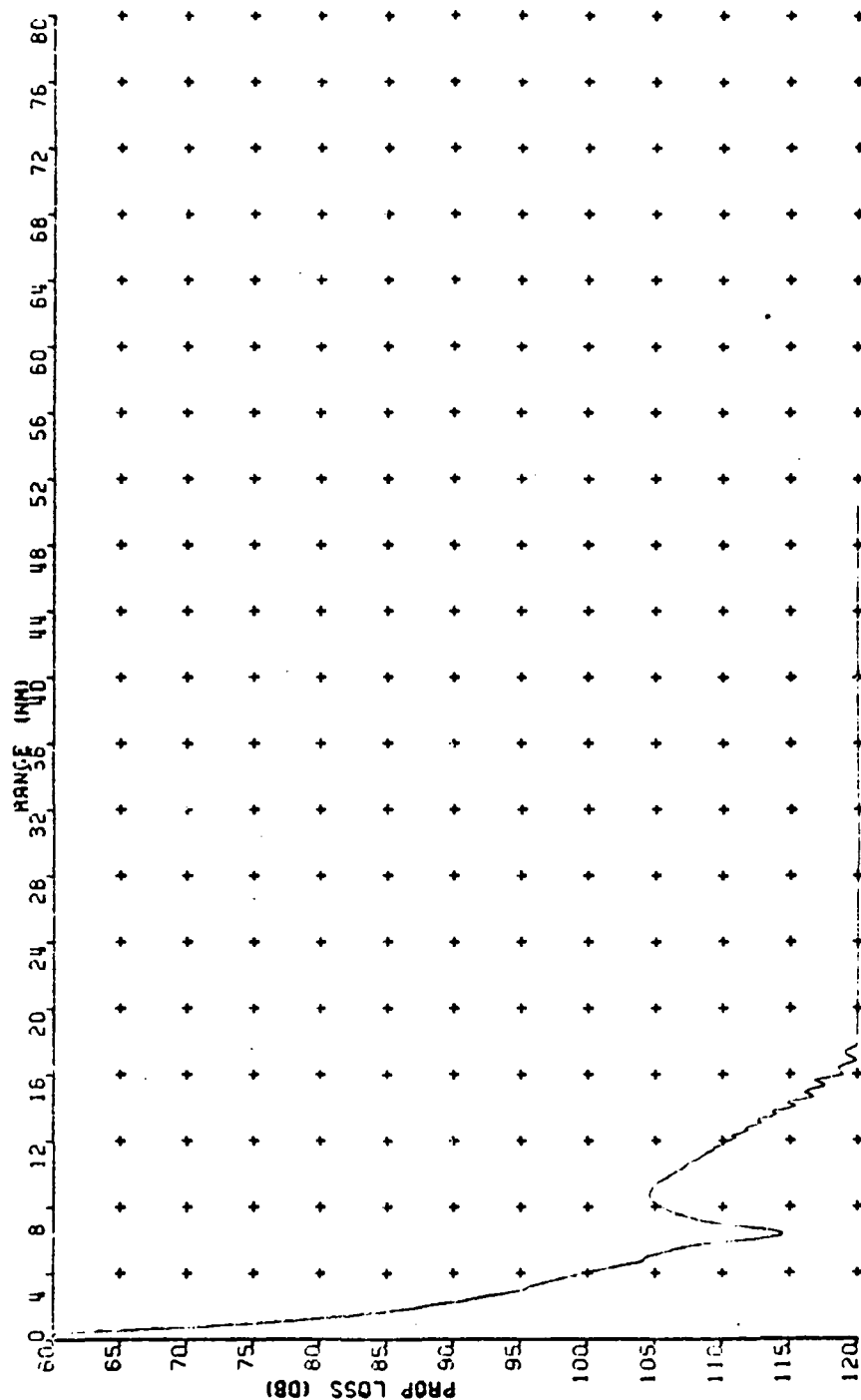
Figure 6. Fully Absorbing SL=2 Bottom (50 Hz)

26
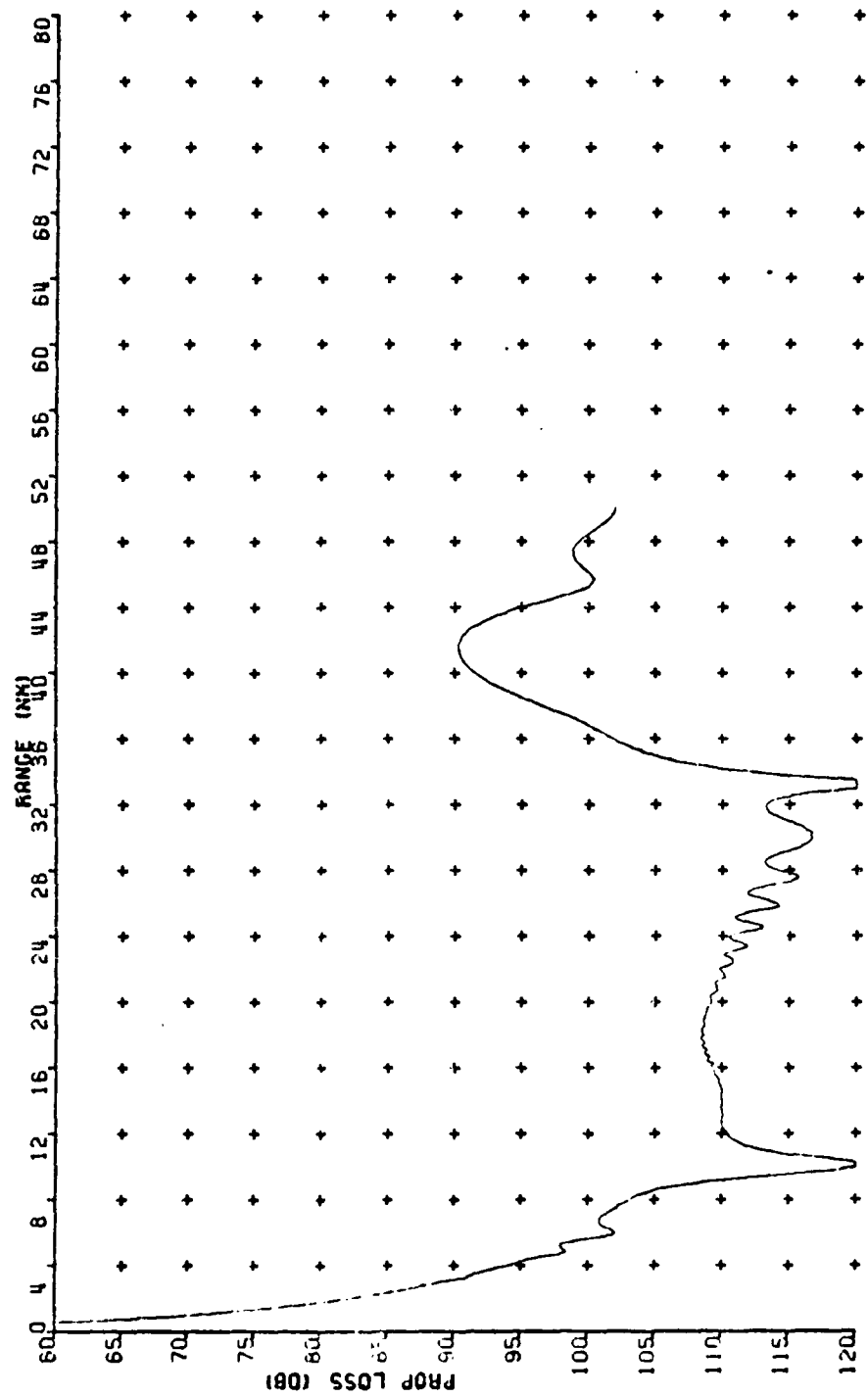
Figure 7.   Fully Absorbing Flat Bottom (100 Hz)

27
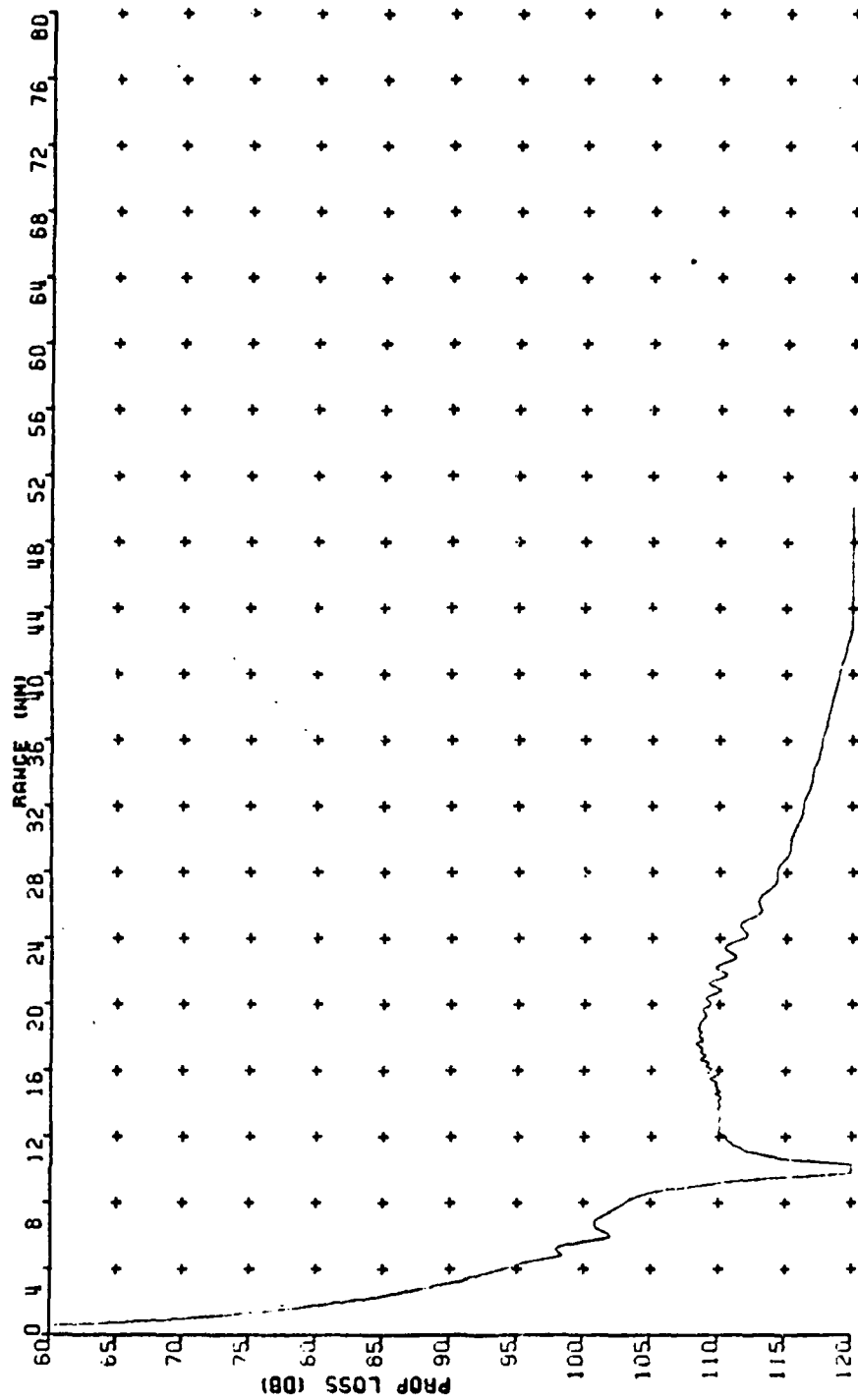
Figure 8. Fully Absorbing SL=1 Bottom (100 Hz)

28
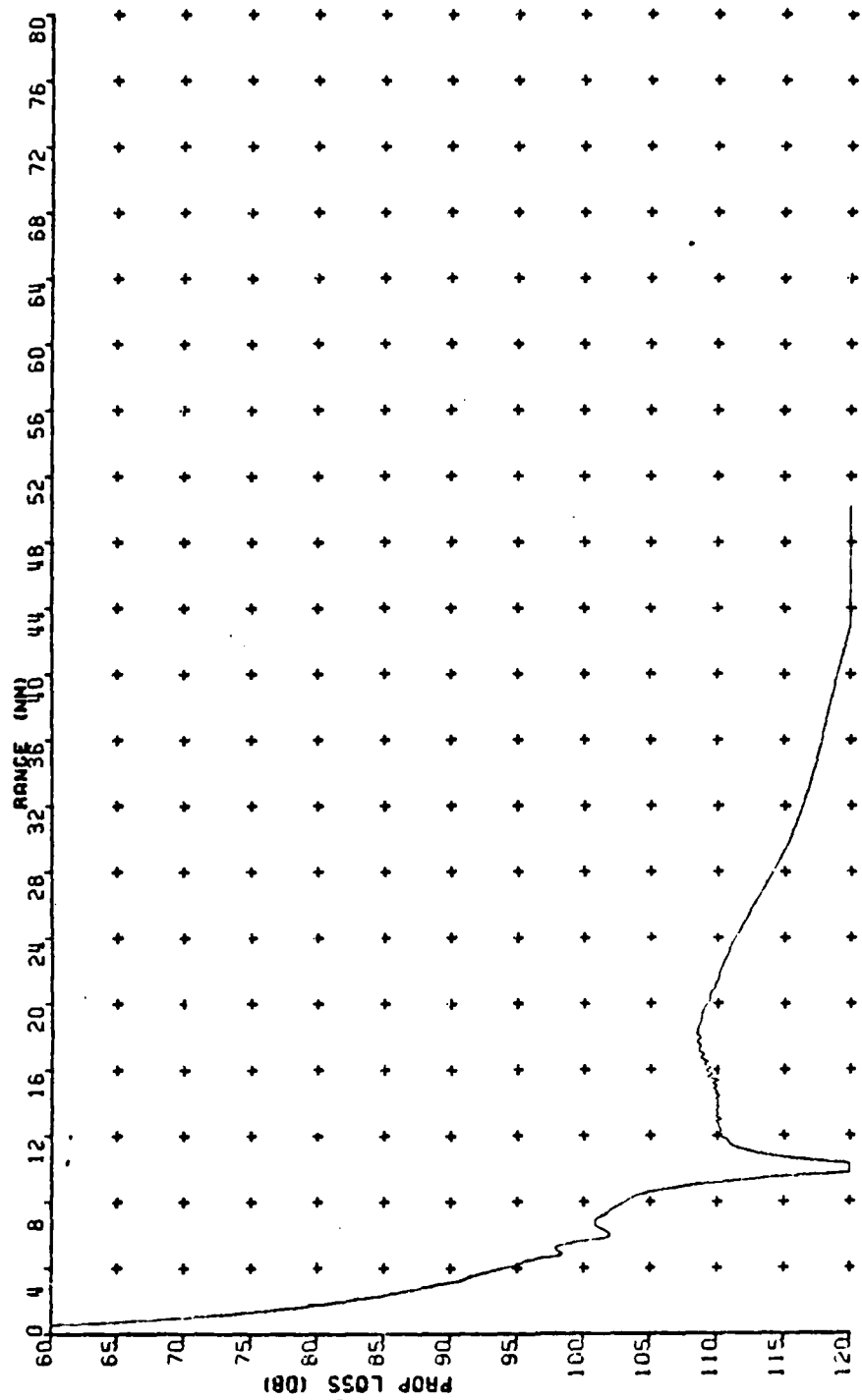
Figure 9. Fully Absorbing SL=2 Bottom (100 Hz)

29
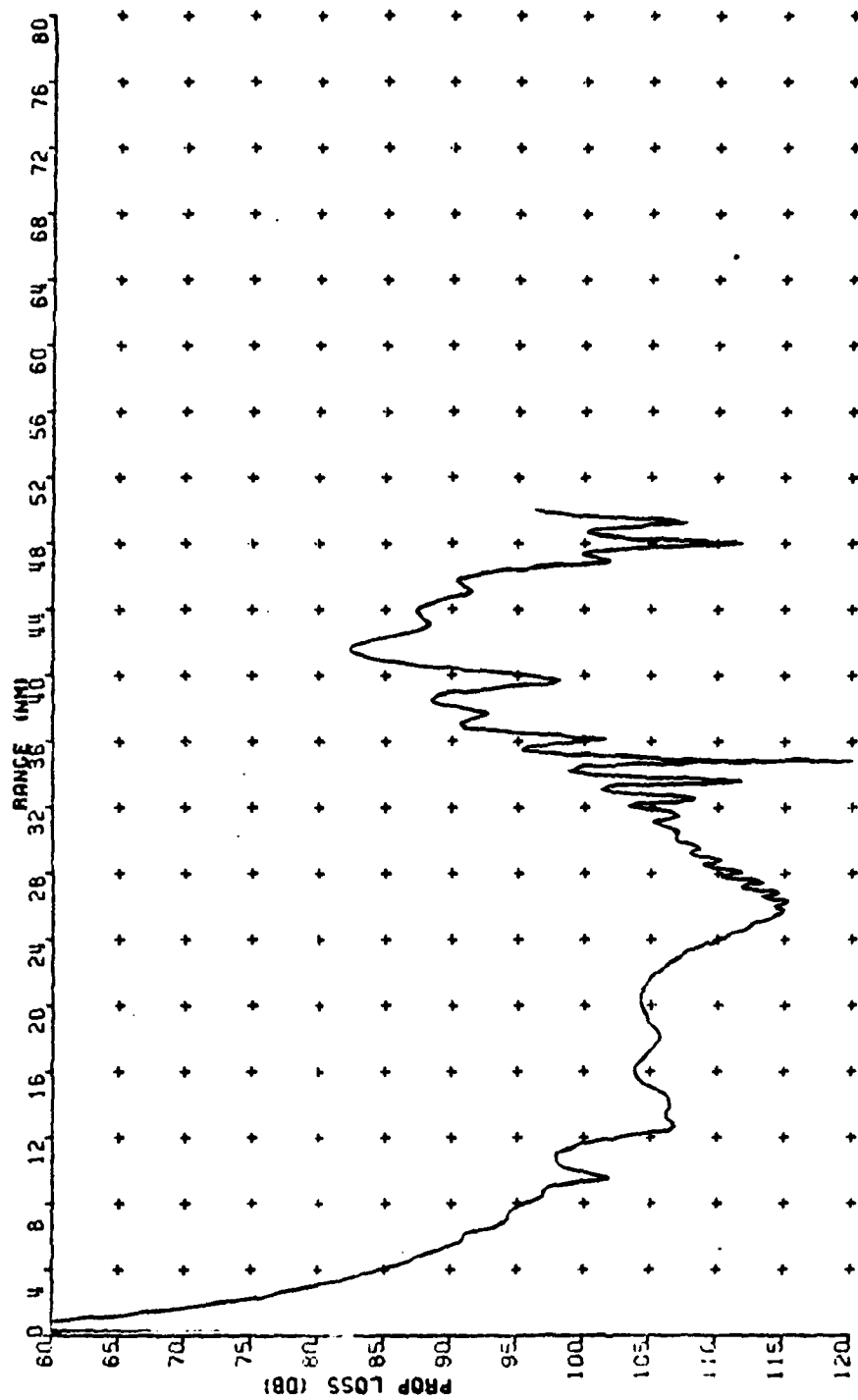
Figure 10.   Fully Absorbing Flat Bottom (300 Hz)
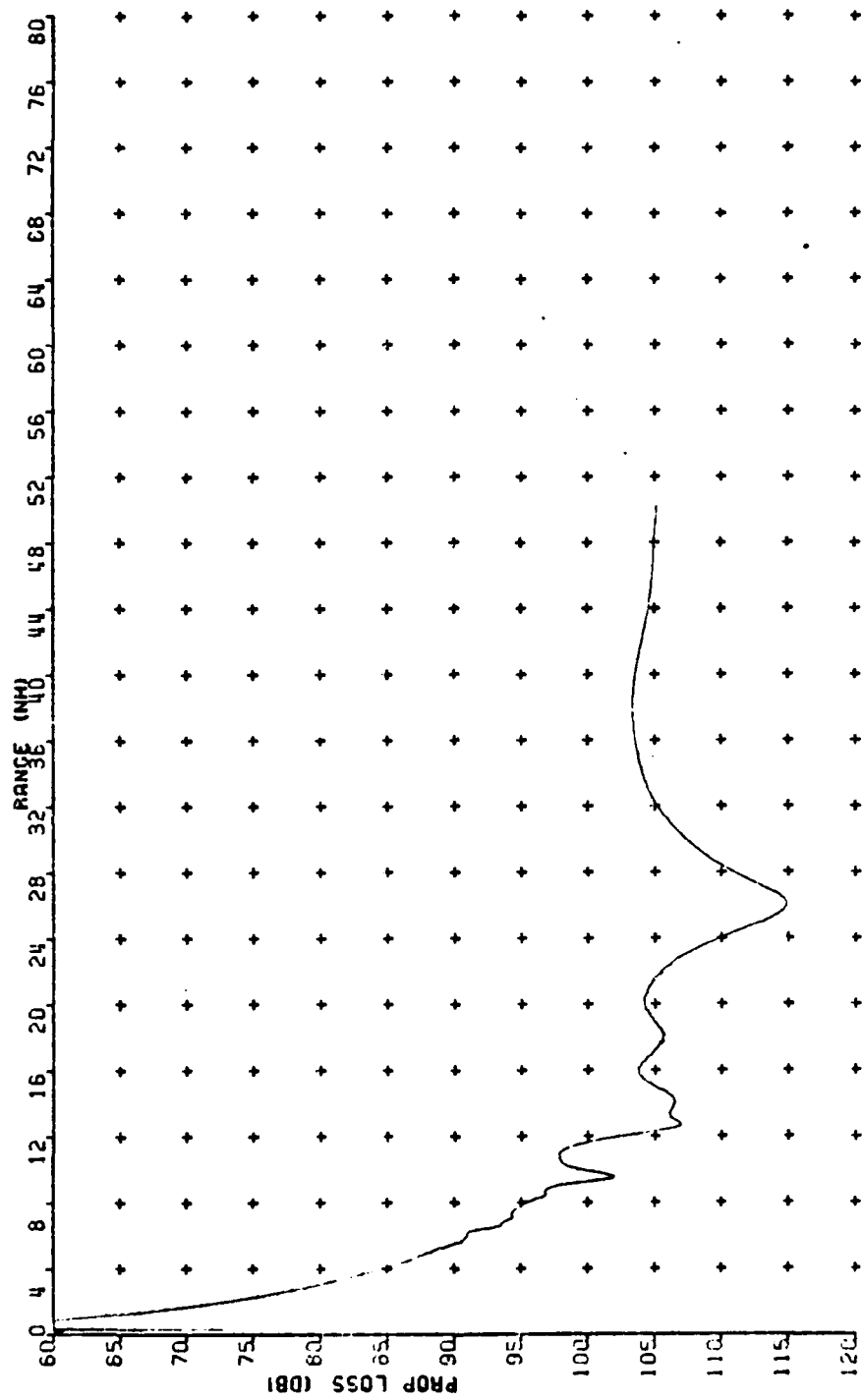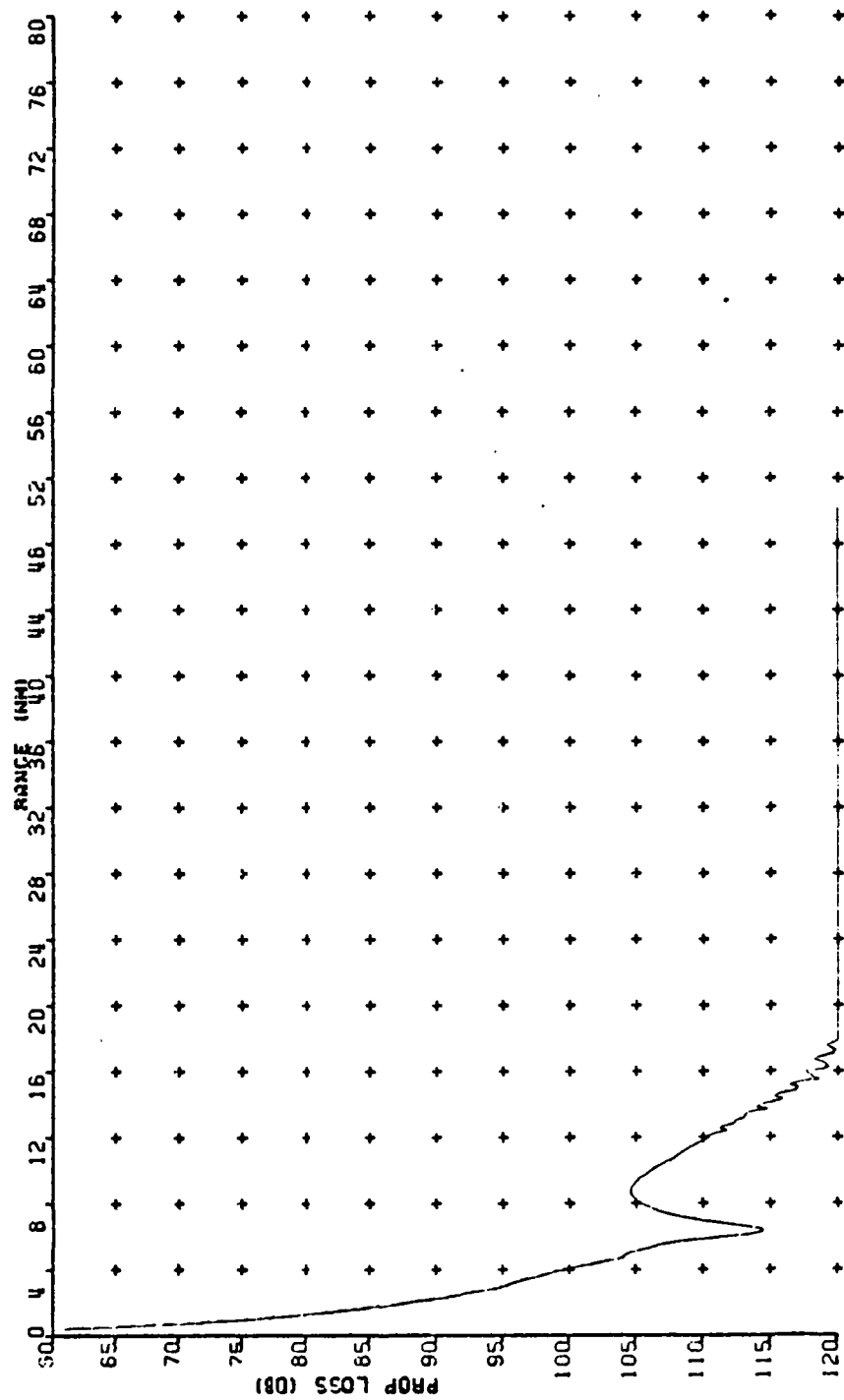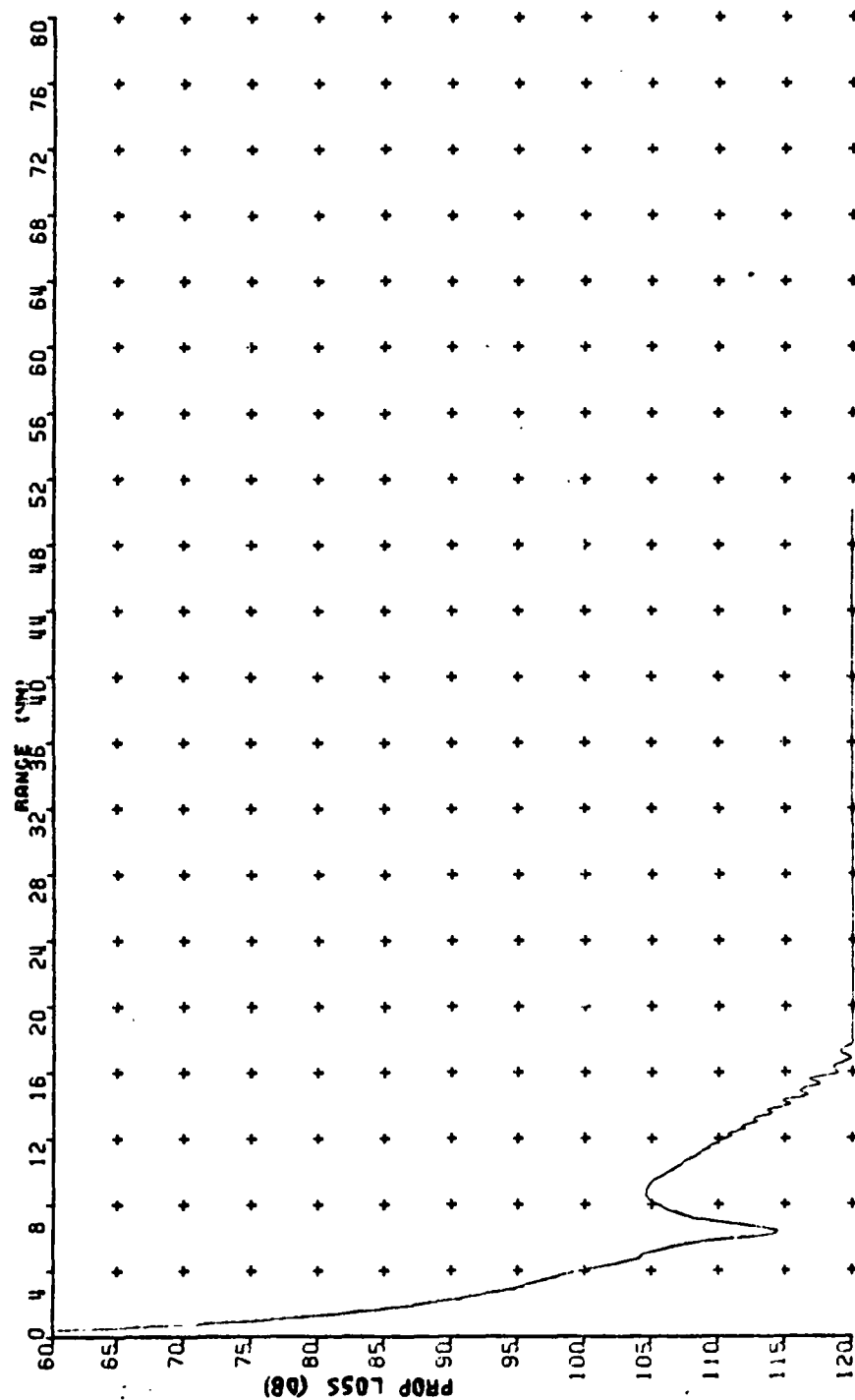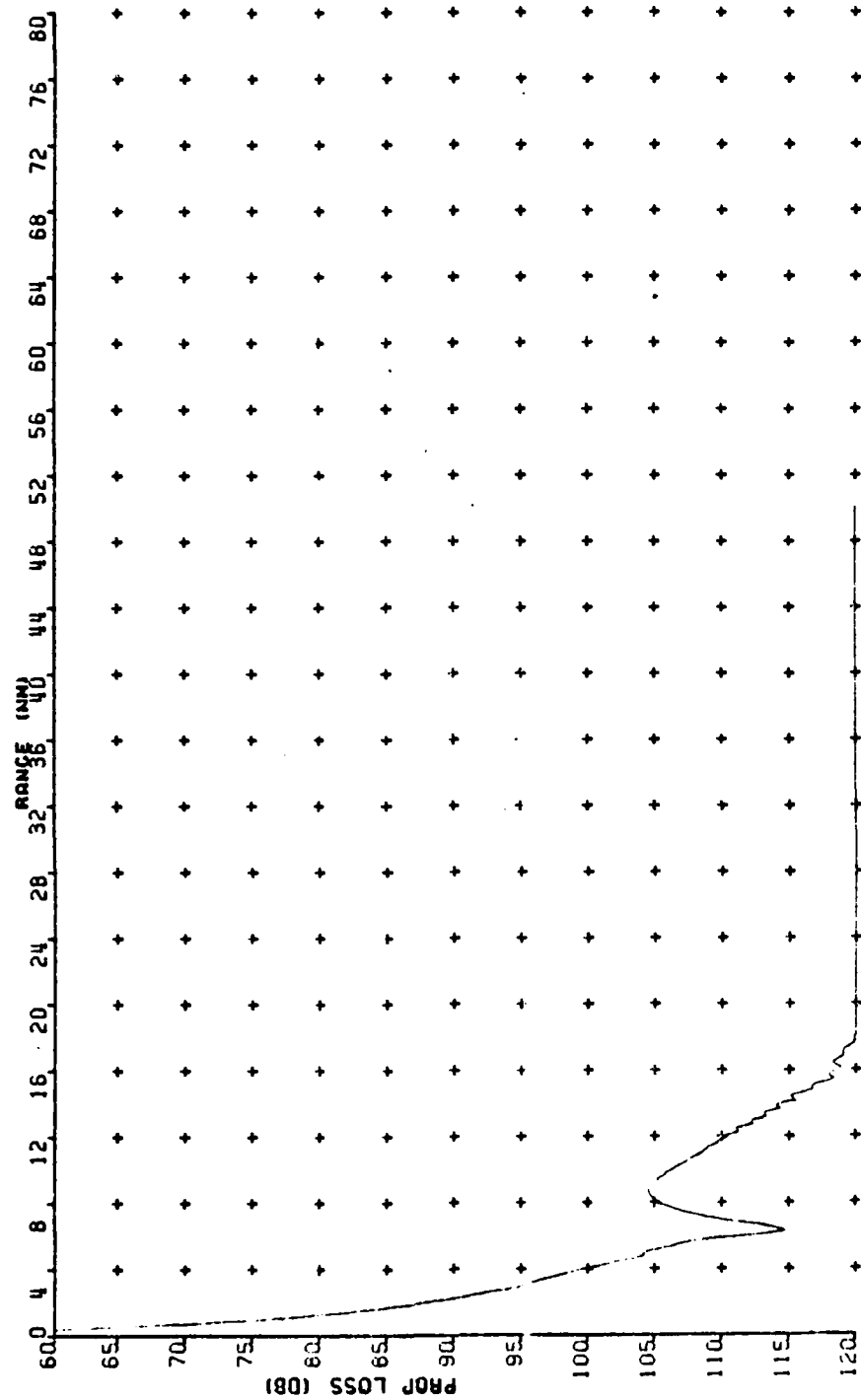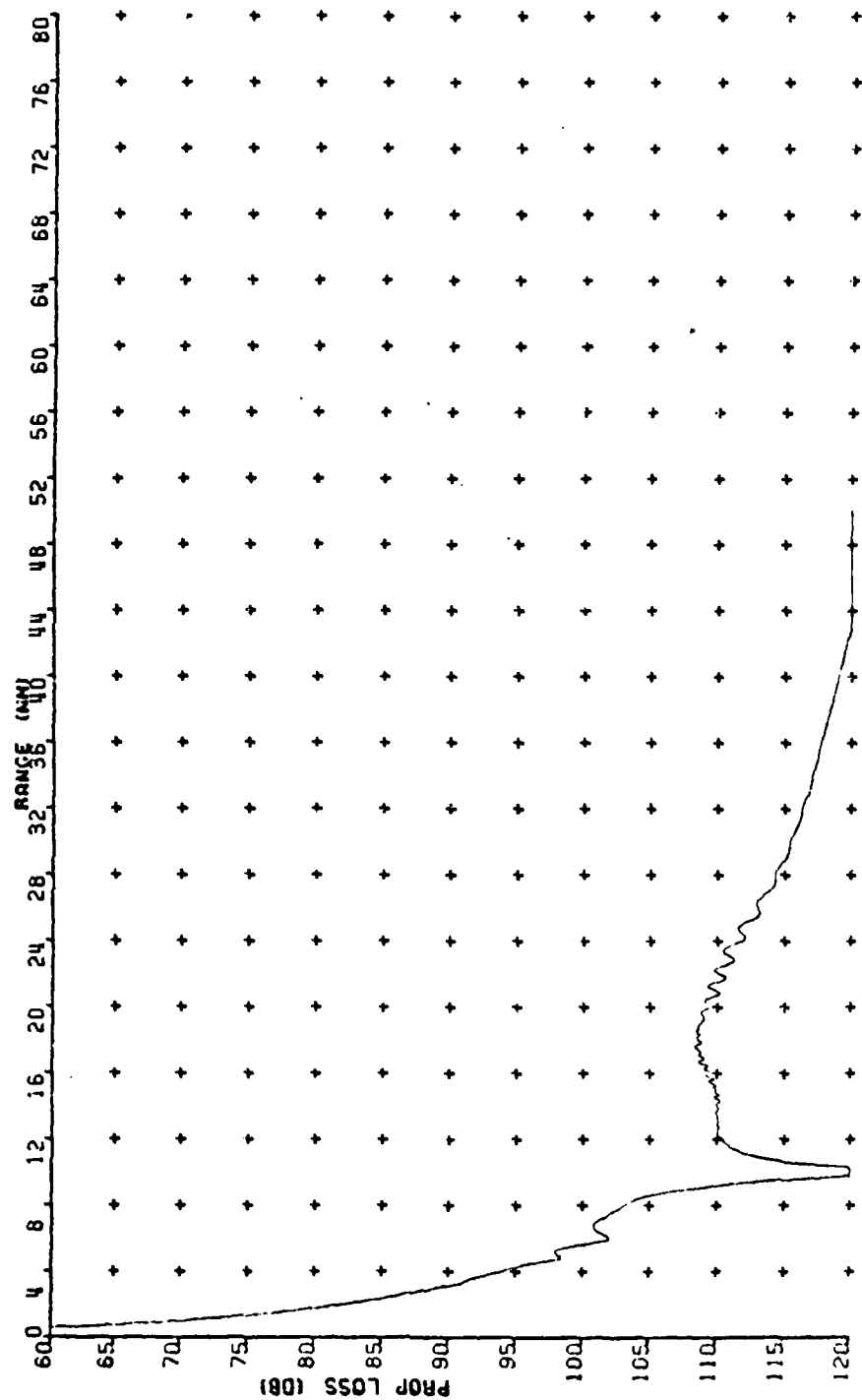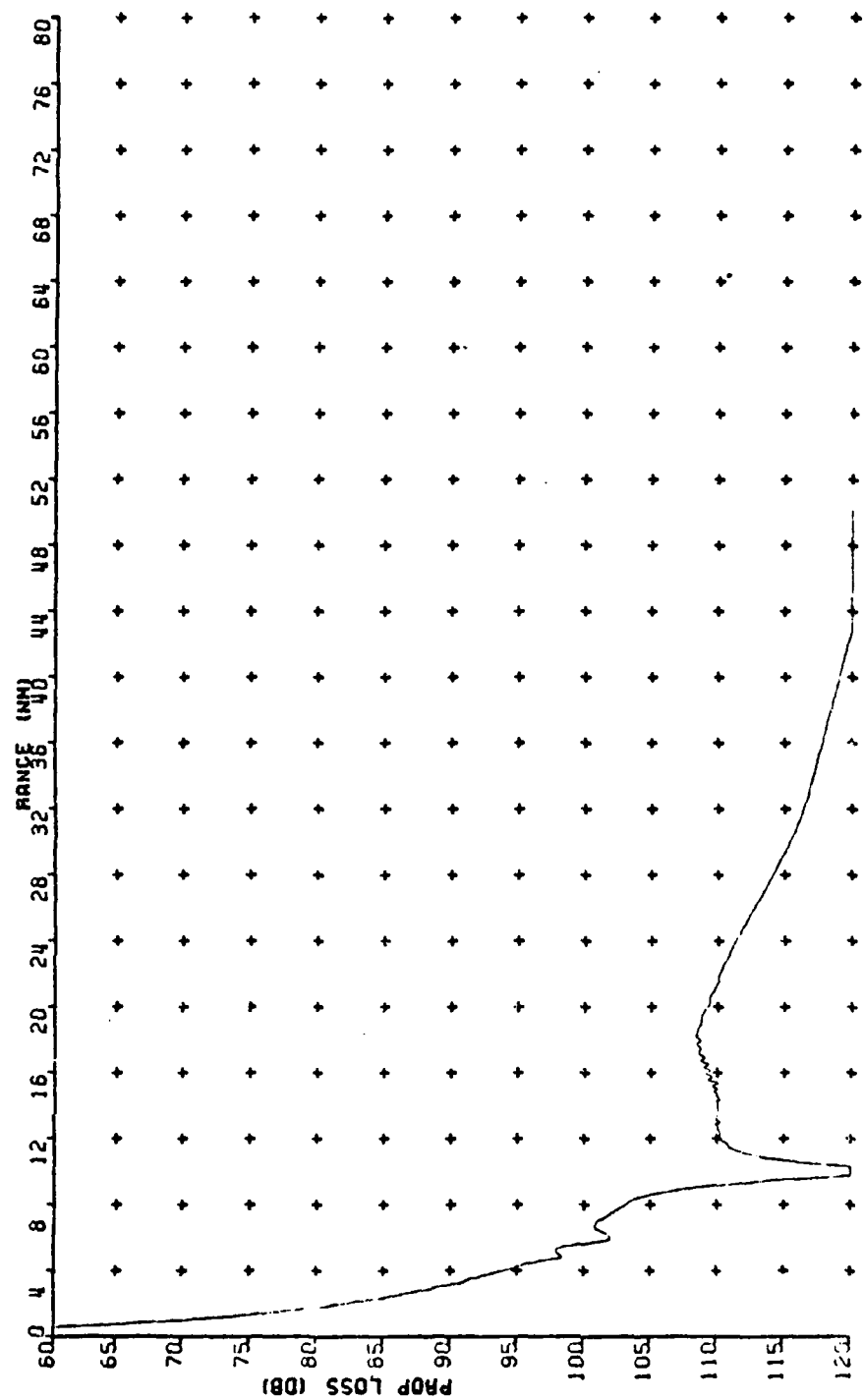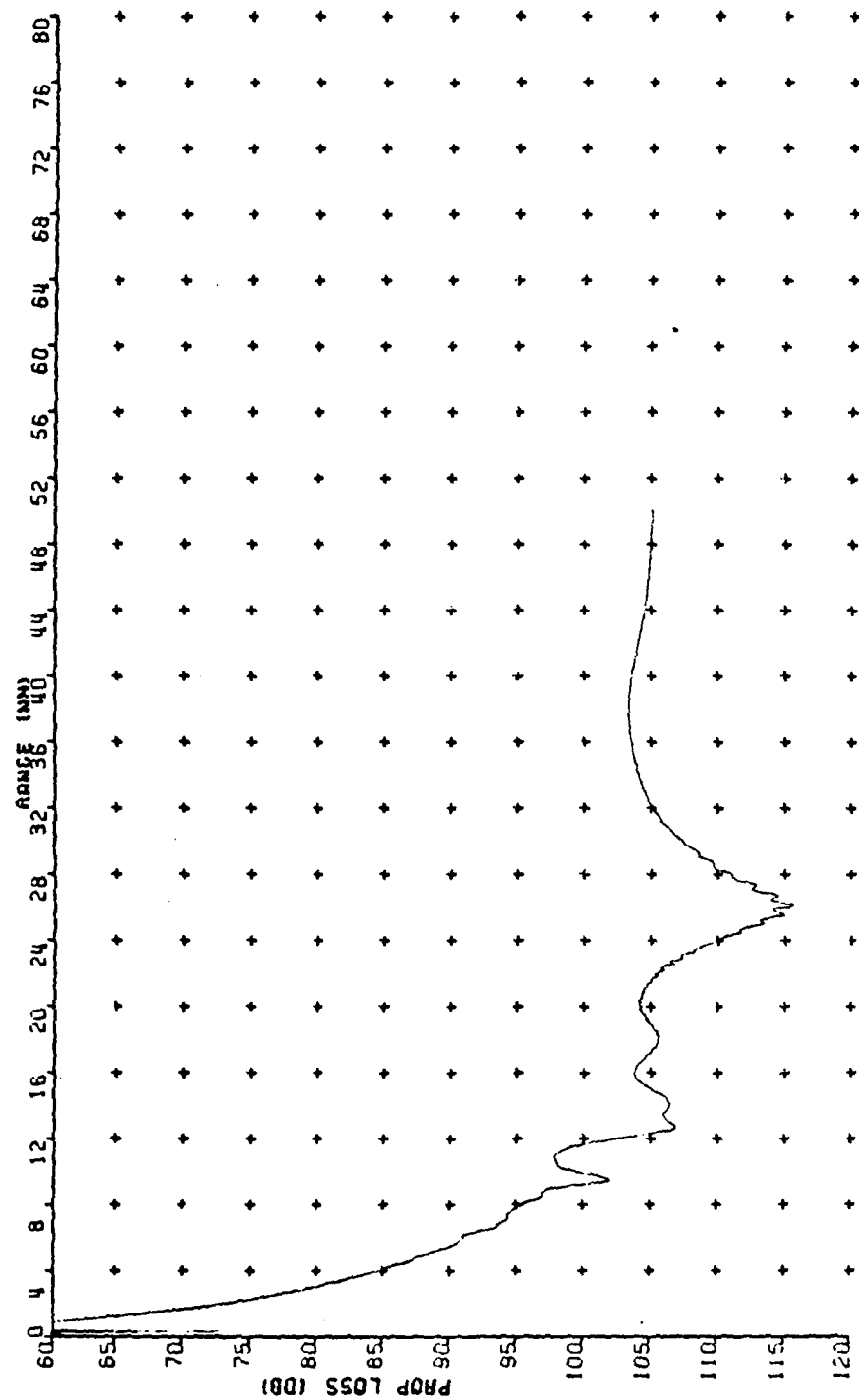
30
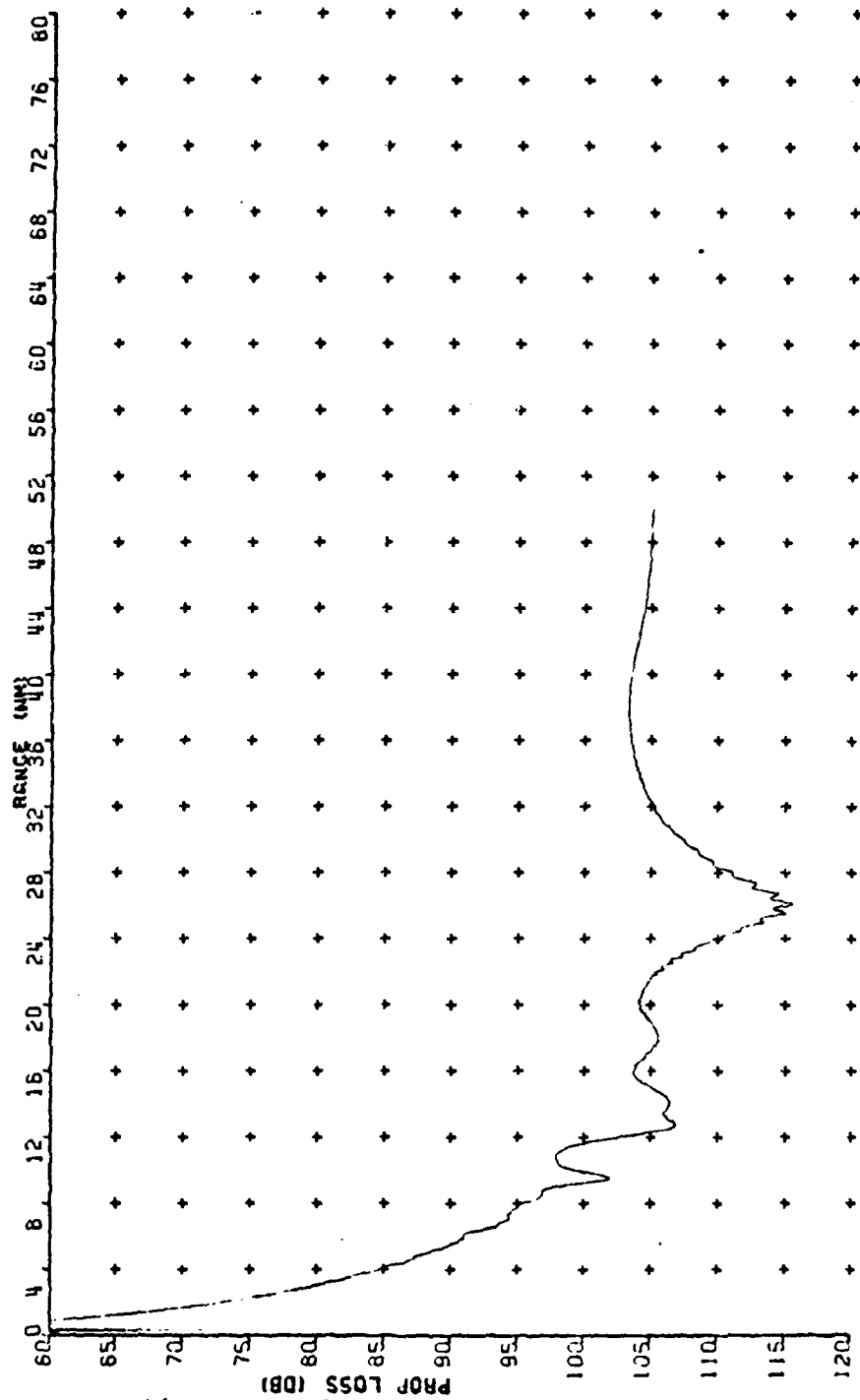
Figure 11.  Fully Absorbing SL=1 Bottom (300 Hz)

31

Figure 12.   Fully Absorbing SL=2 Bottom (300 Hz)

Figure 13.   Fully Absorbing MIXF1 Bottom (50 Hz)
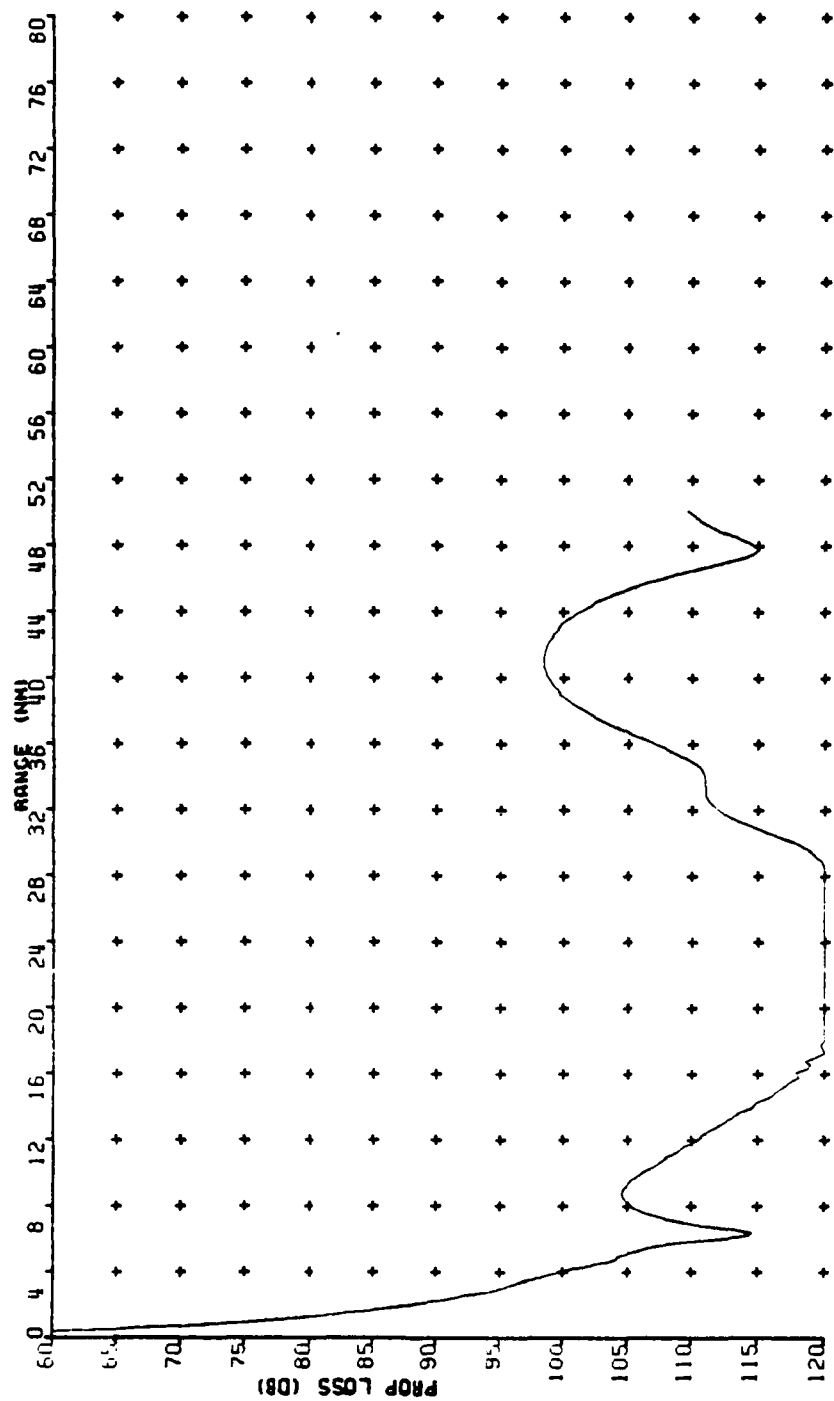
33

Figure 14.   Fully Absorbing MIXF2 Bottom (50 Hz)

34

Figure 15.   Fully Absorbing MIXF3 Bottom (50 Hz)

Figure 16.   Fully Absorbing MIXFl Bottom (100 Hz)
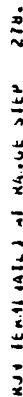
36

Figure 17. Fully Absorbing MIXF2 Bottom (100 Hz)

37

Figure 18.  Fully Absorbing MIXF1 Bottom (300 Hz)

38
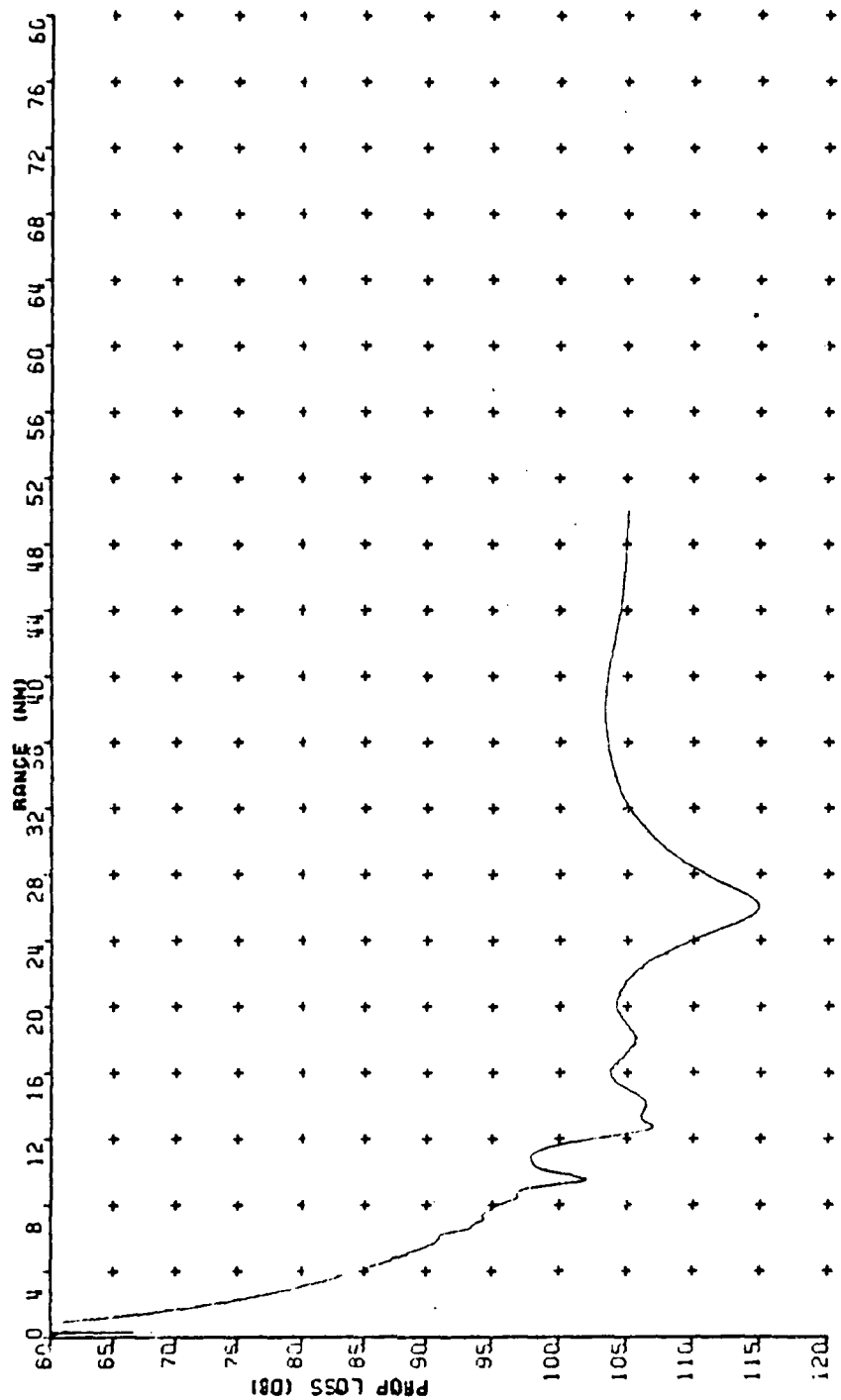
Figure 19.   Fully Absorbing MIXF2 Bottom (300 Hz)

Figure 20. Fully Absorbing and Mixed Bottom (50 Hz)
with Slope at 30 nm from Source

40

Figure 21. Fully Absorbing Mixed Bottom (50 Hz) with
Slope at 30 nm from Source. The symbols
employed are described at the head of the
figure in the TL scale. The bottom is
depicted by the letter B.

41

## B.  PERFECTLY REFLECTING BOTTOM

The same parameters as in the previous case were re-run for a perfectly reflecting bottom with the exception of the 300 Hz tests and some of the 100 Hz tests because of computational-time restraints.  Table II summarizes the cases, according to bottom geometry and frequency.

### Table II

### Perfectly Reflecting Bottom Tests

| FIGURE | BOTTOM GEOMETRY | FREQUENCY |
|--------|-----------------|-----------|
| 22 | F | 50 |
| 23 | SL=1 | 50 |
| 24 | SL=2 | 50 |
| 25 | MIXF1 | 50 |
| 26 | MIXF2 | 50 |
| 27 | MIXF3 | 50 |
| 28 | F | 100 |
| 29 | SL=1 | 100 |
| 30 | SL=2 | 100 |

In the range of 25-50 nm, the analysis of these cases shows the existence of clearly defined convergence or energy-focusing zones that vary according to the specific bottom geometry imposed.  These convergence zones (CZ) are not the typical refracted CZ observed at 40 nm as in previous cases (Figs. 4, 7, 10 and 21), but are the result of focusing of both refracted and bottom reflected rays.

The difference between an upsloping bottom (Figs. 23, 24) and a flat one (Fig. 22) is that of changing the slope of the TL curves.  This effect has been called the funnel effect in reference to the upslope bottom geometry.  Its counterpart is

42

the megaphone effect for downsloping bottoms. The megaphone
and funnel effects are simply changes in acoustic energy
density due to changes in water cross sectional area at any
fixed range.

The cut-off effect observed in Figs. 24 and 30 appears
to be independent of frequency and hence difficult to explain
in the mode-mode coupling context. There are, however, two
possible explanations for this effect. The first is associated
with a model restriction; if the grazing angle becomes greater
than 33°, the bottom becomes fully absorbing, independetly
of what it is specified by the user. Hence, the propagating
energy that intersects the bottom is lost. Because of the
funnel effect, the energy propagates upslope intercepting
the bottom at steeper angles as it progresses in range. This
could lead eventually to the limiting grazing angle that would
cause the energy cut off observed.

The second possible explanation is a result of the ray
theory. If the reflected angle becomes equal or less than
the angle of the slope, the energy reflects backwards (for
an isovelocity fluid), creating interferences with the pro-
pagating energy at less distance from the source. This could
happen for a very steep slope where

$$\text{slope angle} = 90° - \text{grazing angle} \geq 57°,$$

as the grazing angle is model-limited to a maximum value of
33° where the bottom becomes fully absorbing. This leads to
values for the slope that are not considered in this study.
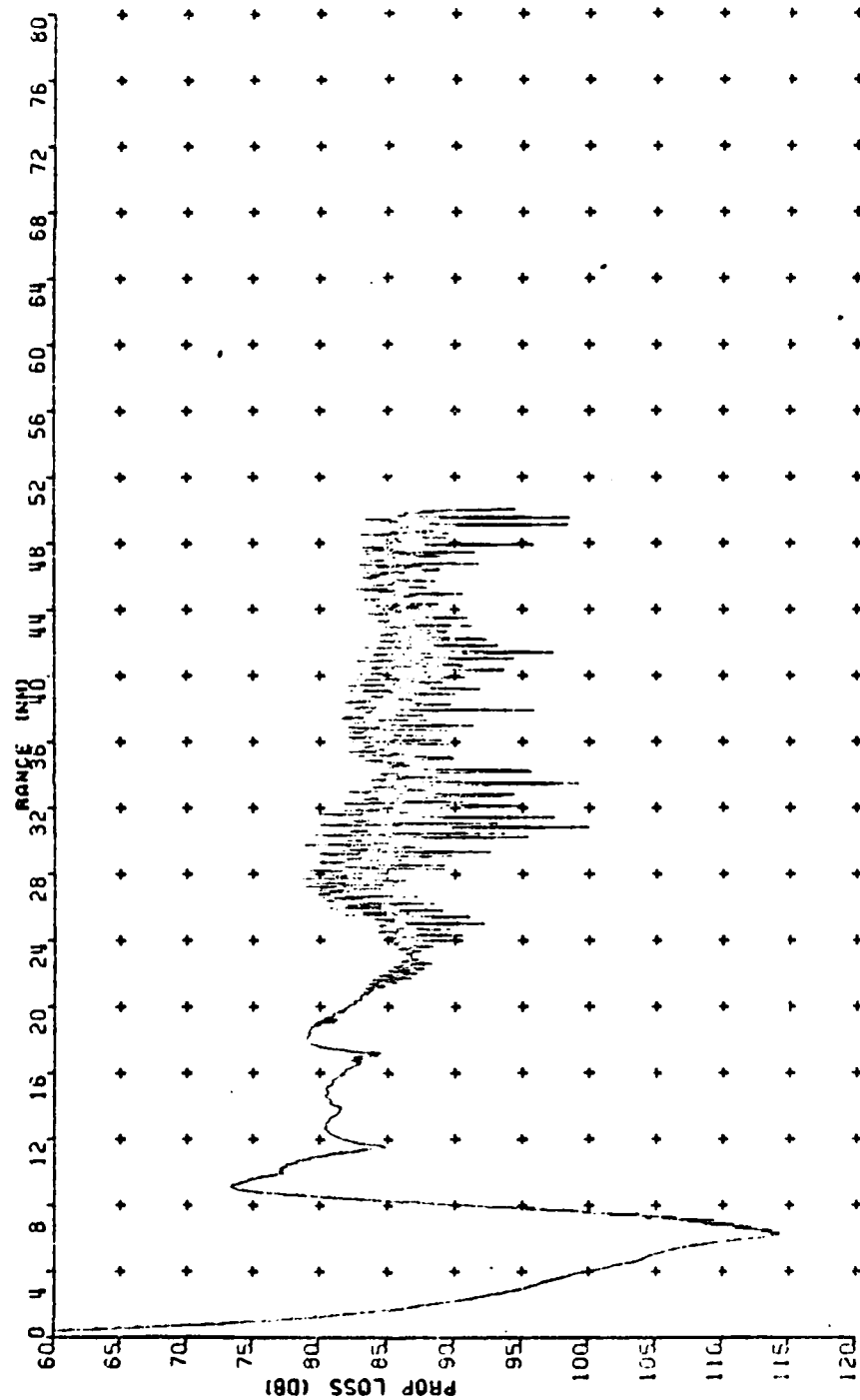Hence, only the first explanation is possible.

43

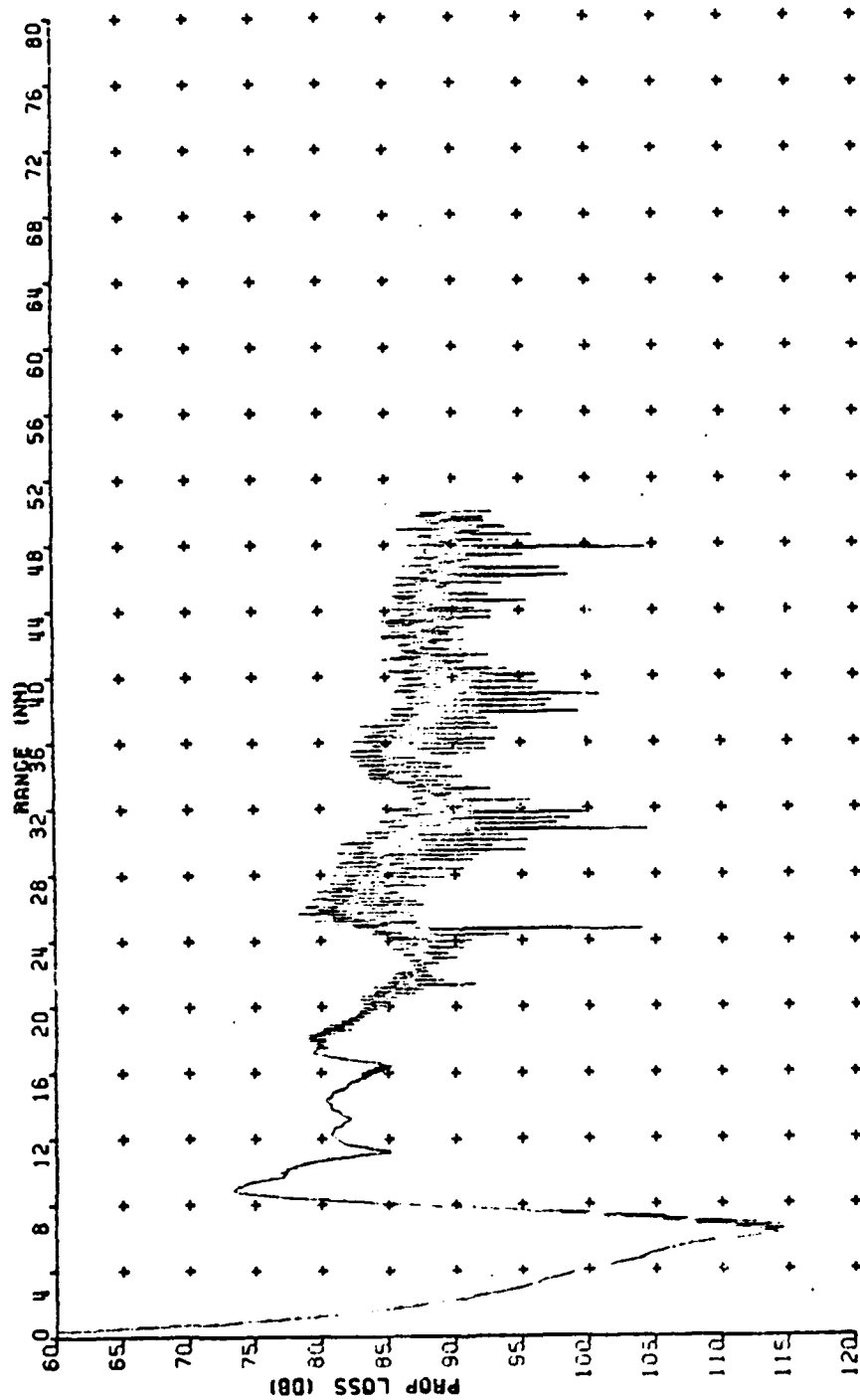Figure 22.   Perfectly Reflecting Flat Bottom (50 Hz)

44

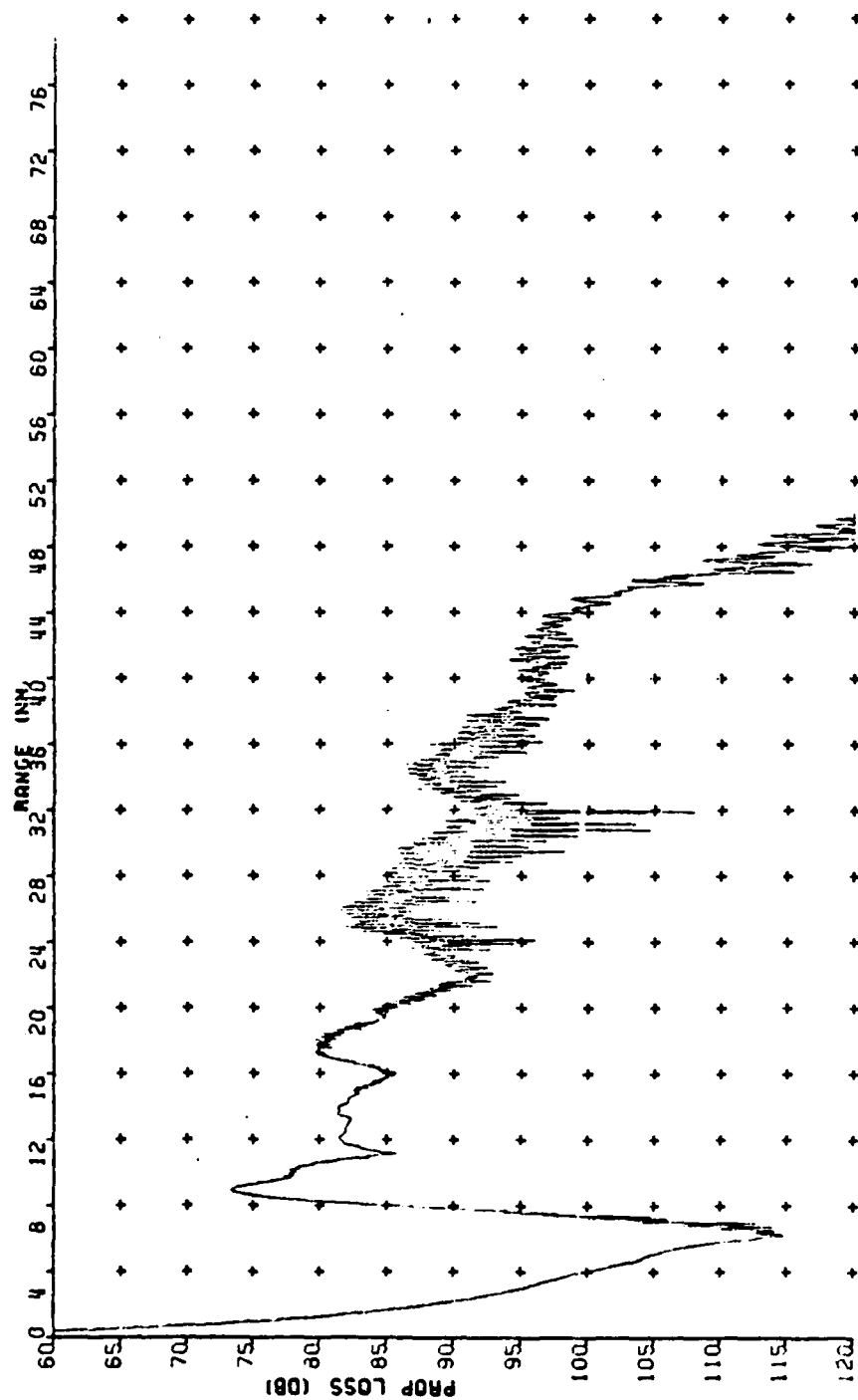Figure 23.  Perfectly Reflecting SL=1 Bottom (50 Hz)

45

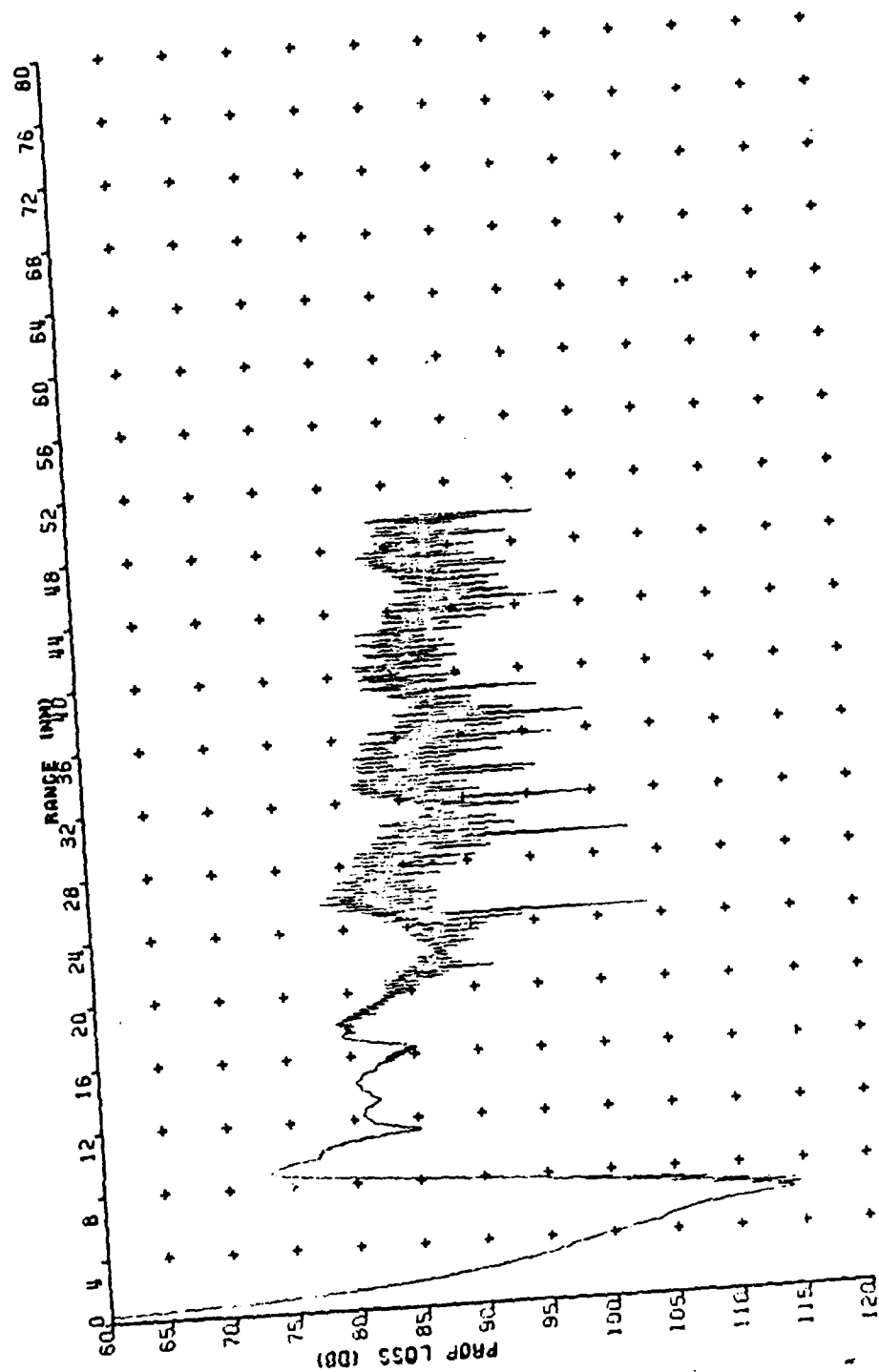Figure 24. Perfectly Reflecting SL=2 Bottom (50 Hz)

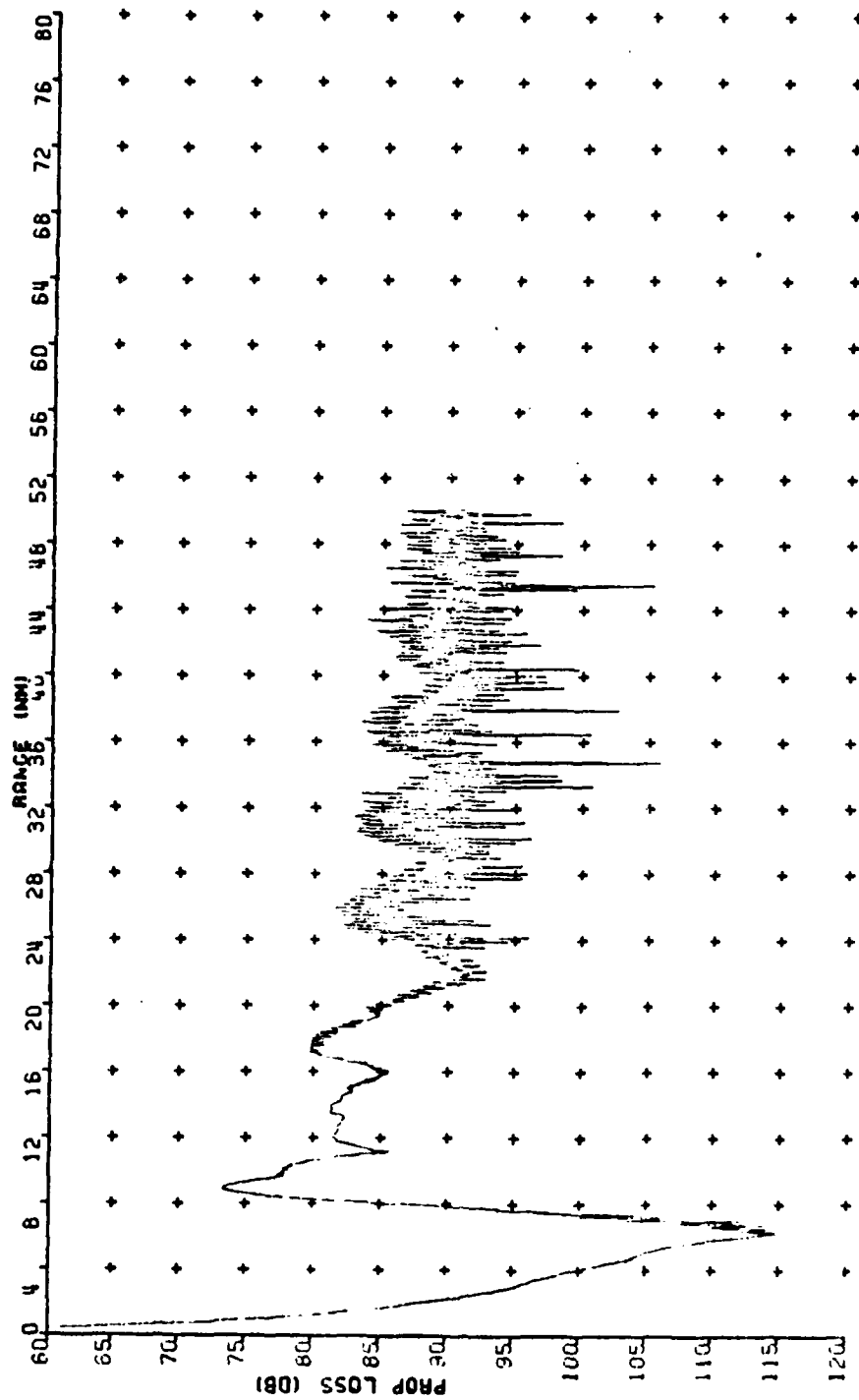Figure 25.  Perfectly Reflecting MIXF1 Bottom (50 Hz)

47

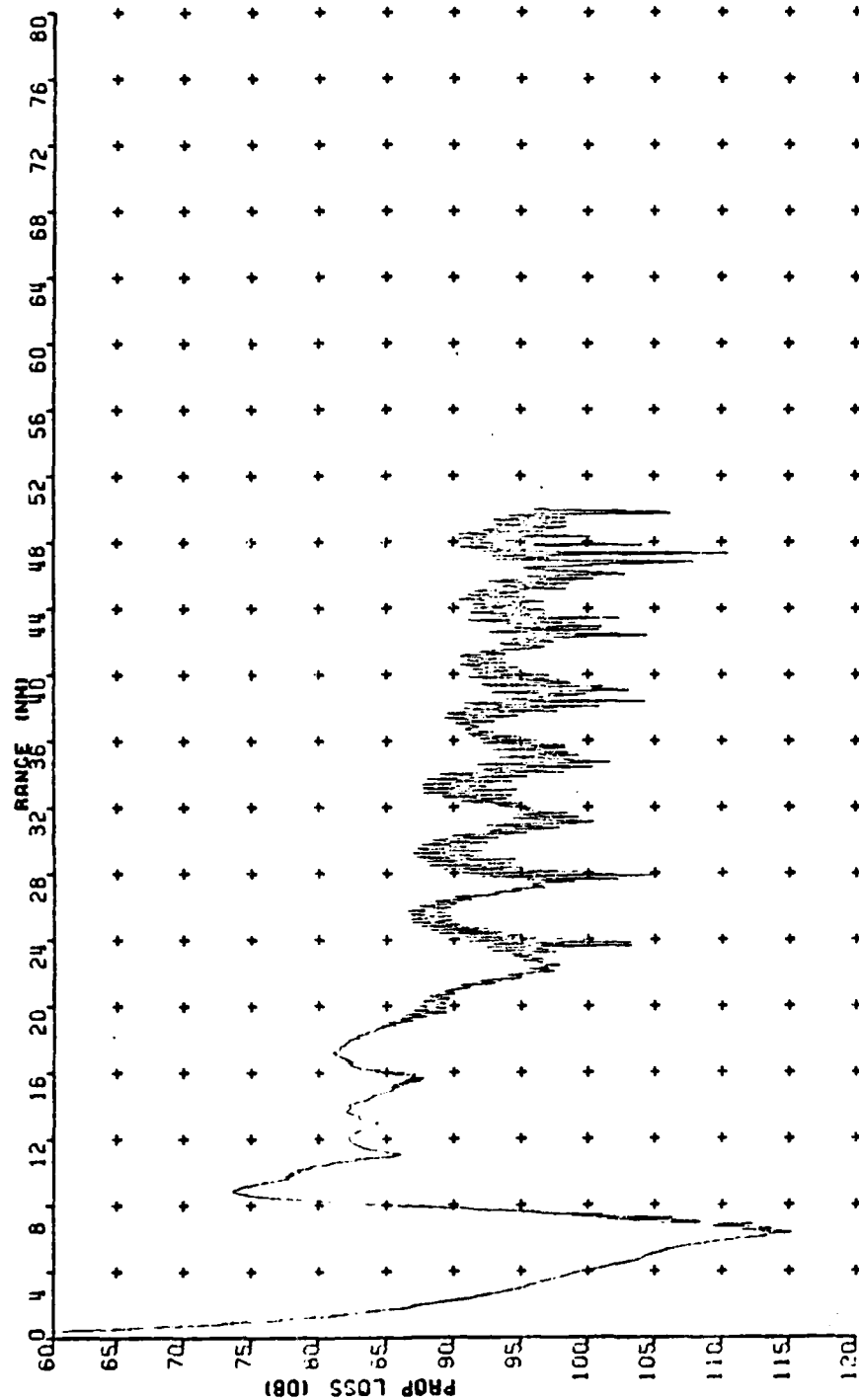Figure 26.   Perfectly Reflecting MIXF2 Bottom (50 Hz)
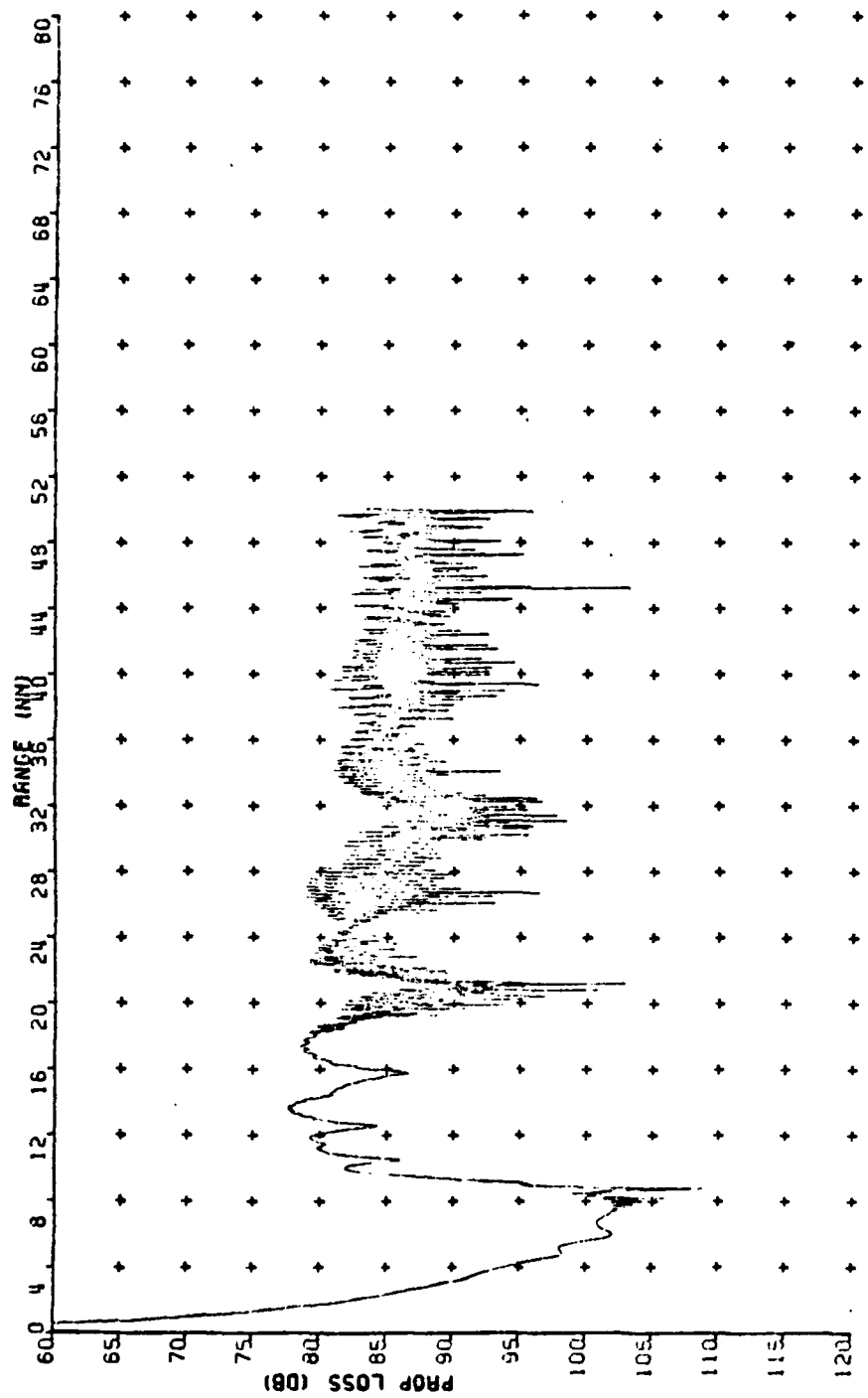
48

Figure 27. Perfectly Reflecting MIXF3 Bottom (50 Hz)

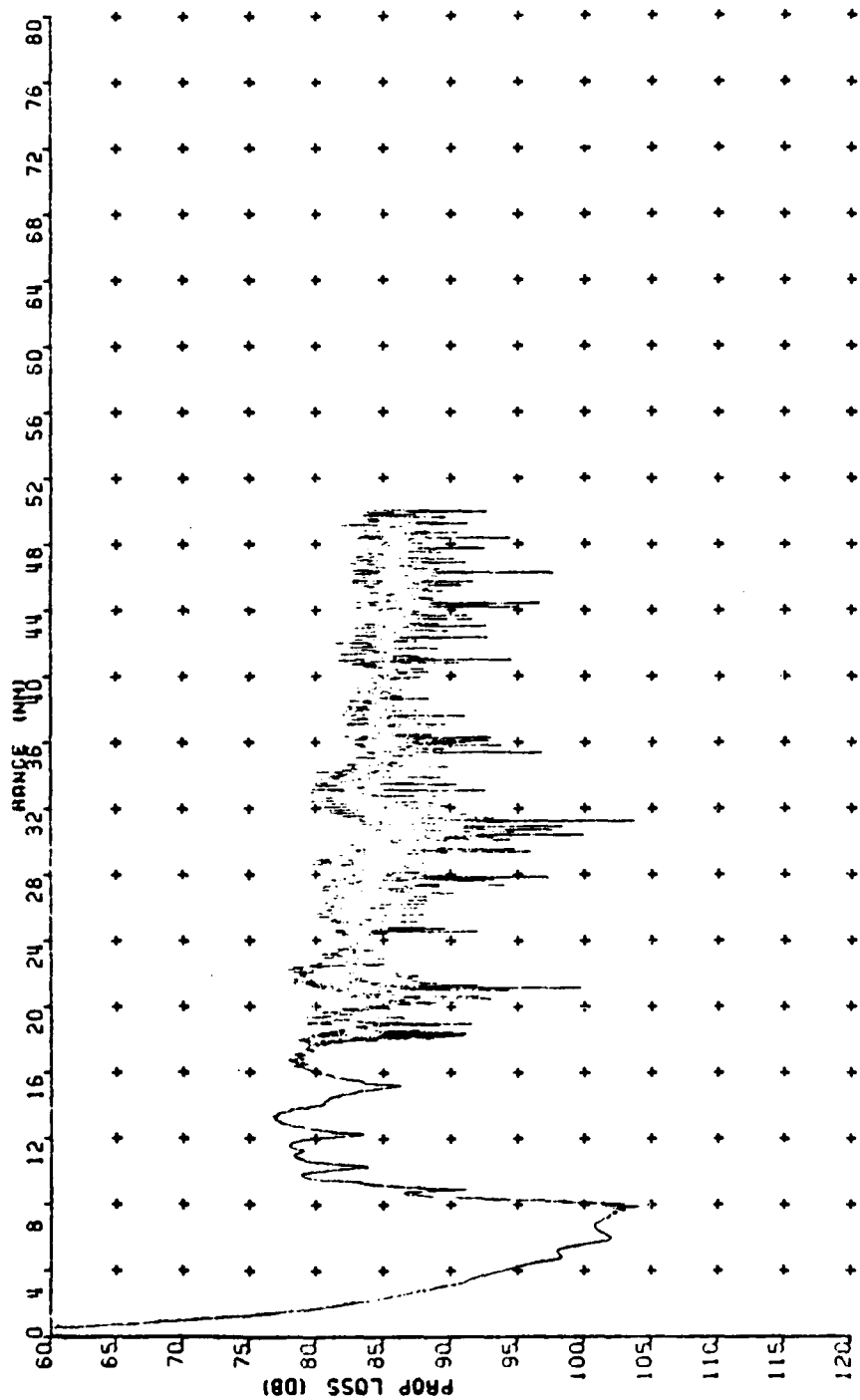Figure 28.  Perfectly Reflecting Flat Bottom (100 Hz)

50

Figure 29. Perfectly Reflecting SL=1 Bottom (100 Hz)
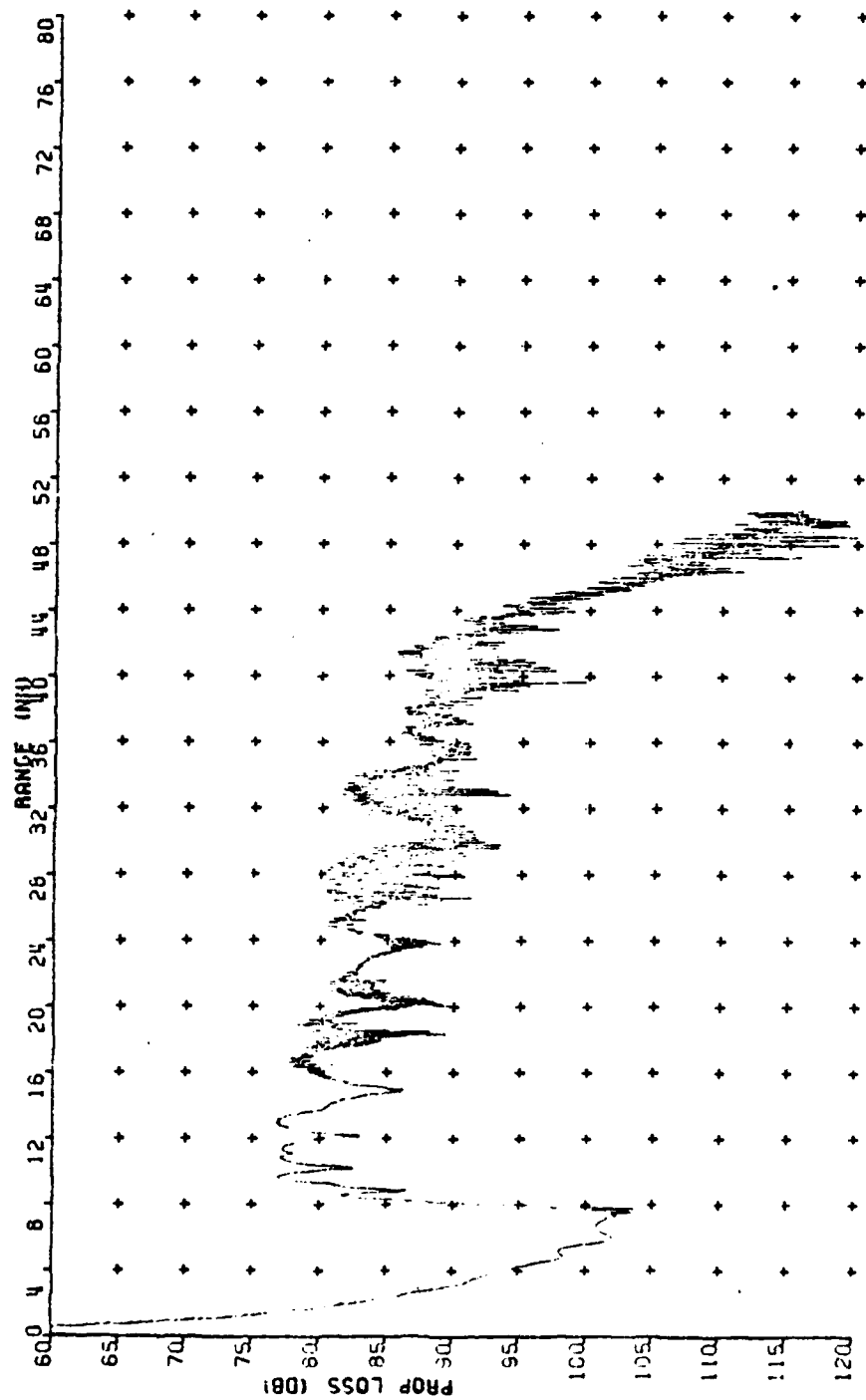
51

Figure 30. Perfectly Reflecting SL=2 Bottom (100 Hz)

The study of the other cases (Figs. 22, 25, 26, 27) is more interesting. From 0-25 nm all the four cases are very similar. However, a smoothing of the curves shows that the number of convergence zones over a given increment of range is a function clearly related to the slope of the bottom geometry. The shape of the TL curve has a strong sinusoidal pattern. The wavelength of this periodic occurrence of convergence zones was plotted versus bottom slope for each of the four cases (Fig. 31). This figure shows a quasi-linear relationship between the slope of the bottom and the wavelength of the convergence peak.
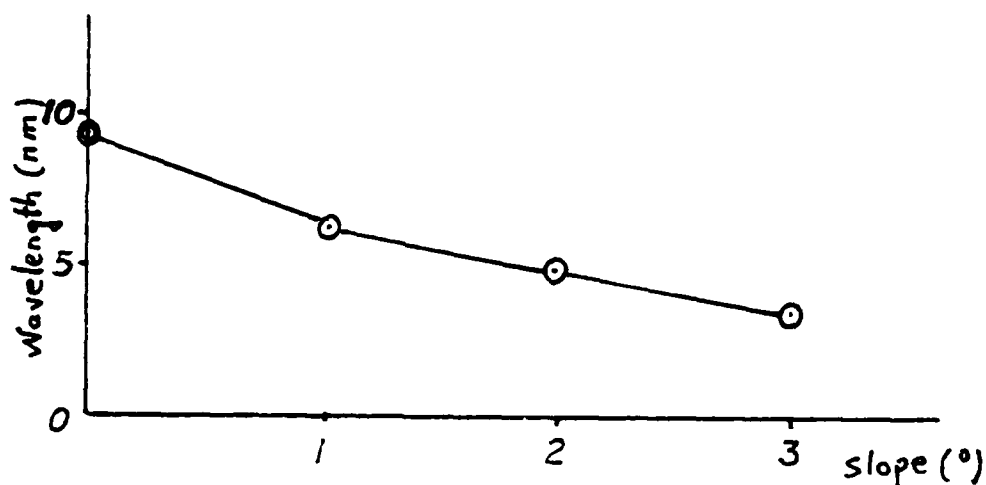


Figure 31.  Wavelength of observed convergence zones
as a function of the slope of the bottom.

## C.  A MORE REALISTIC BOTTOM

In this section a more realistic bottom has been chosen to perform tests similar to those in previous sections. The

degree of reflection from the sea floor is modeled using the formulation of Christensen and shown in Urick (1979), corresponding to a compilation of bottom loss at low frequencies (Fig. 32). This bottom loss formulation has been called U1 for the sake of simplification.

As before, TL vs. range graphs were analyzed and the results compared against those for the fully absorbing and perfectly reflecting bottom cases. The tests performed are listed in Table III.
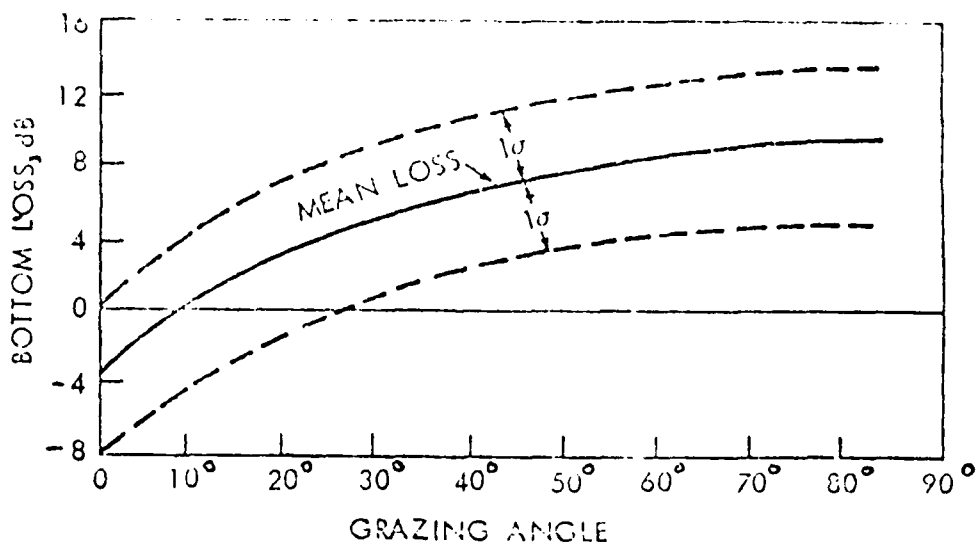


Figure 32. Results of a compilation of low frequency measurements of bottom loss. Dashed curves show limits of one standard deviation. Compiled by R. Christensen (from Urick, 1979).

Table III

U1 Bottom Tests

| FIGURE | BOTTOM GEOMETRY | FREQUENCY |
|--------|-----------------|-----------|
| 33 | F | 50 |
| 34 | SL=1 | 50 |
| 35 | SL=2 | 50 |
| 36 | F | 100 |
| 37 | SL=1 | 100 |
| 38 | SL=2 | 100 |
| 39 | F | 300 |
| 40 | MIXF1 | 50 |
| 41 | MIXF2 | 50 |
| 42 | MIXF3 | 50 |
| 43 | MIXF1 | 100 |
| 44 | MIXF2 | 100 |
| 45 | MIXF3 | 100 |

The following conclusions may be drawn from an analysis of the results:

First, the behavior of the acoustic energy using this more realistic type of bottom loss formulation is practically the same as for the perfectly reflecting bottom (Figs. 22 to 30). Except for more losses due to the partially absorbing characteristics of this bottom, the same general patterns for each geometry and frequency are found (Figs. 33 to 45).

Second, it appears to be possible to apply the general characteristics for perfectly reflecting bottoms to partially absorbing bottoms, if one first establishes the limits or envelope of the TL vs. range plots for the realistic bottoms in question.

Based upon this finding, the tests of the following section were performed utilizing only the perfectly reflecting bottom.
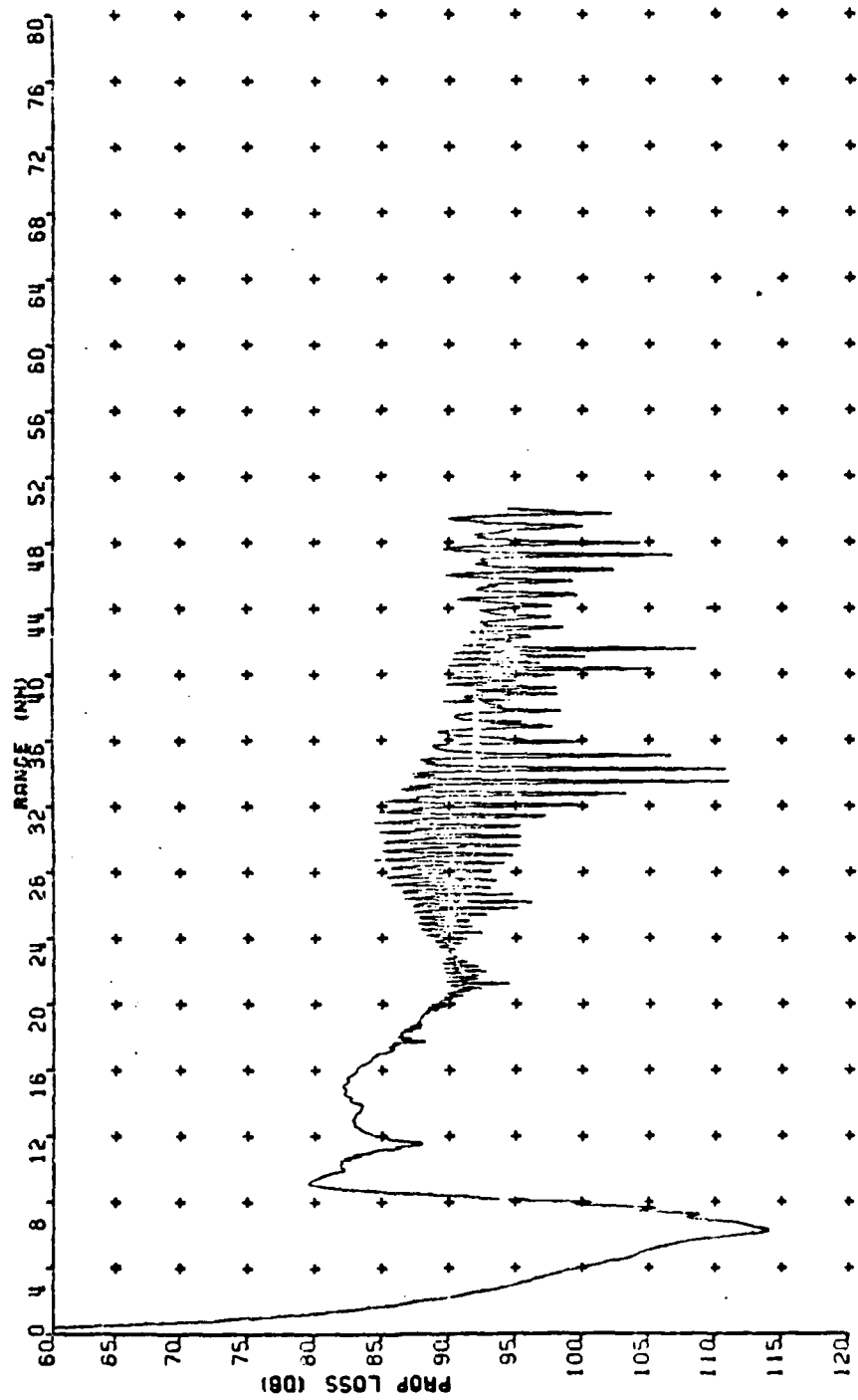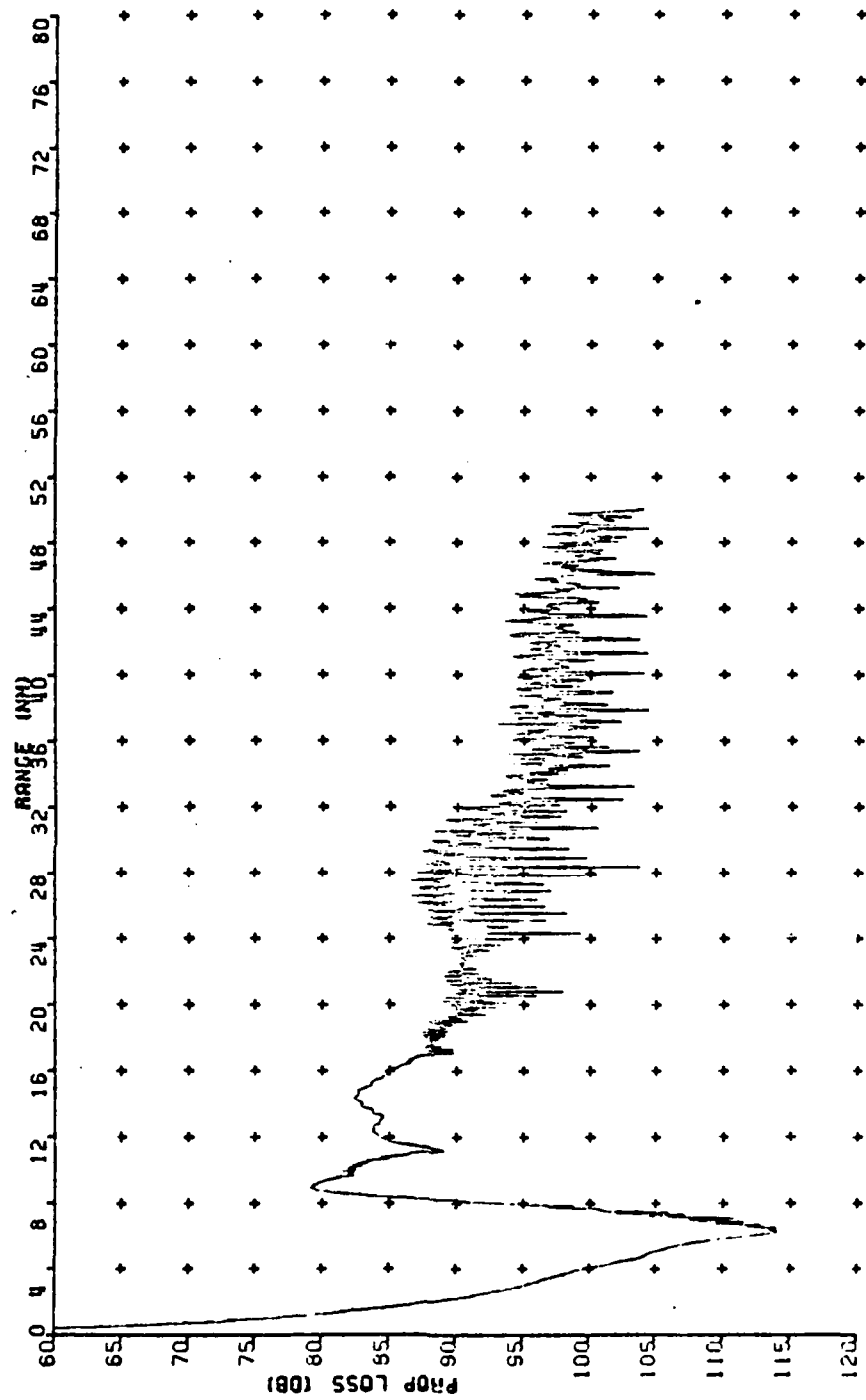
Figure 33.  U1 Flat Bottom (50 Hz)
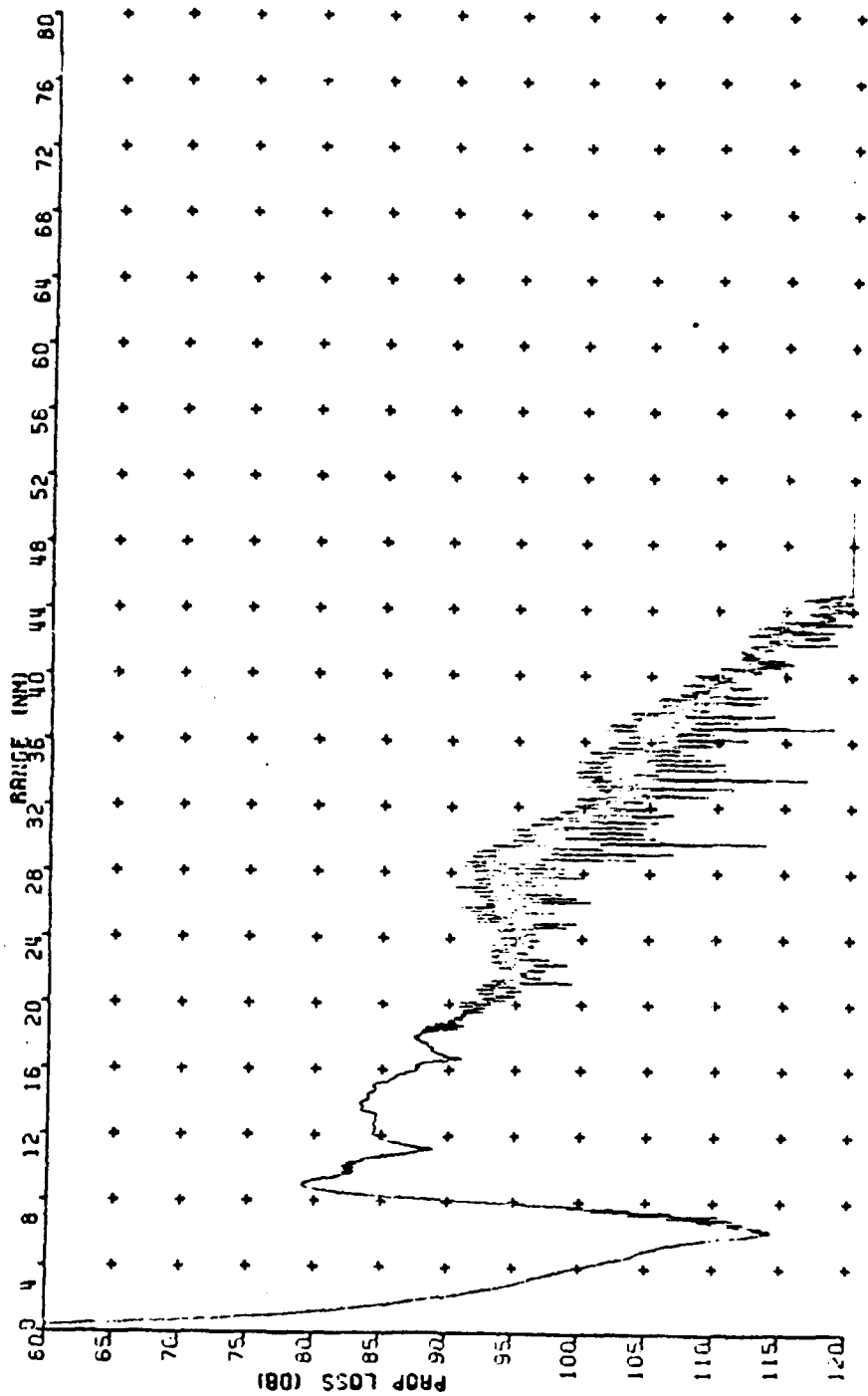
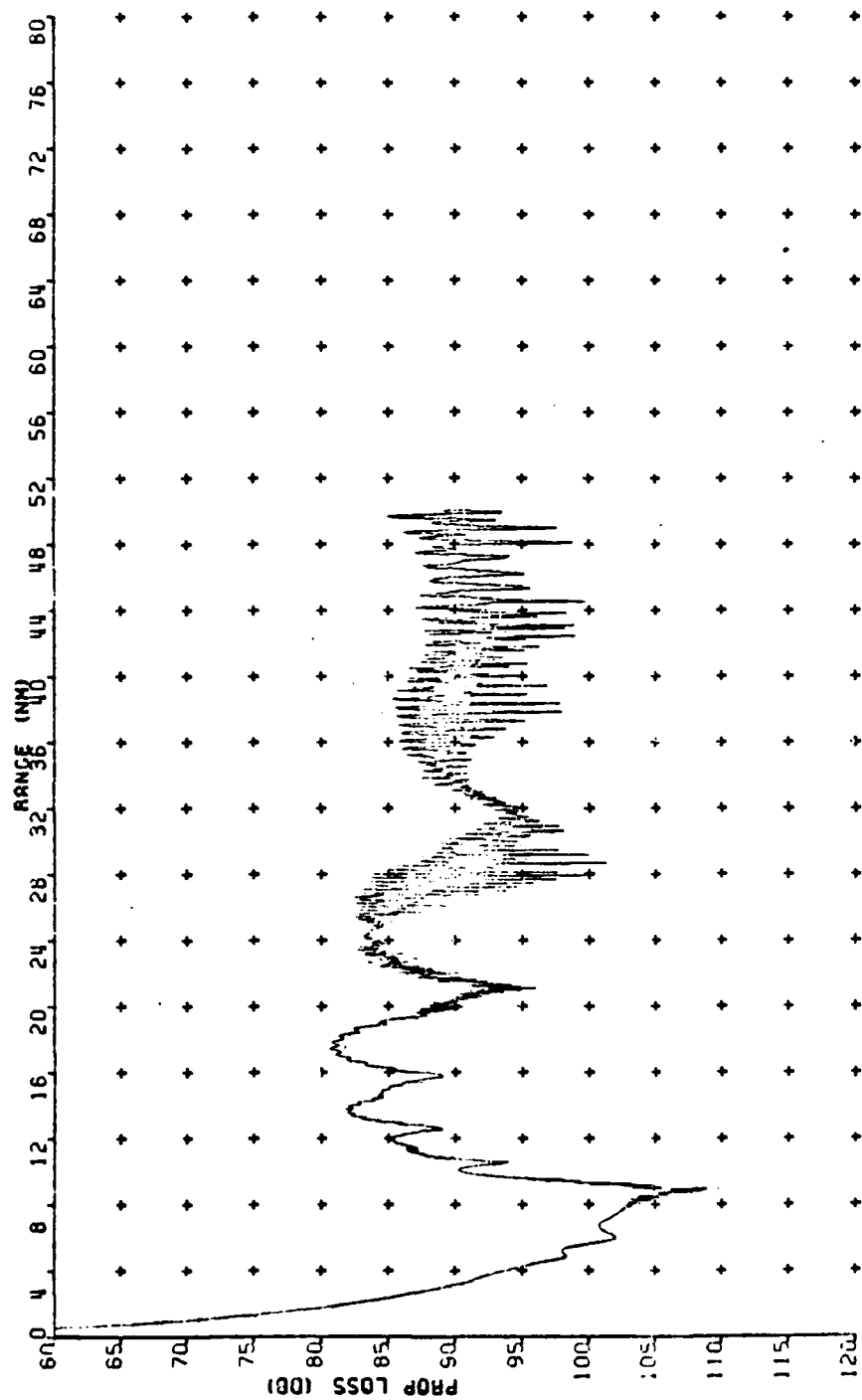Figure 34.   U1 SL=1 Bottom (50 Hz)

57

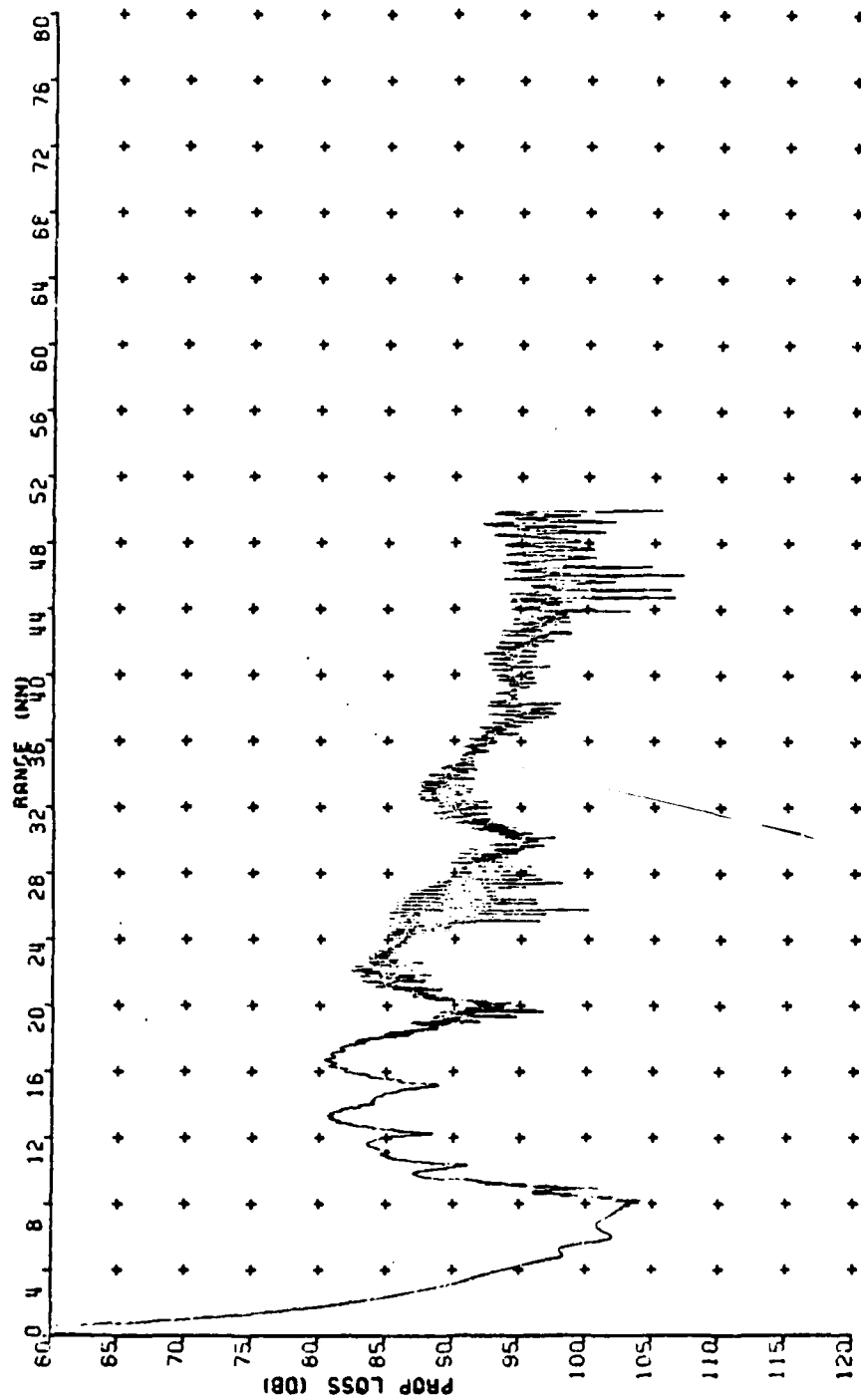Figure 35. U1 SL=2 Bottom (50 Hz)

Figure 36. U1 Flat Bottom (100 Hz)
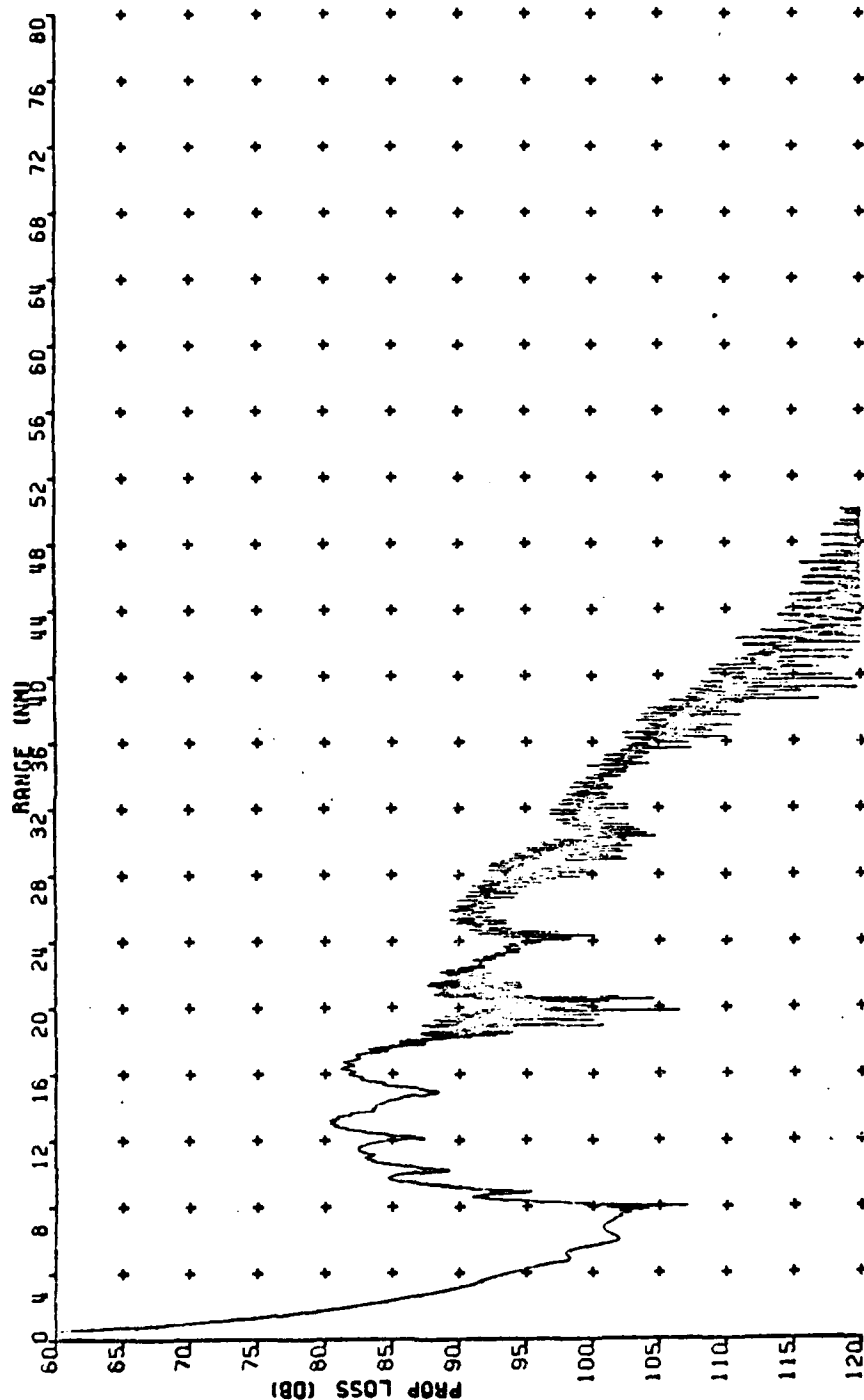
Figure 37.   U1 SL=1 Bottom (100 Hz)
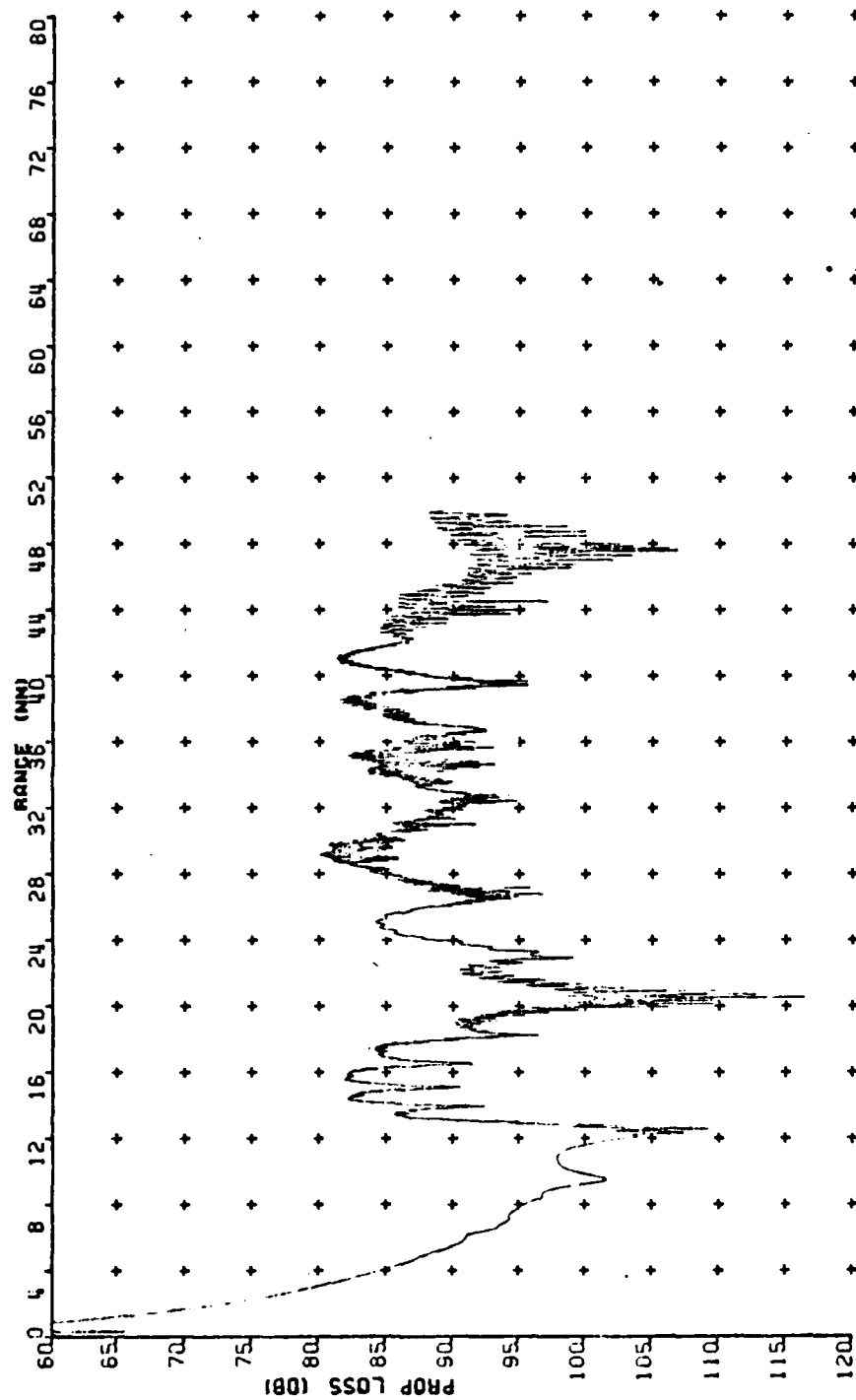
60

Figure 38. Ul SL=2 Bottom (100 Hz)

61

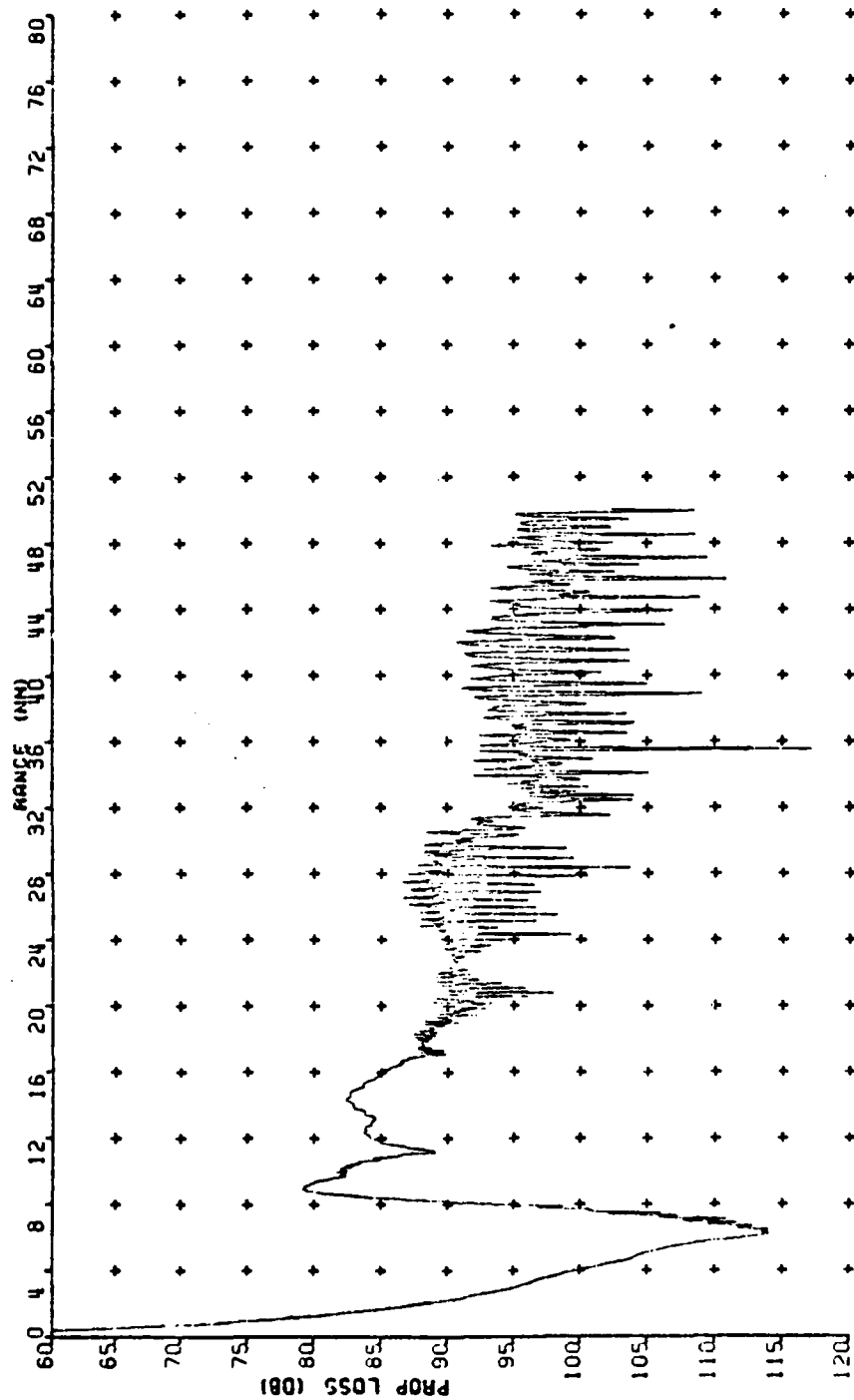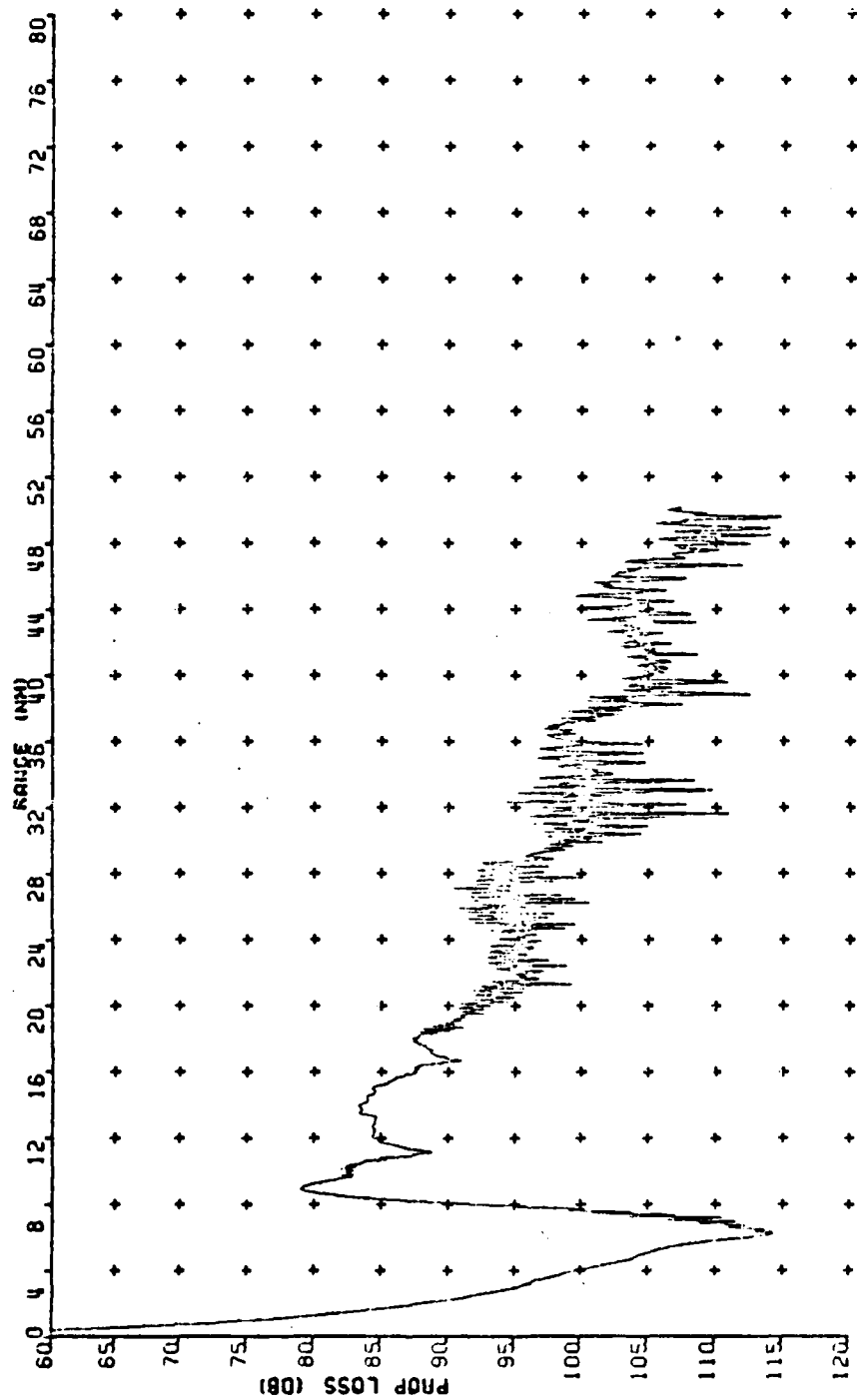Figure 39.   U1 Flat Bottom (300 Hz)

Figure 40.   U1 MIXF1 Bottom (50 Hz)

63

Figure 41.   U1 MIXF2 Bottom (50 Hz)
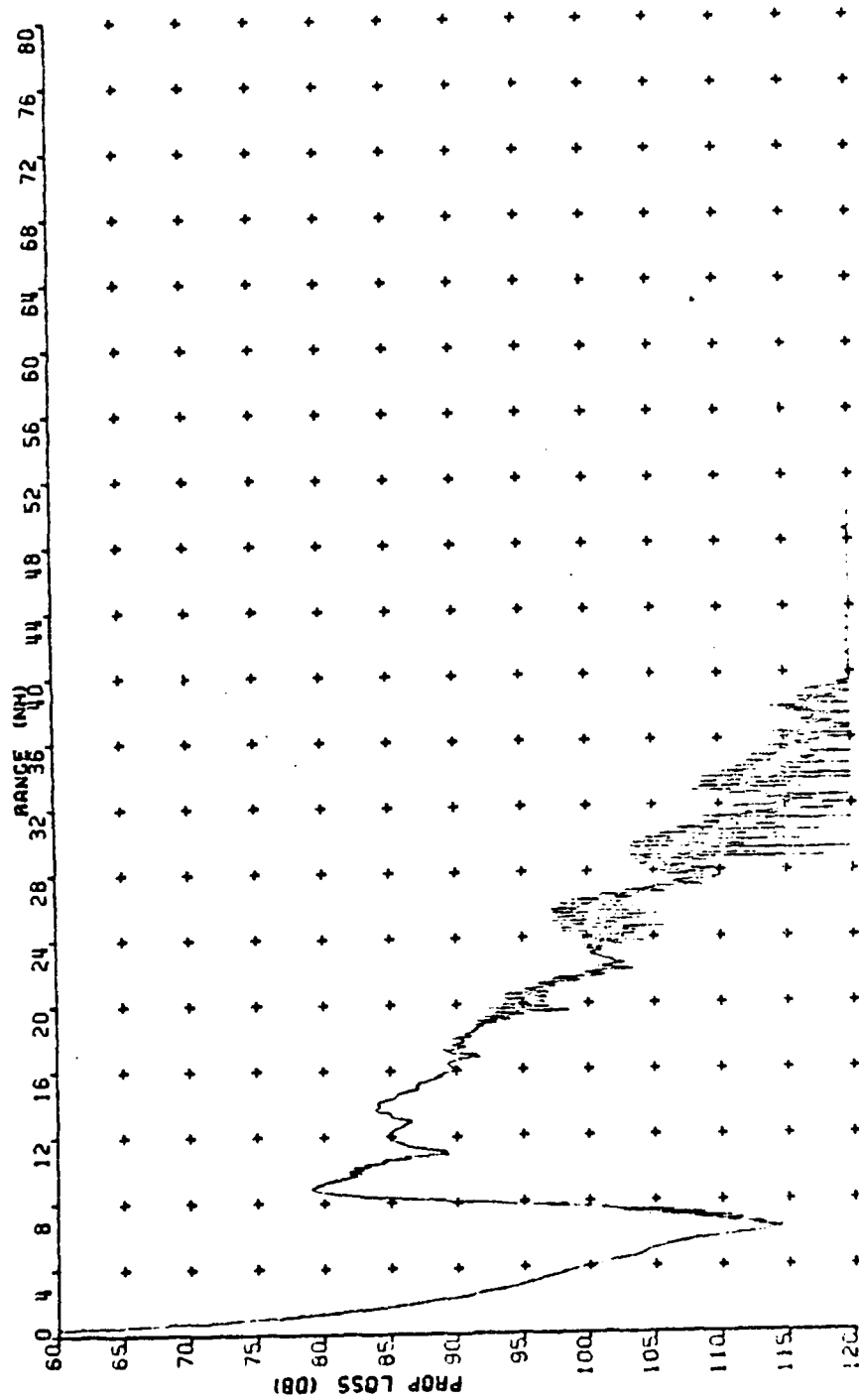
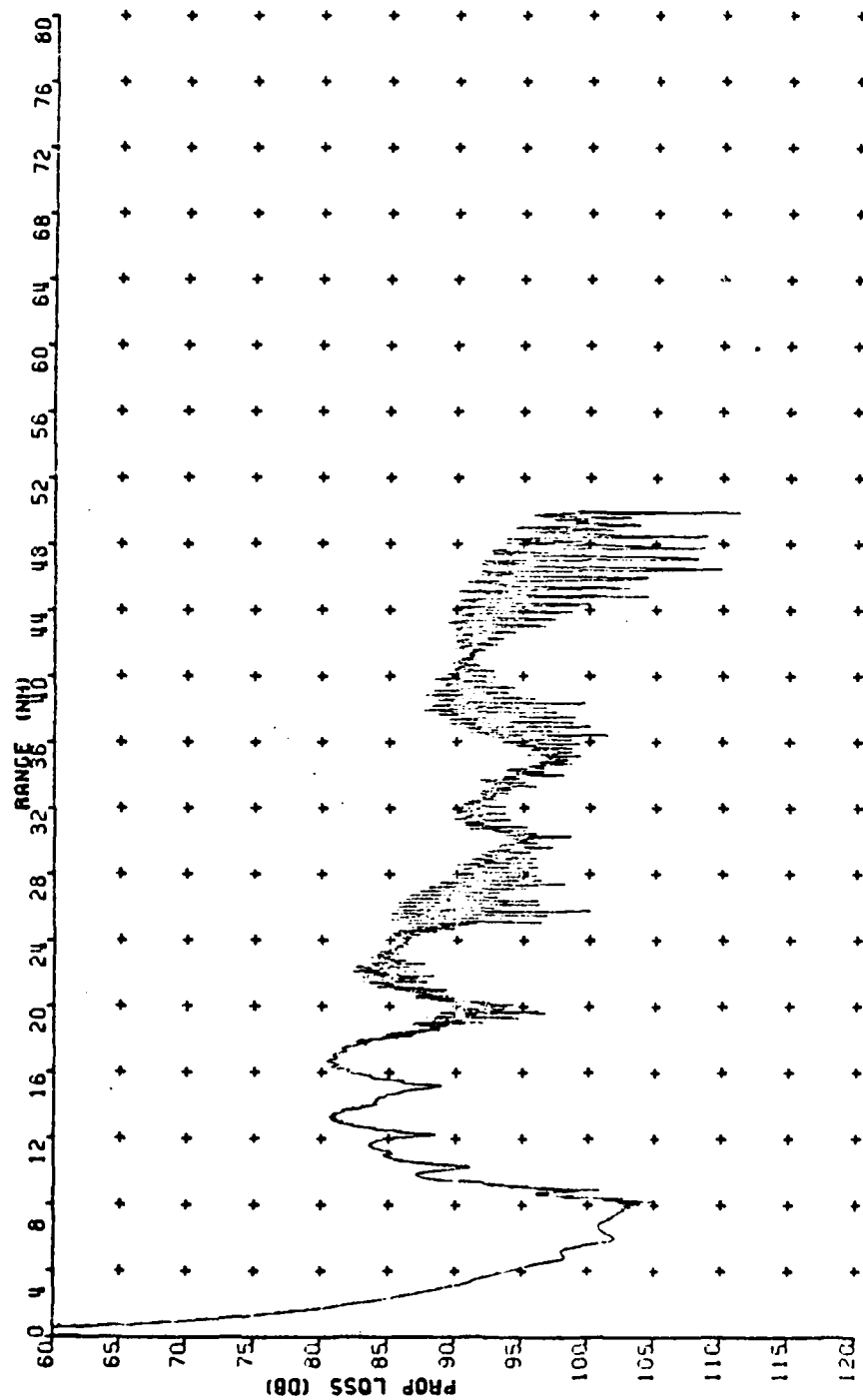64

Figure 42.   U1 MIXF3 Bottom (50 Hz)
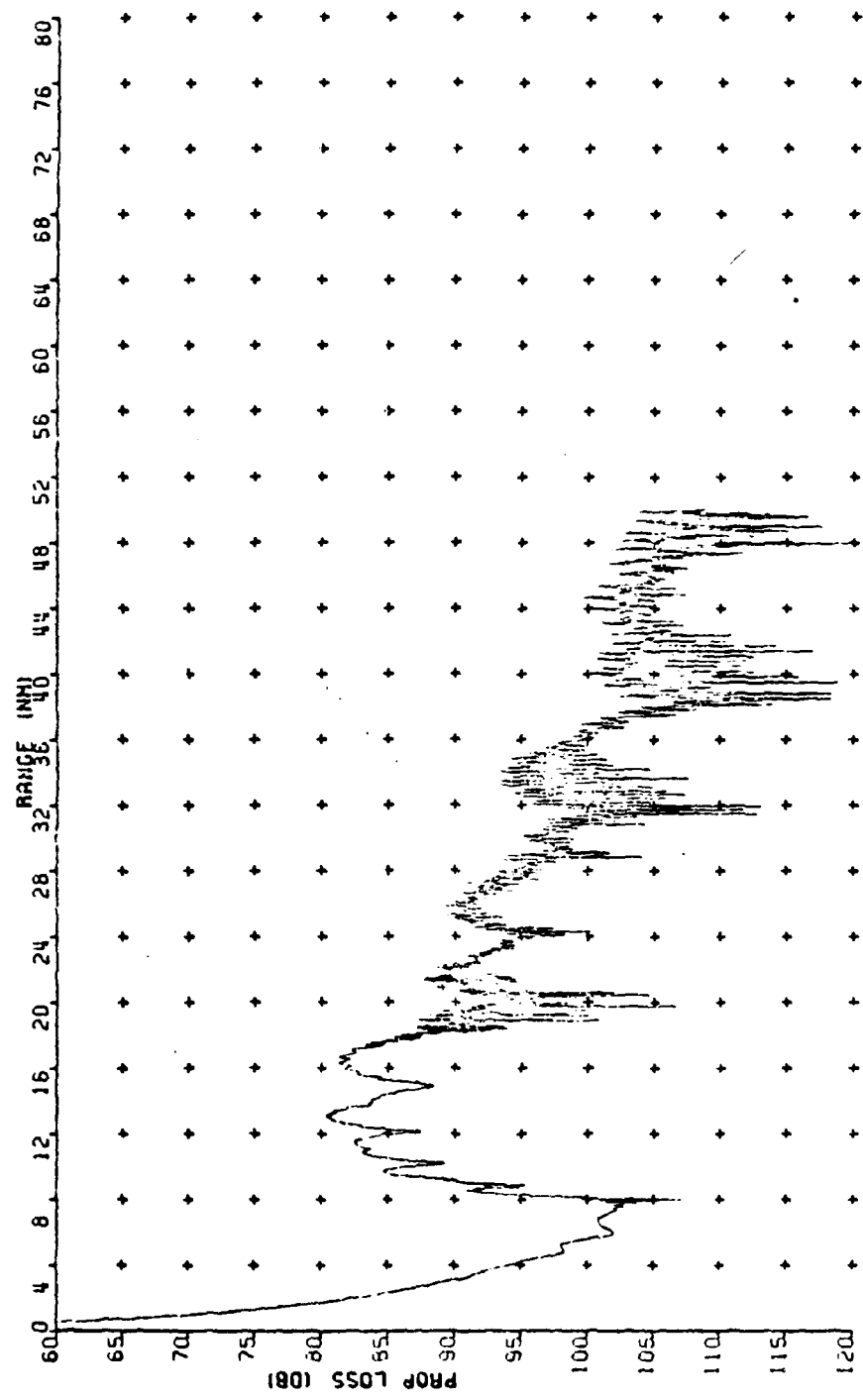
65

Figure 43.   U1 MIXF1 Bottom (100 Hz)

Figure 44.   U1 MIXF2 Bottom (100 Hz)

67
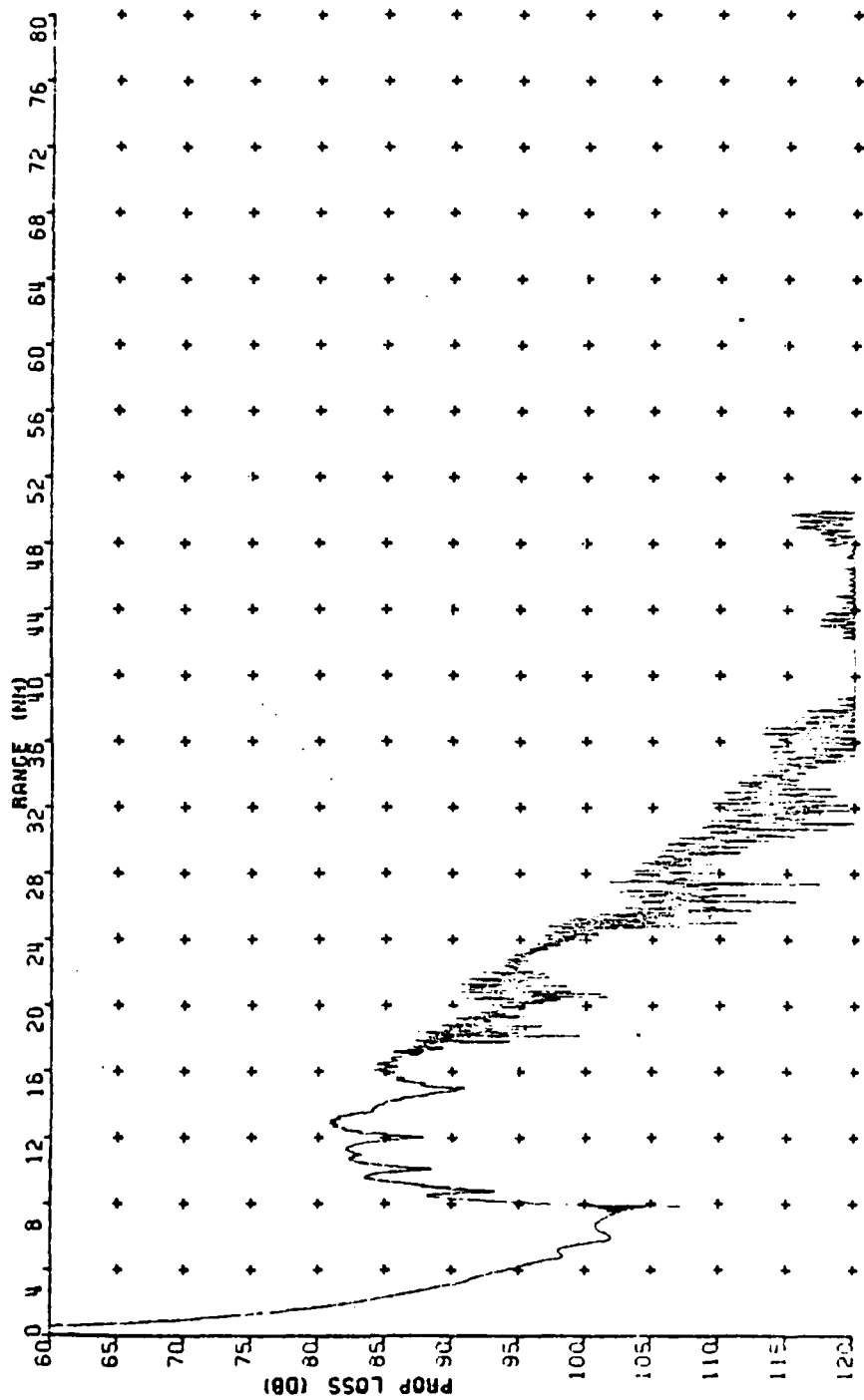
Figure 45.   U1 MIXF3 Bottom (100 Hz)

68

## D.  THE SLOPING-STEP GEOMETRY

The following cases are all for flat bottoms having a single upward-sloping section of varying steepness.  A maximum water depth of 5000 ft was chosen because the objective of these tests were to determine the importance of the changing steepness of the sloping section on the energy reflected paths.  As a consequence, it was considered convenient to eliminate the refractive effect observed in previous runs of the model.  In addition, computational time was saved without detriment to the results obtained.

Range = 50 nm.

SVP = PROF1.

Source Depth = 50 ft.

Receiver Depth = 300 ft.

Maximum Water Depth = 5000 ft.

Frequency = 50 Hz.

Table IV lists the tests performed forthis bottom geometry.

### Table IV

### Perfectly Reflecting Upsloping Bottom

| FIGURE | BOTTOM GEOEMTRY | FREQUENCY |
|--------|-----------------|-----------|
| 46 | SL=1 MXF | 50 |
| 47 | SL=2 MXF | 50 |
| 48 | SL=3 MXF | 50 |
| 49 | SL=4 MXF | 50 |
| 50 | SL=5 MXF | 50 |
| 51 | SL=6 MXF | 50 |
| 52 | SL=7 MXF | 50 |
| 53 | SL=8 MXF | 50 |

The results of the analysis show that: first, only negligible TL differences occur in the first 10 nm (Figs. 46 to 53). This conforms with expectations because of the same bottom geometry over this range for the previous cases studied.

Second, the steepness of the bottom slope is clearly manifested in the subsequent large changes in the TL curves in the range of 10-15 nm. It is possible to measure this change in TL, from the maximum at 12 nm to the first maximum appearing at or immediately after 15 nm. This drop in intensity is related to the geometry of the bottom; ranges from less than 1 dB (SL=1 MXF, Fig. 46) up to 10 dB (SL=8 MXF, Fig. 53) are observed.

Apparently, this is in disagreement with the observed slope enhancement reported by Hawker et al., (1976) when using a reflecting slope. The reason for this loss of energy is attributable to the previously mentioned limitation of the model when reaching an energy propagation angle of 33°, where the bottom literally absorbs all the energy arriving with this and greater grazing angles.

Another interesting effect has already been observed in the previous MIXF cases (Figs. 25, 26, 27): the presence of periodic convergence zones in the range 15 nm to about 30 nm. This effect is more easily seen in Figs. 50, 51, 52 and 53, and seems to be wavelength-related to the angle of the slope, as was found earlier. There remain, however, some

unanswered questions as to the cause of this effect: why are they more apparent in some figures than in others, and why are the peaks so low compared to Figs. 25-27? Hopefully, these and other questions will be solved after a numerical smoothing is incorporated into the parabolic equation model and Fourier Transforms are employed to accurately determine the wavelengths involved. Intuitively, it appears that the cause is purely geometrical and that the relative intensity of the peaks is a function of the length of the slope for a given angle.

Several more cases were tested with a downsloping bottom segment. For these tests all the parameters were the same except that the minimum depth was limited to 1000 feet. Table V lists the tests performed.

Table V

Perfectly Reflecting Downsloping Bottom

| FIGURE | BOTTOM GEOMETRY | FREQUENCY |
|--------|-----------------|-----------|
| 54 | ISL=1 MXF | 50 |
| 55 | ISL=2 MXF | 50 |
| 56 | ISL=3 MXF | 50 |
| 57 | ISL=4 MXF | 50 |
| 58 | ISL=5 MXF | 50 |
| 59 | ISL=6 MXF | 50 |
| 60 | ISL=7 MXF | 50 |
| 61 | ISL=8 MXF | 50 |

The resultant TL vs. range graphs (Figs. 54-61) show a noteworthy aspect: the almost total absence of large interference, or small spatial scale variations, in comparison to

71

the flat or upslope cases. This is particularly true for slopes of 4° or more in the range 15-50 nm (Figs. 57 to 61). This is due to the fact that with increasing downward slope the number of bottom reflections decreases for the same range. All the high frequency noise is at close range where frequent bottom reflections take place due to shallower depths. On the other hand, rays which were bottom reflected at close range become refracted rays as the bottom slopes downward. Hence, CZ-type peaks appear. The effect of increasing slope angle on the overall TL is to decrease the intensity of the energy locally, principally due to the megaphone effect cited before and not to any kind of energy absorption process. If the downslope is increased sufficiently, the energy becomes purely refracted, creating zones of energy peaks as expected for the typical CZ's in a fully absorbing bottom (where no reflected paths exist).

Figure 45.   Perfectly Reflecting SL=1 MXF Bottom (50 Hz)

73

Figure 46.  Perfectly Reflecting SL=2 MXF Bottom (50 Hz)

Figure 47.  Perfectly Reflecting SL=3 MXF Bottom (50 Hz)

Figure 48. Perfectly Reflecting SL=4 MXF Bottom (50 Hz)

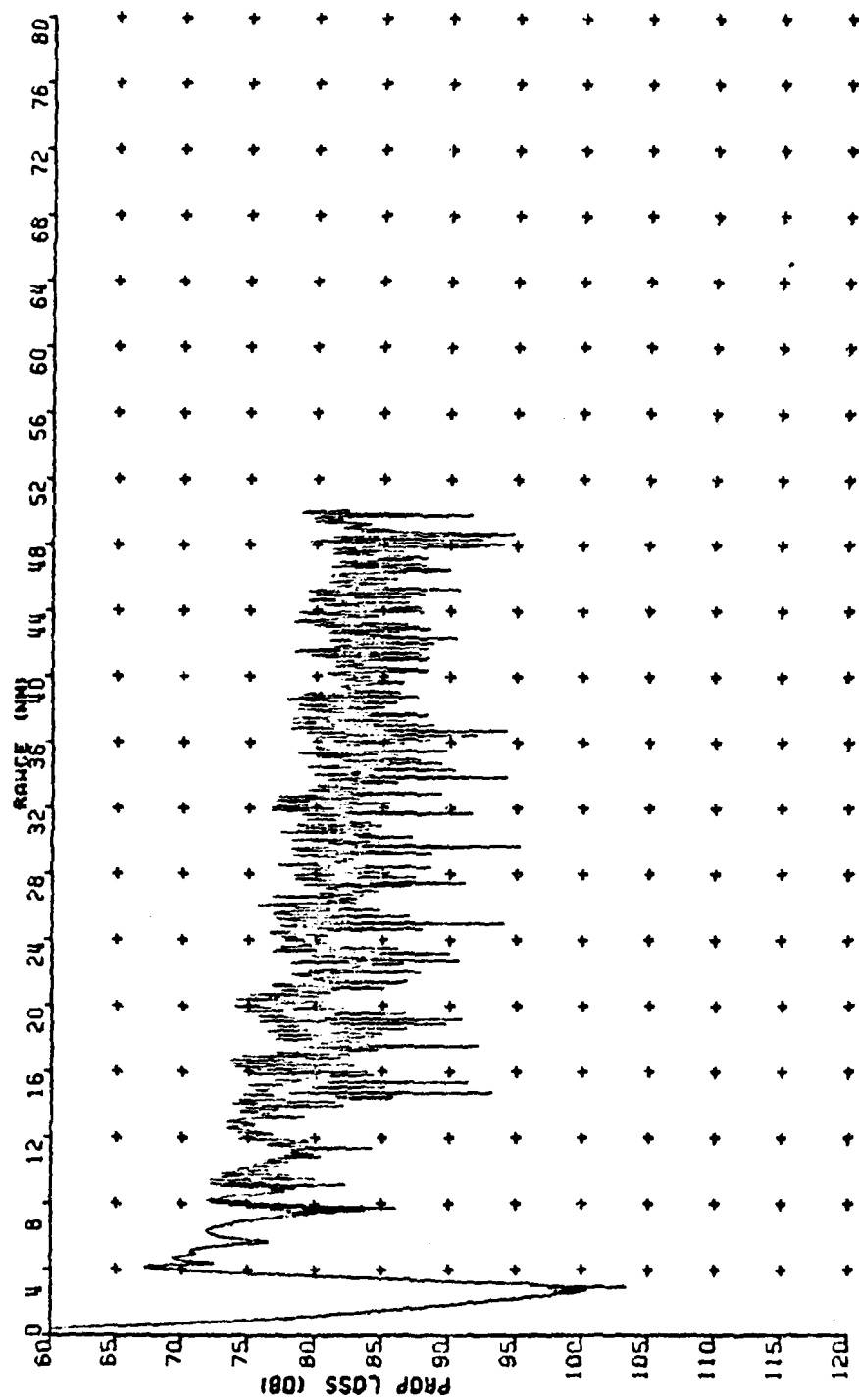Figure 49.  Perfectly Reflecting SL=5 MXF Bottom (50 Hz)
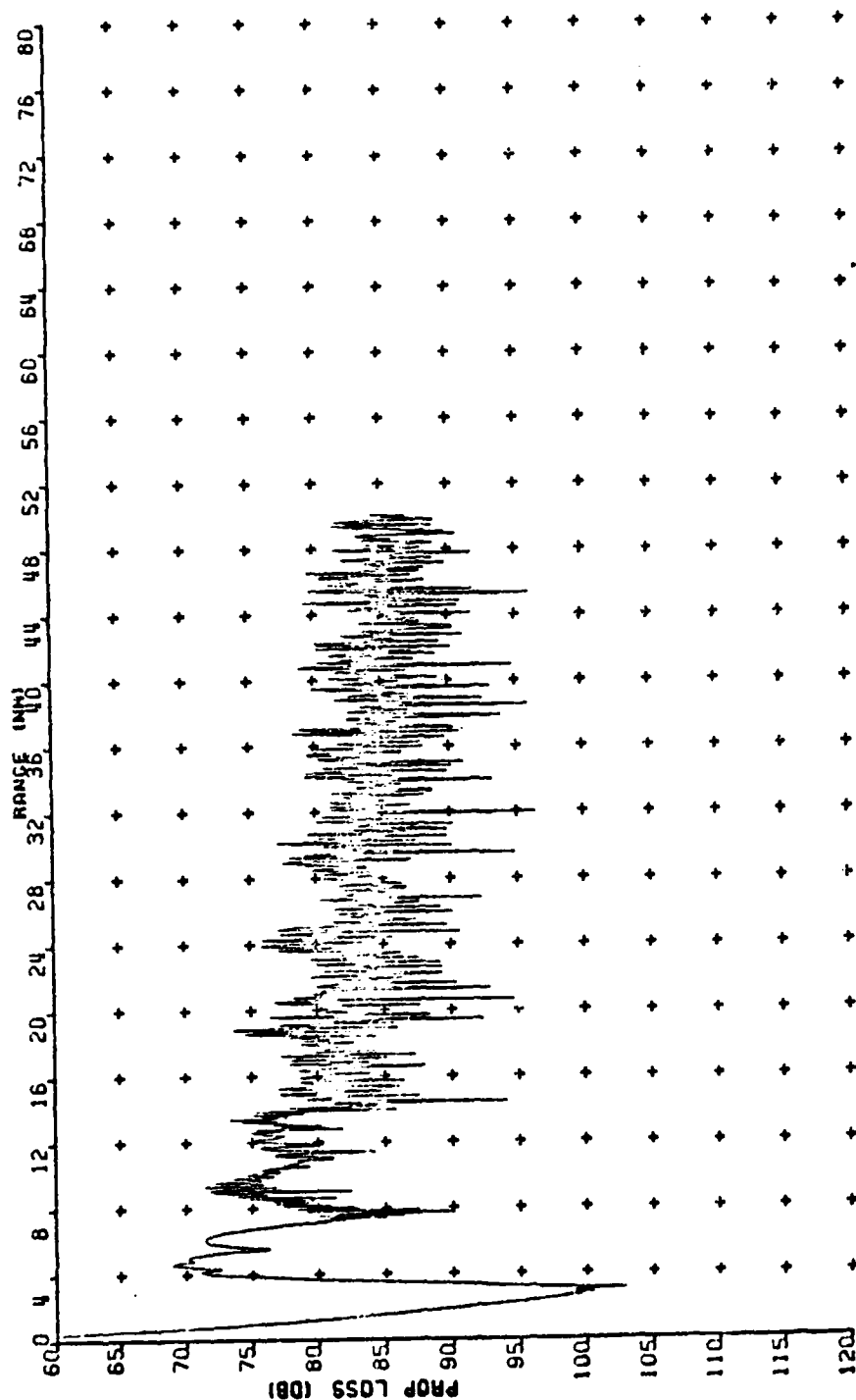
77

Figure 50.   Perfectly Reflecting SL=6 MXF Bottom (50 Hz)

Figure 51.  Perfectly Reflecting SL=7 MXF Bottom (50 Hz)

Figure 52.   Perfectly Reflecting SL=8 MXF Bottom (50 Hz)

Figure 53. Perfectly Reflecting ISL=1 MXF Bottom (50 Hz)

81

Figure 54.  Perfectly Reflecting ISL=2 MXF Bottom (50 Hz)

82

Figure 55.   Perfectly Reflecting ISL=3 MXF Bottom (50 Hz)

83
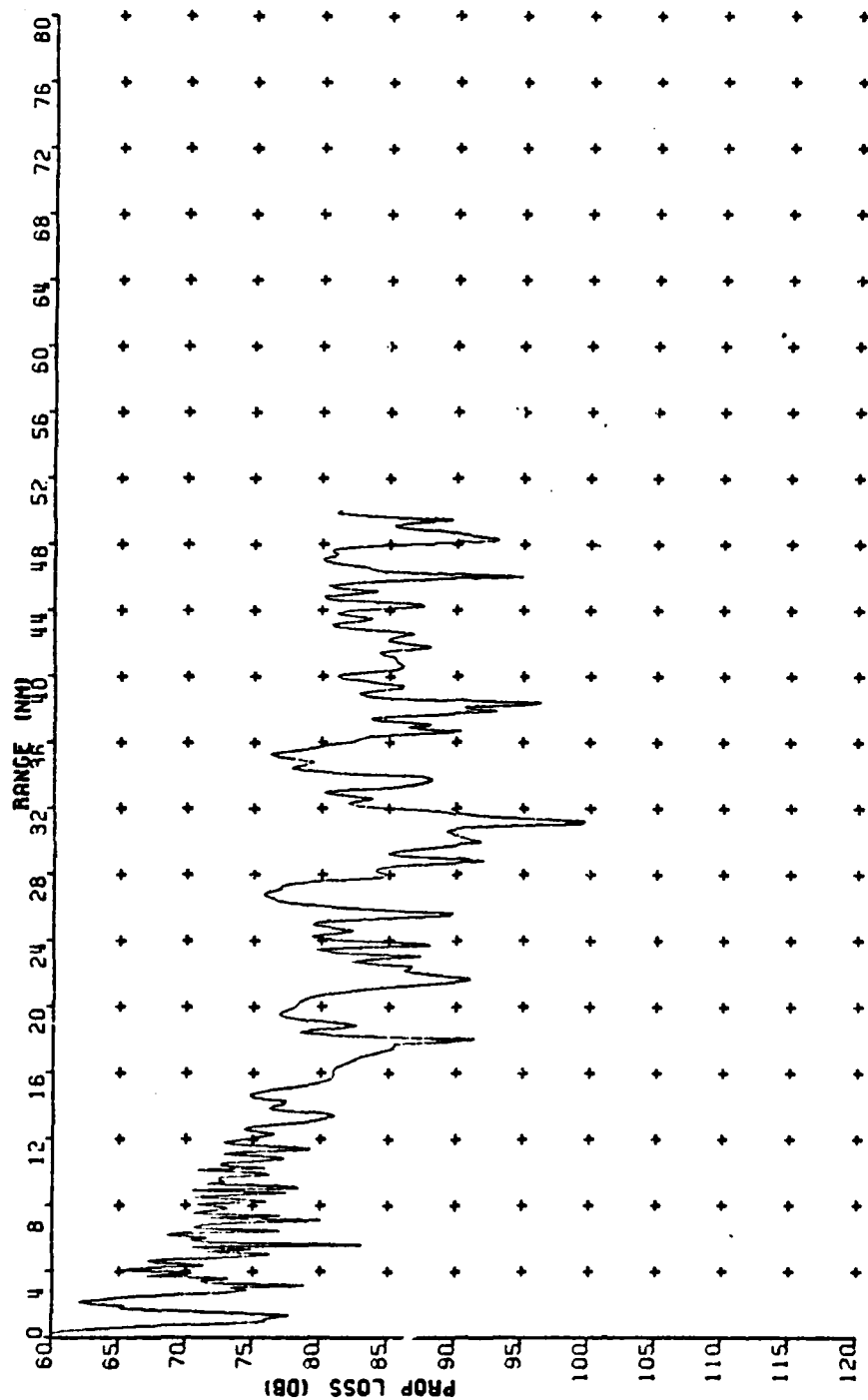
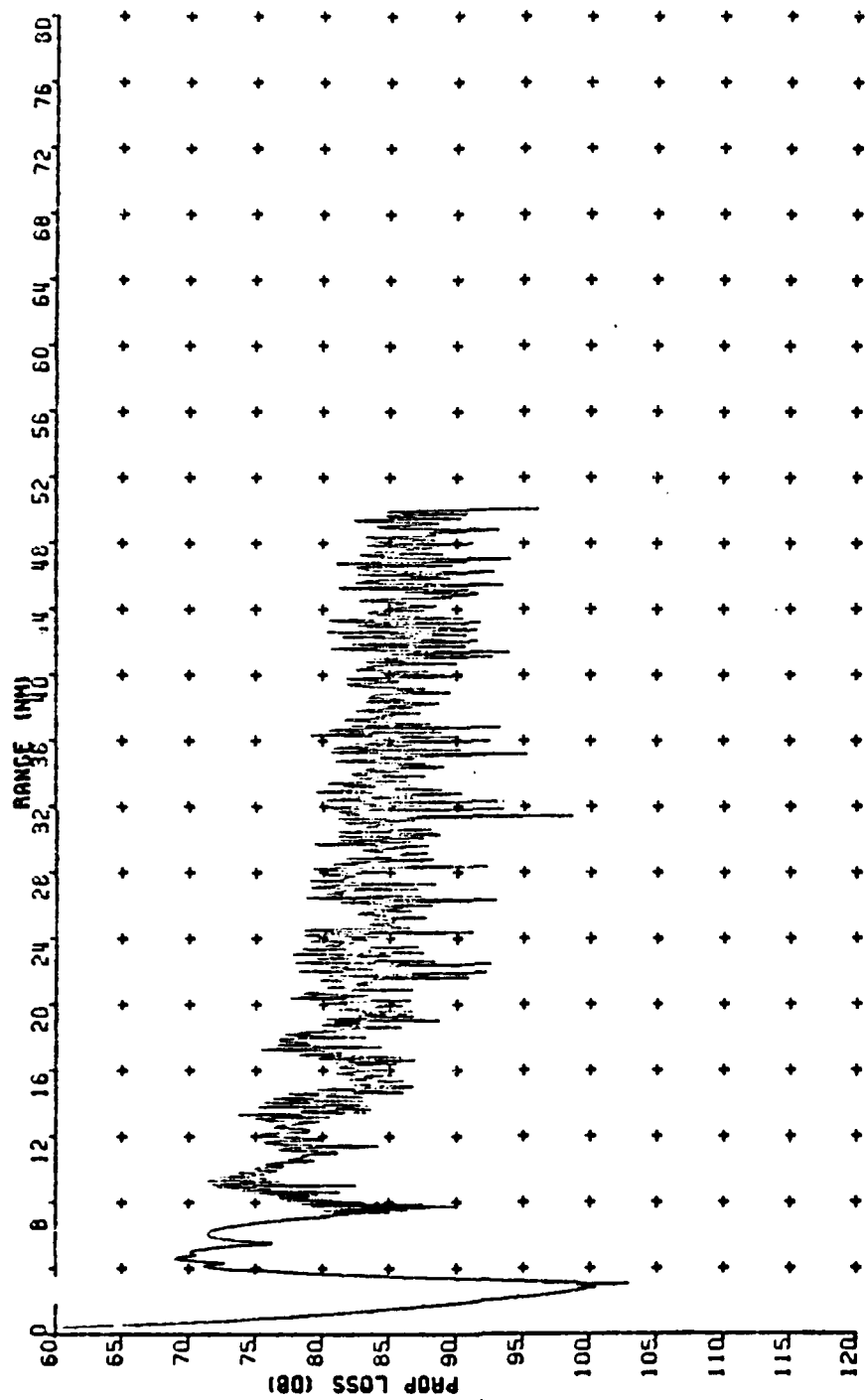Figure 56.   Perfectly Reflecting ISL=4 MXF Bottom (50 Hz)

84
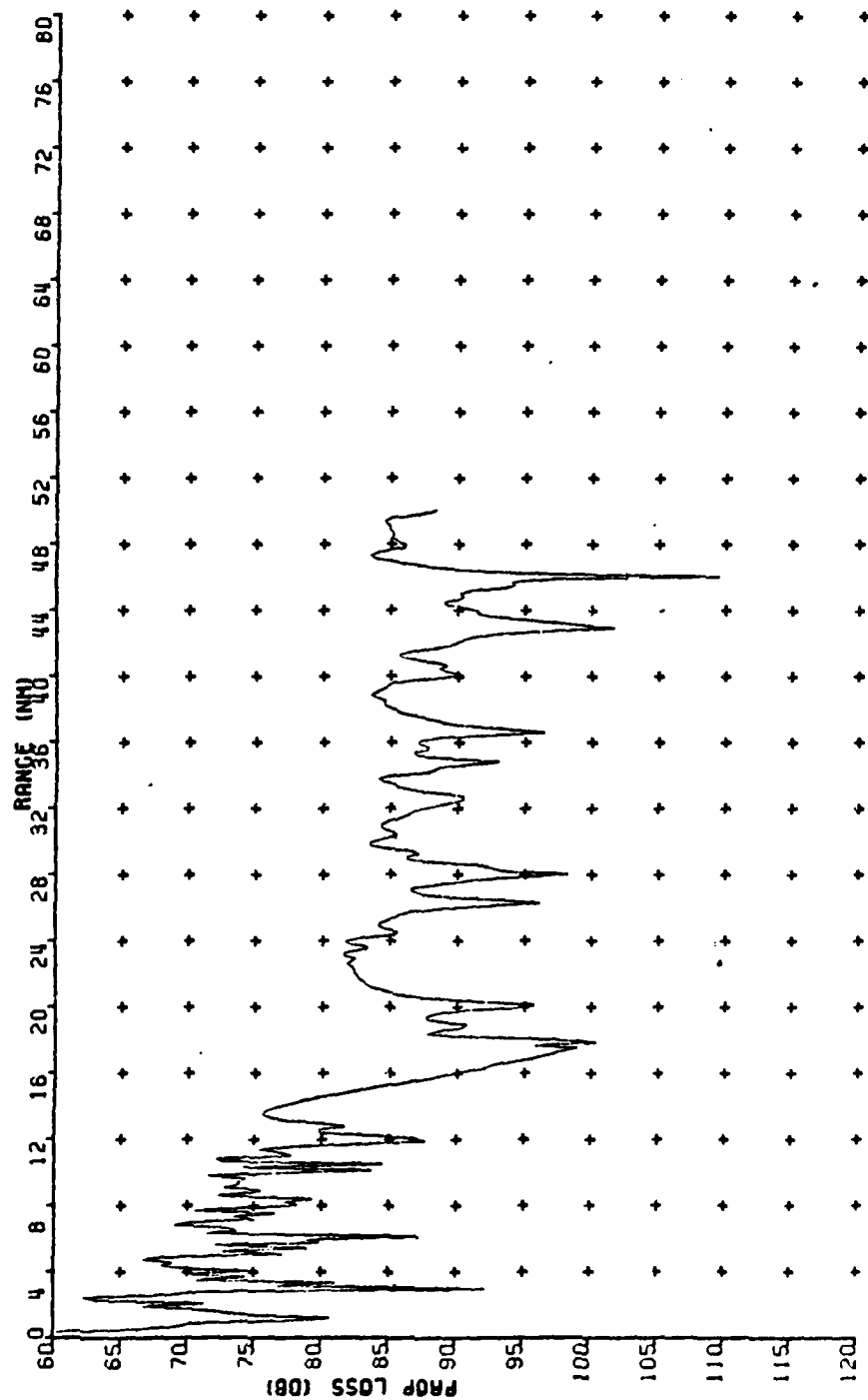
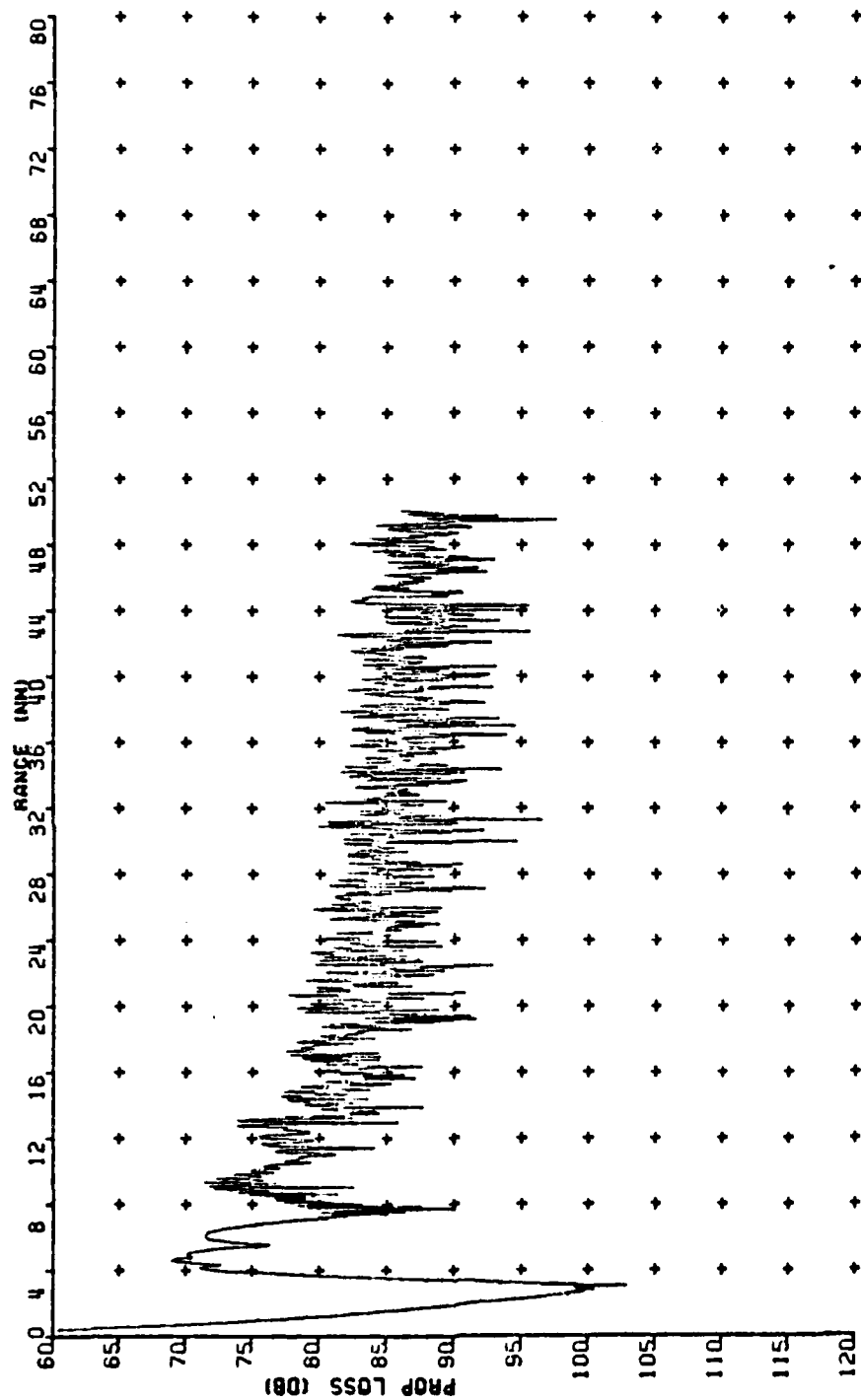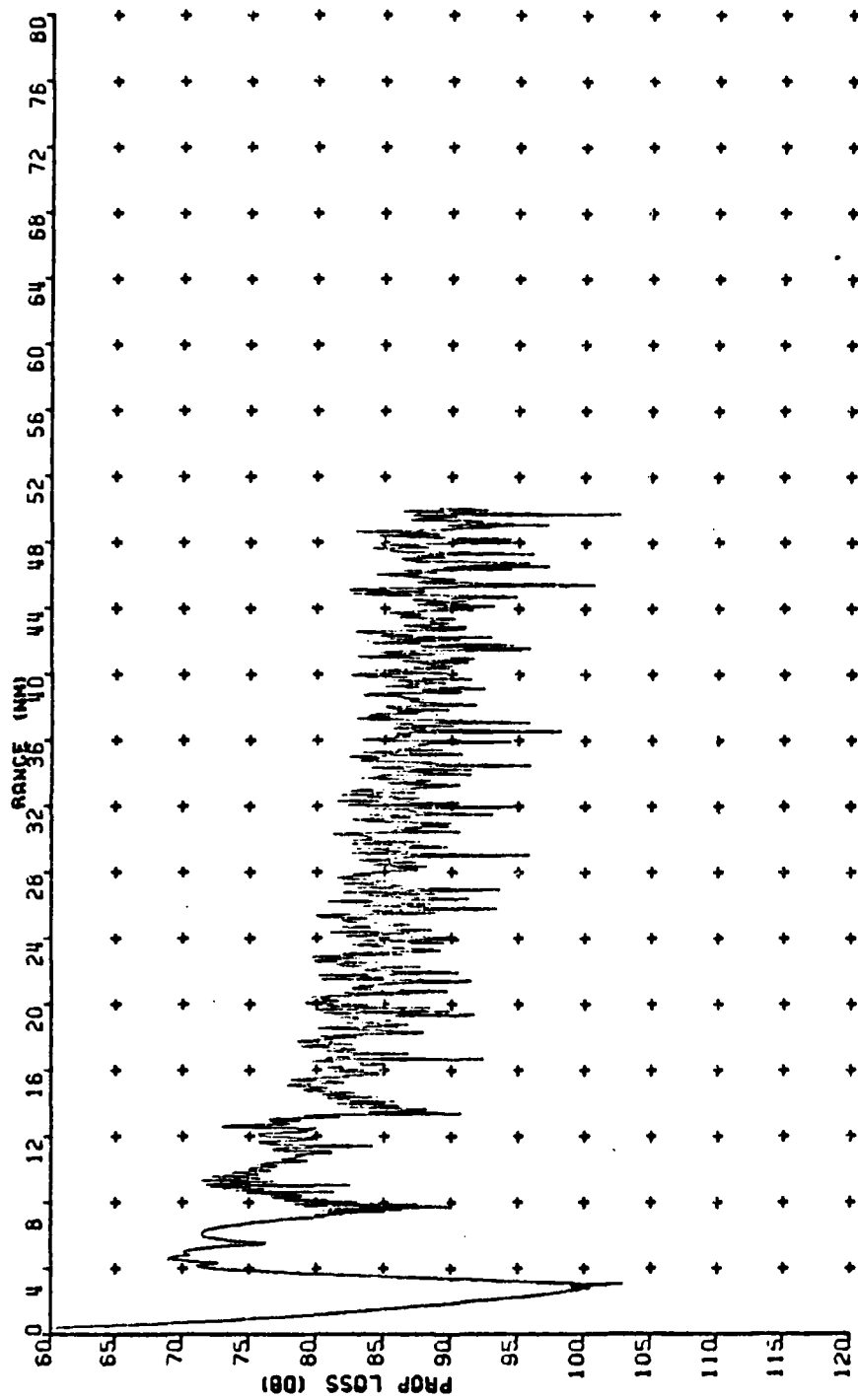Figure 57.   Perfectly Reflecting ISL=5 MXF Bottom (50 Hz)
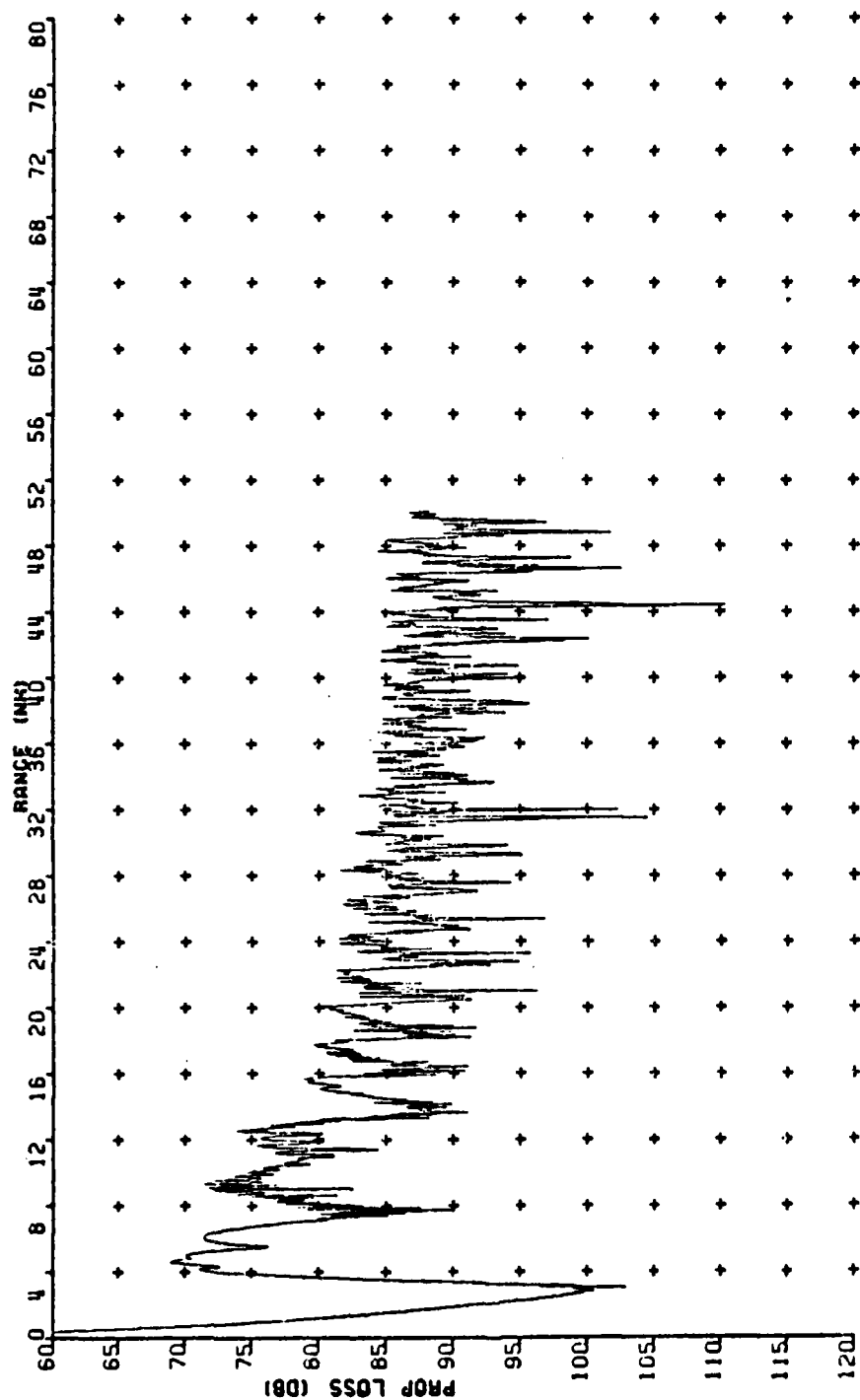
85
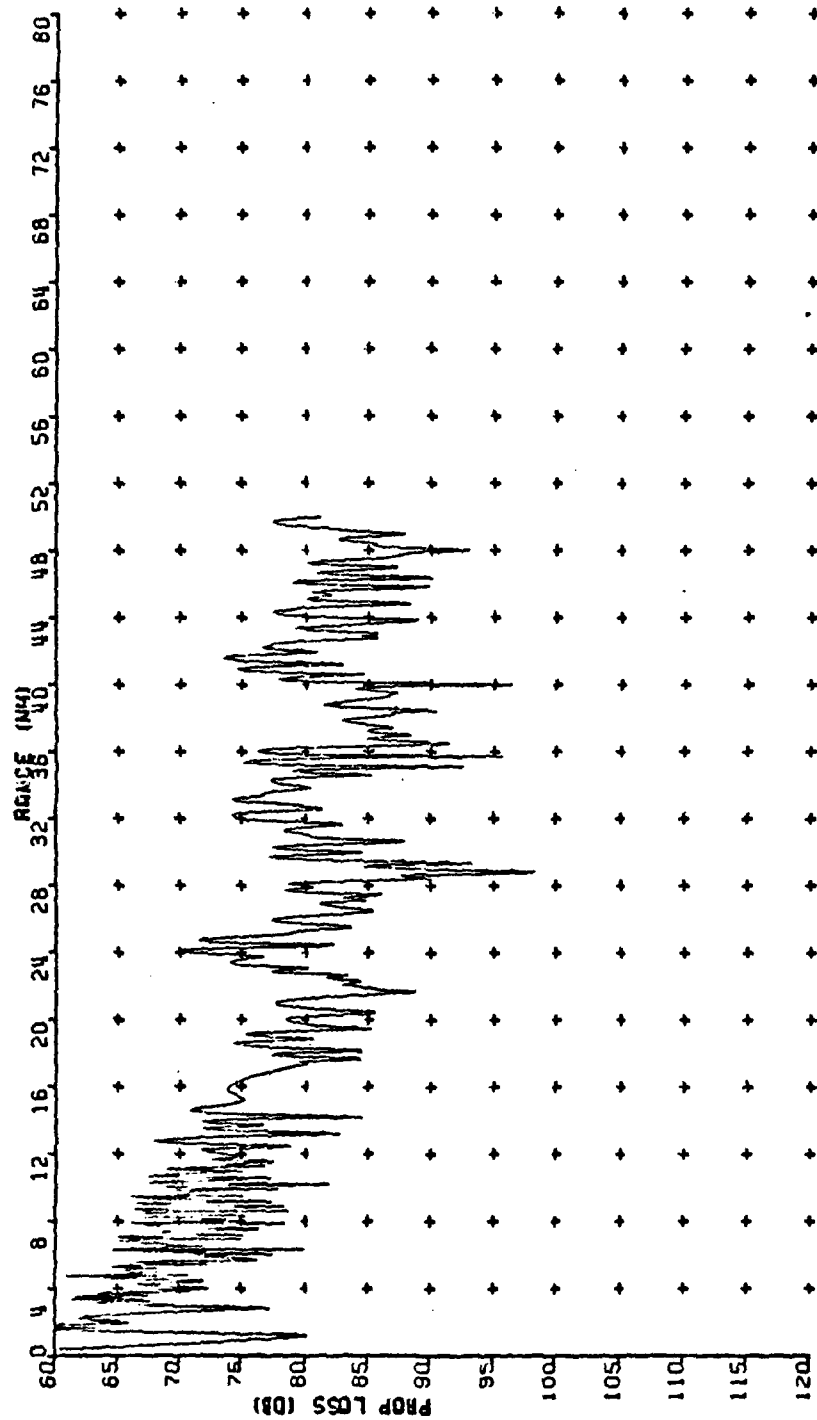
Figure 58.   Perfectly Reflecting ISL=6 MXF Bottom (50 Hz)
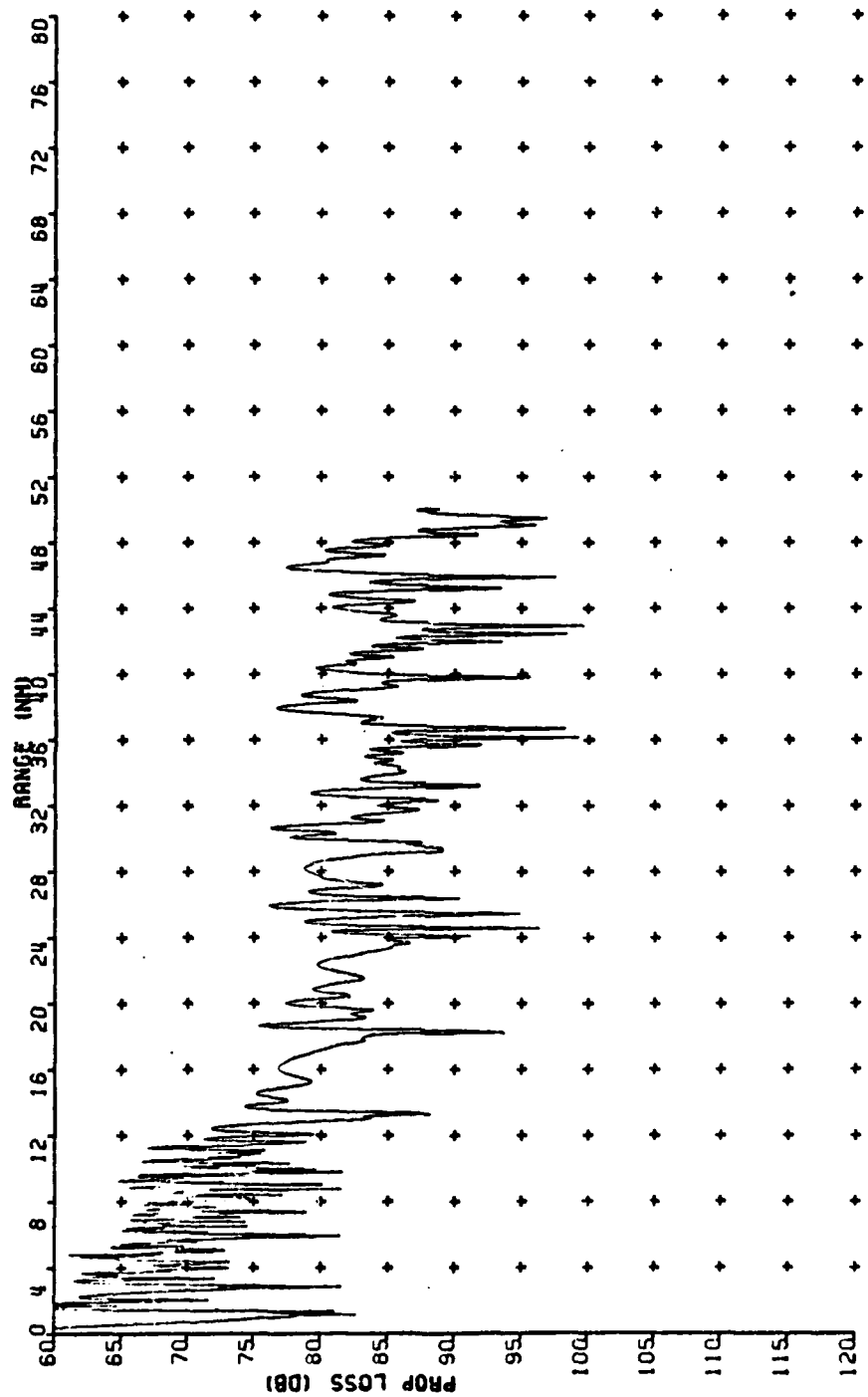
Figure 59.    Perfectly Reflecting ISL=7 MXF Bottom  (50 Hz)

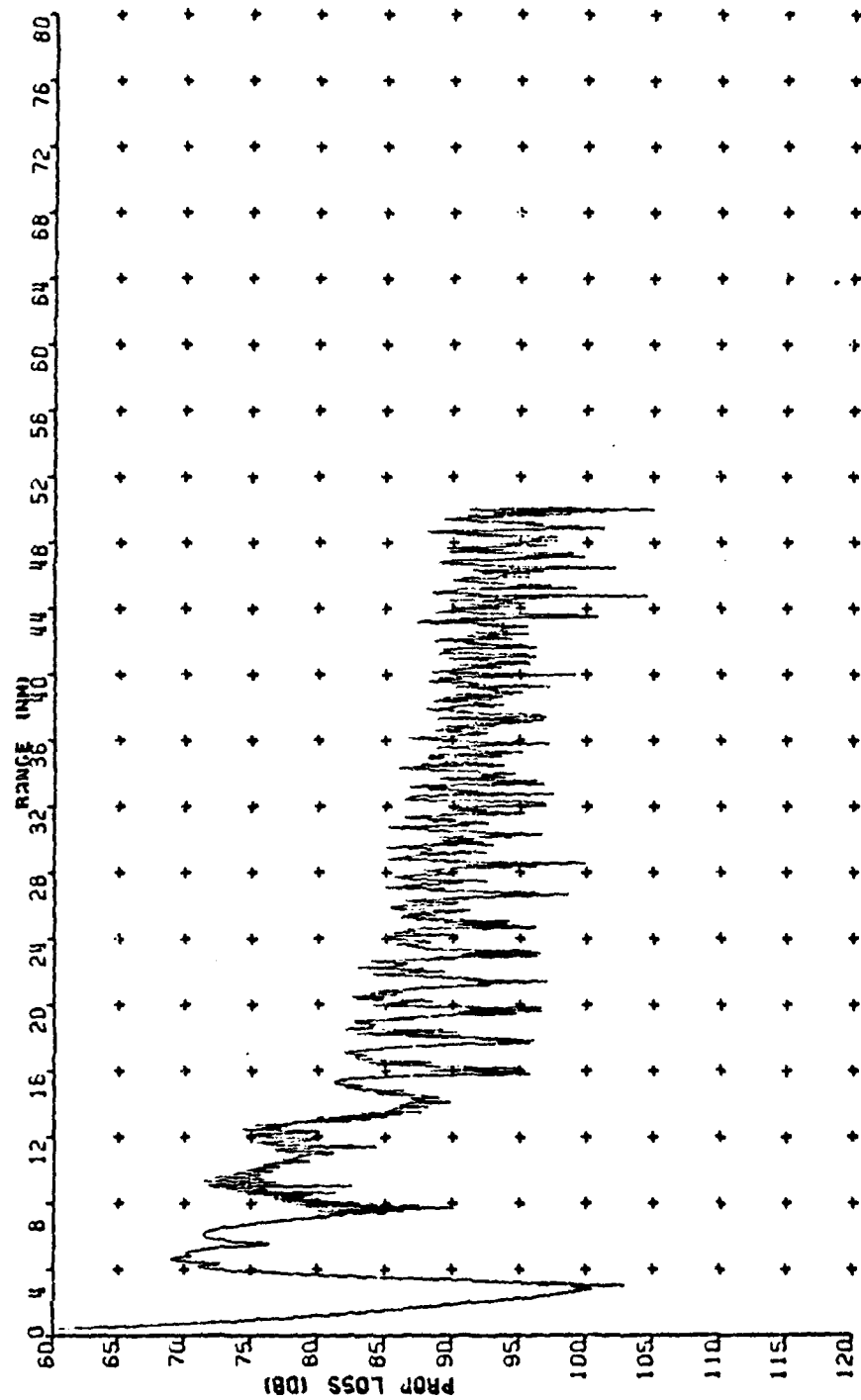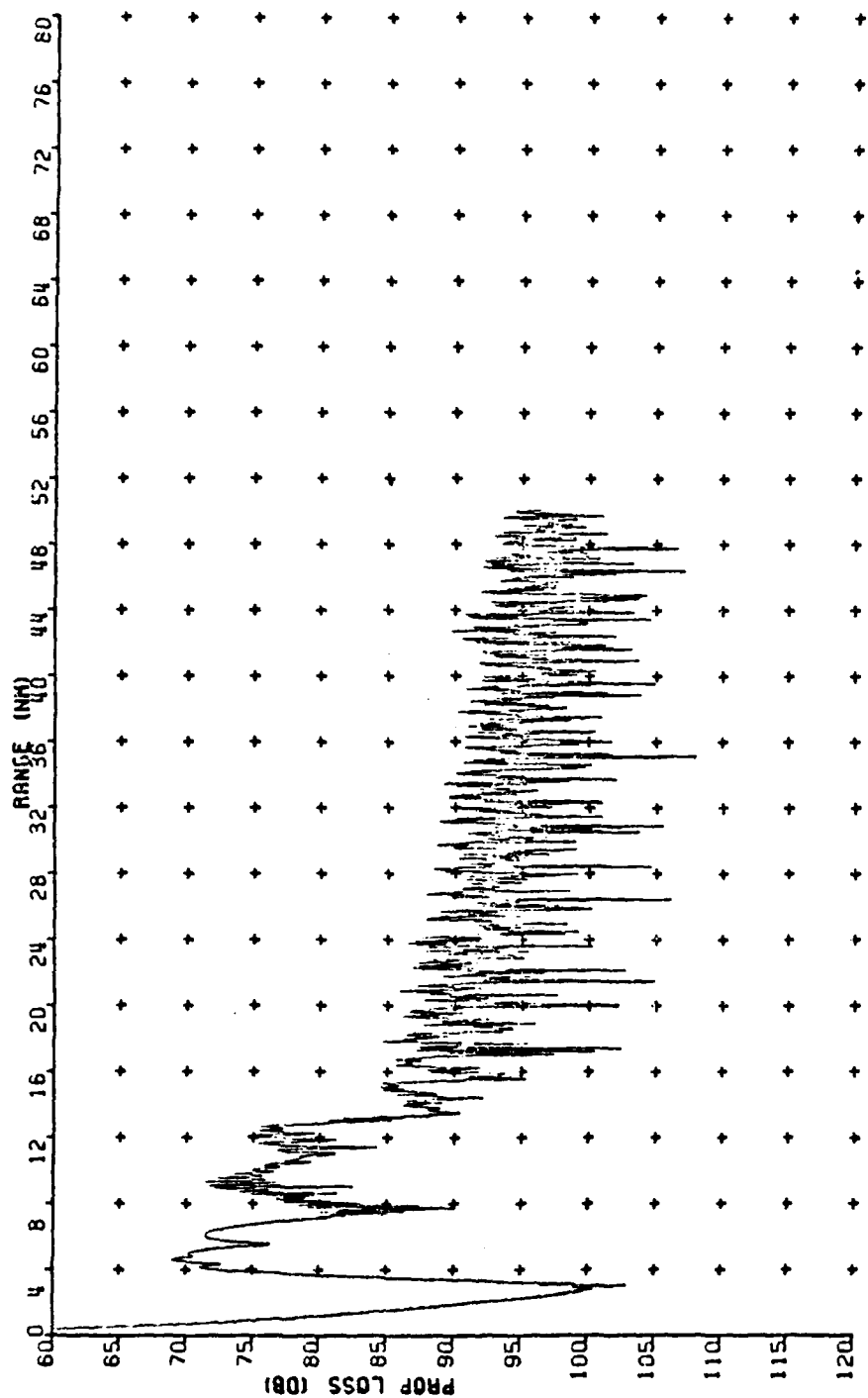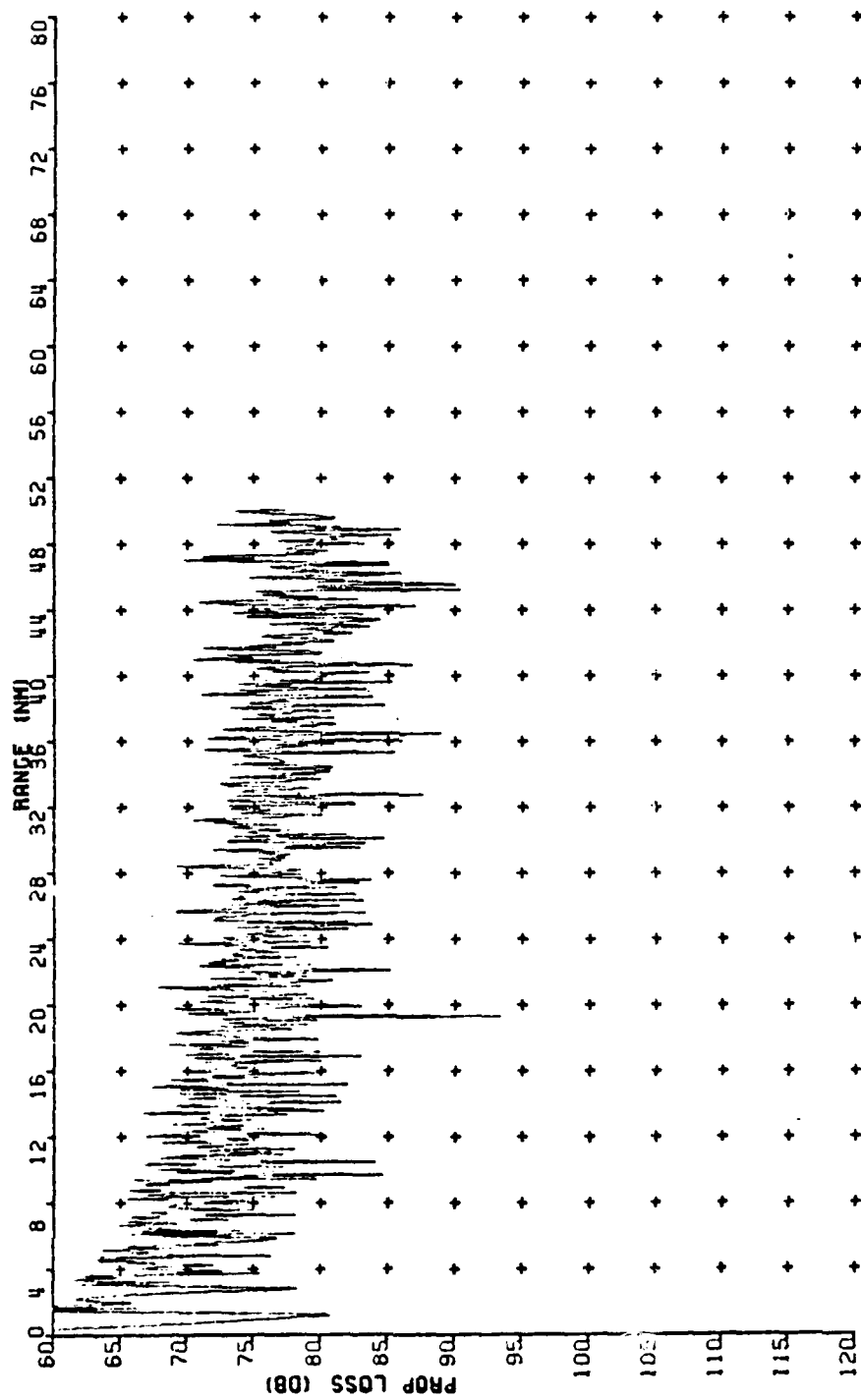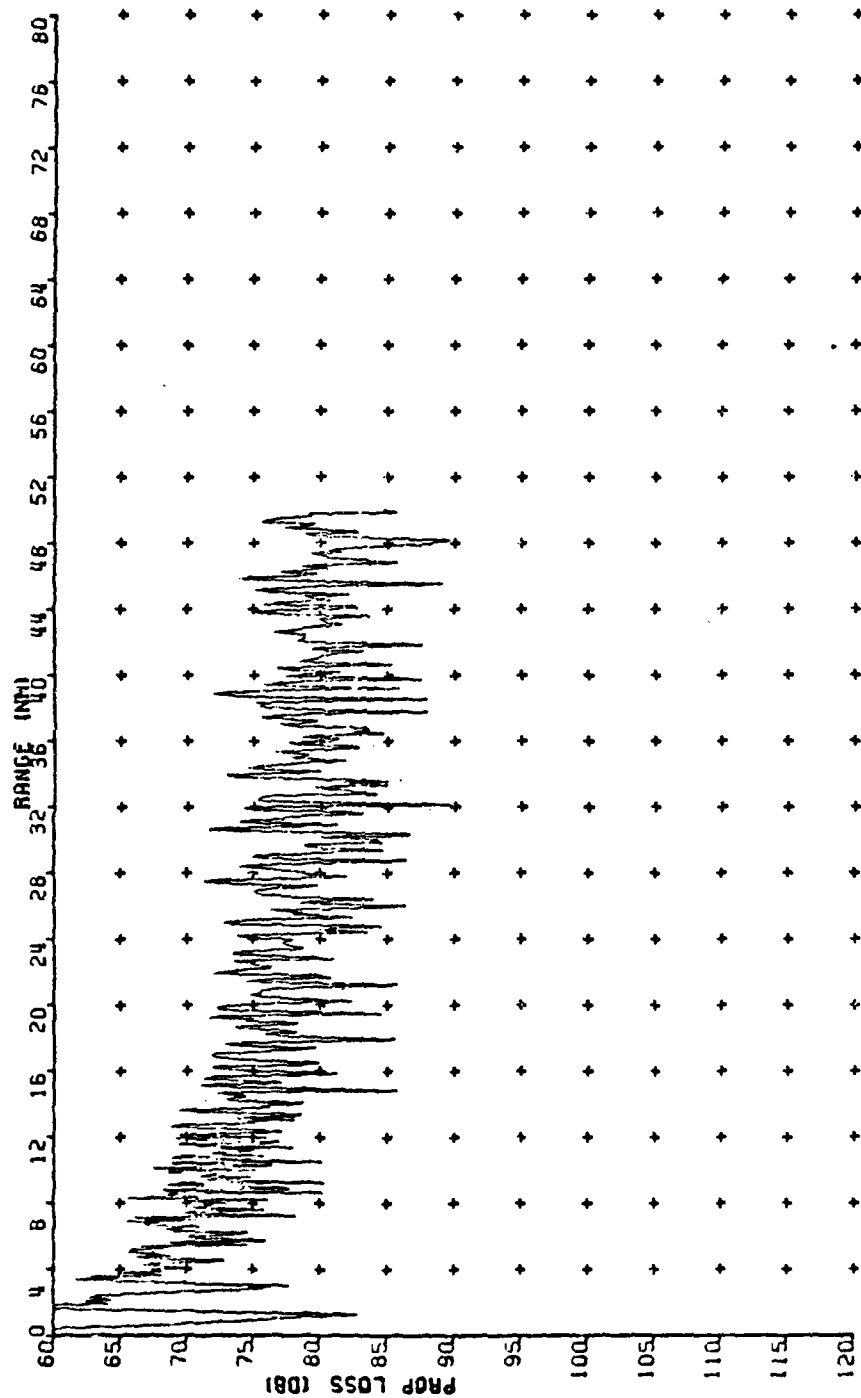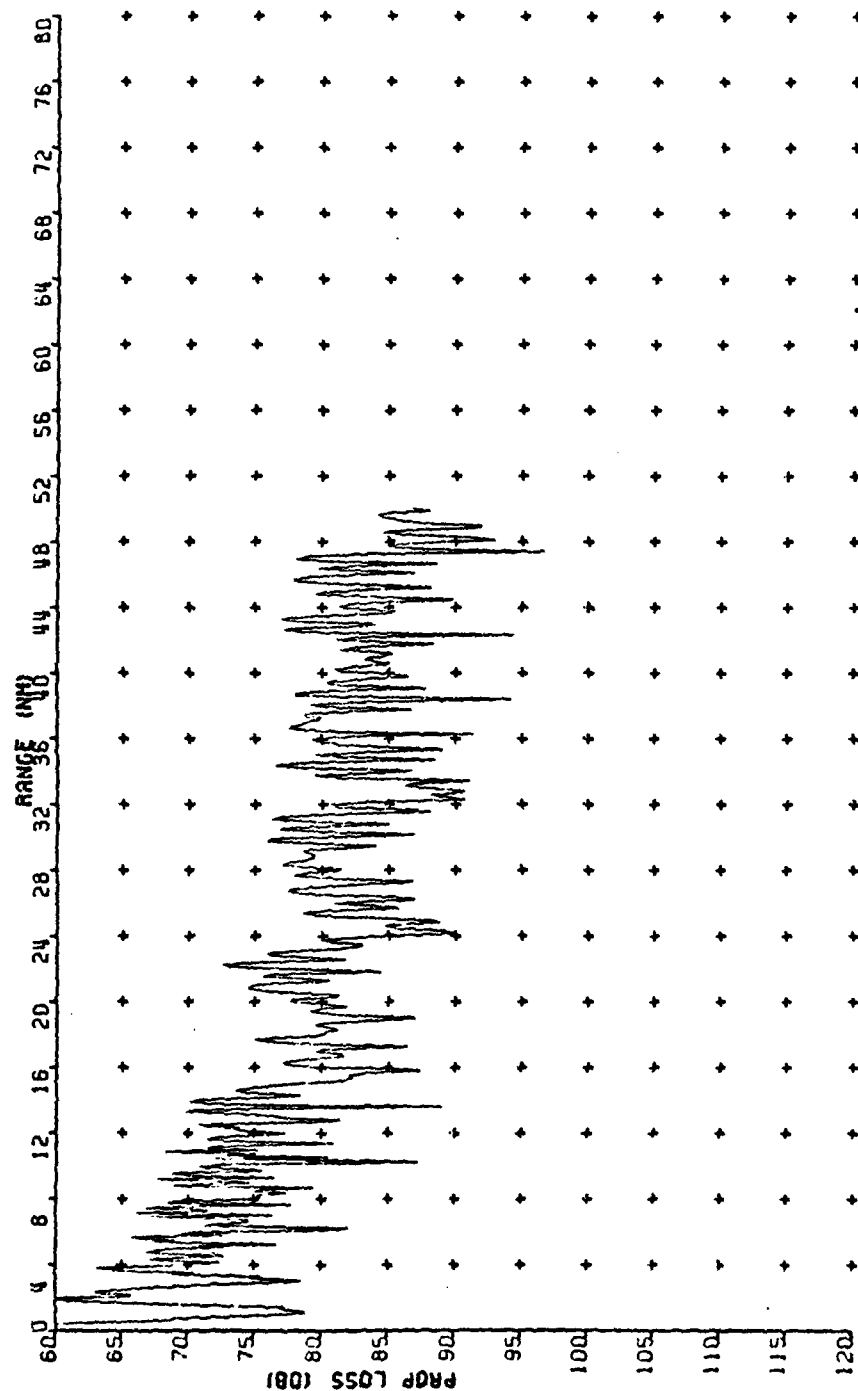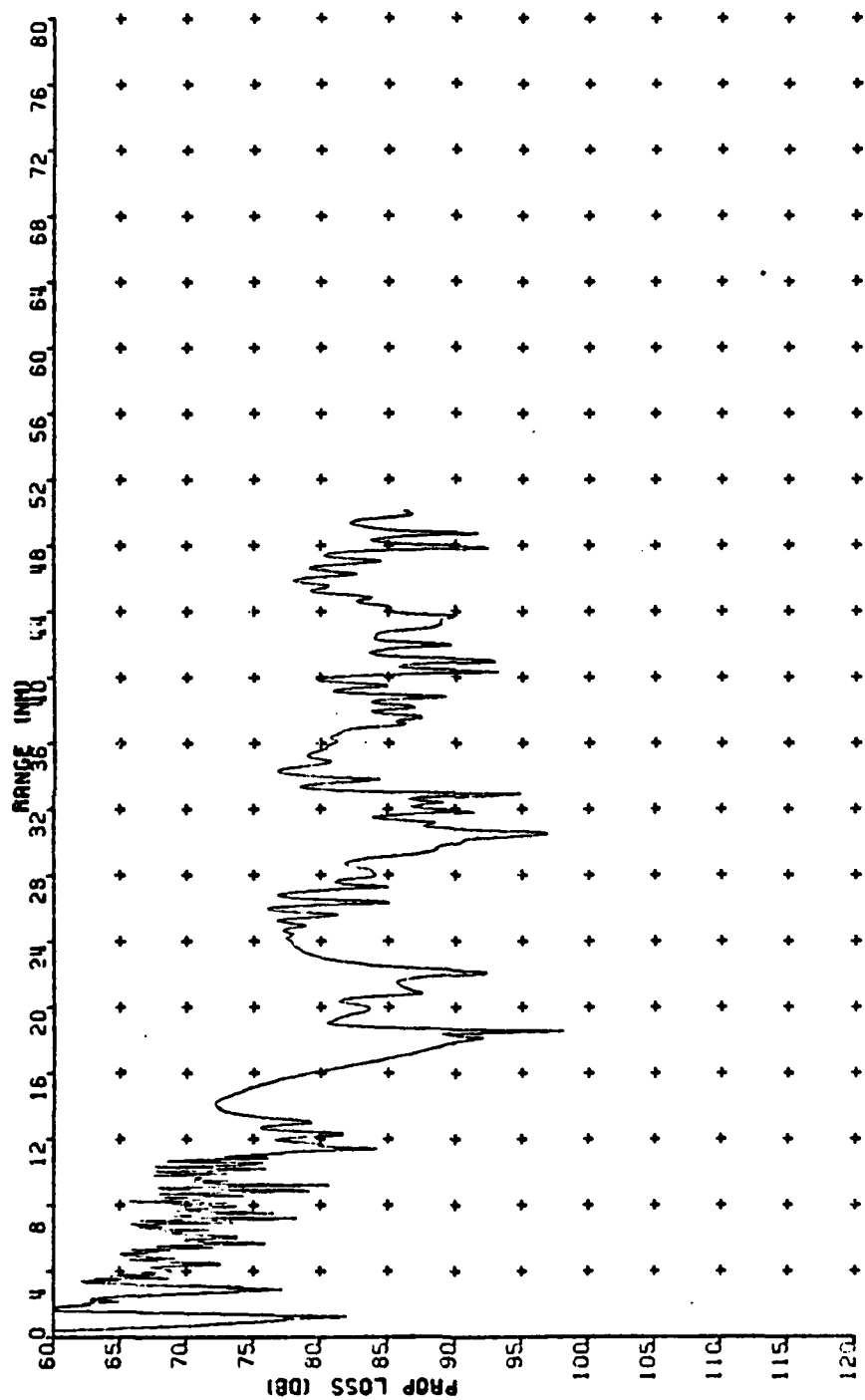Figure 60.   Perfectly Reflecting ISL=8 MXF Bottom (50 Hz)

88

## IV. SUMMARY AND CONCLUSIONS

More than two hundred different cases for the PE model have been computed for both deep and shallow water situations.

The scope of the present work has been, to study the sensitivity of the parabolic equation model to ocean bottom type.

Although this problem is a very broad one, it was chosen to provide experience in the use of the Parabolic Equation technique and to increase our understanding of its capabilities and limitations. Furthermore, it was hoped that it would be possible to determine, first hand, how the bottom interaction affects the propagation of acoustic energy under fairly realistic conditions.

The importance of the present work is obvious from many standpoints. From the theoretical acoustics point of view, it opens a way to determine qualitatively the importance of some of the different environmental parameters for the propagation of the sound. From the applied acoustics point of view, and especially for problems of naval interest, it provides the possibility of evaluating for a known environment any anomalous situation that affects the established pattern of sound propagation.

The conclusions that can be drawn from the present work are the following: with respect to the type of the bottom, only the refracted energy paths remain for a fully absorbing

bottom, making the model insensitive to different bottom geometries when an interaction of the energy with the bottom would otherwise be present. For a perfectly reflecting bottom, both the refracted and reflected paths will be present, but only if there is sufficient depth. The importance of the water depth is closely related to the shape of the SSP. The third bottom type tested was a more realistic compilation of bottom interaction at low frequencies. This bottom type, called Ul in the study, proved to have properties very similar to those of the perfectly reflecting bottom. Based on this fact it was proposed that the study of any realistic bottom should begin by studying the perfectly reflecting bottom. Any partial absorption characteristic of the bottom could then be simply simulated with a simple attenuation coefficient applied to the TL curves.

With respect to the bottom geometry, in the perfectly reflecting bottom cases, the importance of the sloping bottom and sloping-step bottoms was examined. A periodic interference pattern was found in the TL curves. The wavelength of this pattern proved to be inversely related to bottom slope. It is suggested that more general conclusions can be made with regard to this interference pattern after further study that would add a smoothing procedure to the parabolic equation model. Then the results may be studied in the frequency domain.

The funnel and megaphone effects were present in some of the tests, but some deviations from the usually expected

results were found.  This may be attributable to the restrictions in the parameterization of the modeled bottom.

In the downslope cases studied, the transfer of reflected to refracted energy was evident.  This effect was augmented by increasing bottom slope.

More study is clearly necessary in these areas of research using more sophisticated numerical and statistical procedures.  Furthermore, the study should expand to include sensitivity to the roughness of the bottom, to changes in the sound speed profile, and to a variety of source and receiver depths.  Equally interesting should be some laboratory or field experiments in order to establish in a practical way the model-observed dependence between the wavelength of the periodic interference pattern observed for upsloping, perfectly reflecting bottom, and the slope of the bottom.

# BIBLIOGRAPHY

Brock, H.K., "The AESD Parabolic Equation Model", Naval
    Ocean Research and Development Activity, Technical
    Note 12, January 1978.

Hamilton, K.G., Siegmann, W.L., and Jacobson, M.J., "Effects
    of Tidally Varying Sound Speed on Acoustic Propagation
    Over a Sloping Ocean Bottom," J. Acoust. Soc. Am. 66, p.
    1108-1119, 1979.

Hawker, K.E., Anderson, A.L., Focke, K.C., Foreman, T.L.,
    "Initial Phase of a Study of Bottom Interaction of Low
    Frequency Underwater Sound", Texas Univ. at Austin
    Applied Research Labs, Rept. No. ARL-TR-76-14, April
    1976.

Jensen, F. and Kroll, H., "The Use of the Parabolic Method
    in Sound Propagation Modeling", SACLANTCEN Memorandum
    SM-72, 1975.

Jensen, F.B., and Kuperman, W.A., "Environmental Acoustical
    Modeling at SACLANTCEN", SACLANTCEN Report SR-34, November
    1979.

Jensen, F.B., and Kuperman, W.A., "Sound Propagation in a
    Wedge-Shaped Ocean with a Penetrable Bottom", J. Acoust.
    Soc. Am. 67, p. 1564-1566, 1980.

Jensen, F.B., and Martinelli, M.G., "The SACLANTCEN Parabolic
    Equation Model (PAREQ)", SACLANTCEN, June 1980.

Johnson, R. and Norris, R., "Geographic Variation of Sofar
    Speed and Axis Depth in the Pacific Ocean", J. Geoph.
    Res. 73, p. 4695, 1968.

Lee, D. and Papadakis, J.S., "Numerical Solutions of the
    Parabolic Wave Equation: An Ordinary-Differential-
    Equation Approach", p. 1482-1488, 1980.

Northrop, J., Loughridge, M.S. and Wener, E.W., "Effect
    of Near-Source Conditions on Long-Range Sound Propagation
    in the Ocean", J. Geoph. Res. 73, p. 3905-3908, 1968

Spofford, C.W.,"A Synopsis of the AESD Workshop on Acoustic
    Propagation Modeling by Non-Ray Tracing Techniques,"AESD
    Technical Note TN 73-05, November 1973.

Stieglitz, R., Dozier, L., Garon, H.M., and Spofford, C.W., "Incorporation of an Ocean Bottom into the Parabolic Equation (PE) Algorithm", Science Applications, Inc., SAI-79-878-WA, January 1979.

Urick, R.J , <u>Sound Propagation in the Sea</u>, DARPA, 1979.

# INITIAL DISTRIBUTION LIST

|    |                                                                                                               | No. Copies |
|----|---------------------------------------------------------------------------------------------------------------|:----------:|
| 1. | Defense Technical Information Center<br>Cameron Station<br>Alexandria, VA  22314                               | 2          |
| 2. | Library, Code 0142<br>Naval Postgraduate School<br>Monterey, CA  93940                                        | 2          |
| 3. | Department Chairman, Code 68Mr<br>Department of Oceanography<br>Naval Postgraduate School<br>Monterey, CA  93940 | 1        |
| 4. | Department Chairman, Code 63Rd<br>Department of Meteorology<br>Naval Postgraduate School<br>Monterey, CA  93940 | 1         |
| 5. | Department Chairman, Code 61Dy<br>Department of Physics and Chemistry<br>Naval Postgraduate School<br>Monterey, CA  93940 | 1 |
| 6. | Department Chairman, Code 71<br>ASW Academic Group<br>Naval Postgraduate School<br>Monterey, CA  93940        | 1          |
| 7. | Professor R.W. Garwood, Code 68Gd<br>Department of Oceanography<br>Naval Postgraduate School<br>Monterey, CA  93940 | 2    |
| 8. | Professor R.H. Bourke, Code 68Bf<br>Department of Oceanography<br>Naval Postgraduate School<br>Monterey, CA  93940 | 1     |
| 9. | Antonio Ruiz Cañavate<br>Teniente de Navio<br>Instituto Hidrografico de la Marina<br>Cadiz, Spain             | 4          |
| 10.| Director<br>Naval Oceanography Division<br>Naval Observatory<br>34th and Massachusetts Avenue NW<br>Washington, D.C.  20390 | 1 |

94

11. Commander                                              1
    Naval Oceanography Command
    NSTL Station
    Bay St. Louis, MS   39522

12. Commanding Officer                                     1
    Naval Oceanographic Office
    NSTL Station
    Bay St. Louis, MS   39522

13. Commanding Officer                                     1
    Fleet Numerical Oceanography Center
    Monterey, CA   93940

14. Commanding Officer                                     1
    Naval Ocean Research and Development
      Activity
    NSTL Station
    Bay St. Louis, MS   39522

15. Office of Naval Research (Code 480)                    1
    Naval Ocean Research and Development
      Activity
    NSTL Station
    Bay St. Louis, MS   39522

16. Scientific Liaison Office                              1
    Office of Naval Research
    Scripps Institution of Oceanography
    La Jolla, CA   92037

17. Commander                                              1
    Oceanography Systems Pacific
    Box 1390
    Pearl Harbor, HI   96860

18. Almirante Director                                     2
    Instituto Hidrografico de la Marina
    Cadiz, Spain

19. Jose M. Fernandez Lopez                                1
    Capitan de Corbeta
    Instituto Hidrografico de la Marina
    Cadiz, Spain